Solo Dwarf Galaxy Survey: The Sagittarius Dwarf Irregular Galaxy

by

Clare Higgs
B.Sc.H., Queen's University, 2012

A Thesis Submitted in Partial Fulfillment of the
Requirements for the Degree of

MASTER OF SCIENCE

in the Department of Physics and Astronomy

Solo Dwarf Galaxy Survey: The Sagittarius Dwarf Irregular Galaxy

by

Clare Higgs
B.Sc.H., Queen's University, 2012

Supervisory Committee

Dr. Alan McConnachie, Co-Supervisor
(Department of Physics & Astronomy)

Dr. Kim Venn, Co-Supervisor
(Department of Physics & Astronomy)

Supervisory Committee

Dr. Alan McConnachie, Co-Supervisor
(Department of Physics & Astronomy)

Dr. Kim Venn, Co-Supervisor
(Department of Physics & Astronomy)

ABSTRACT

Galaxy evolution depends on a diverse suite of factors, from the environment in which the galaxy exists to the number of supernovae that explode throughout its history. The structure and stellar populations present will also be altered by a galaxy's merger history, stellar mass, star formation rate, among other influences. Some factors, like mergers, are dependent on the environment of the galaxy, while others, like feedback from star formation, are intrinsic to the galaxy themselves. Dwarf galaxies are sensitive to many of these factors due to their smaller masses, hence shallower potential wells. Dwarfs are also interesting in themselves as the least massive structures that can form stars, forming the faint limit of galaxy types. There is some indication that the evolutionary pathway of dwarfs might be different than their more massive counterparts. Indeed, some dwarfs may be the stripped remnants of larger galaxy after a major interaction. Regardless, dwarfs are thought to be the building blocks of larger galaxies via hierarchical galaxy formation and understanding these small dwarfs helps us build a more complete picture of galaxy formation and evolution at all masses.

As dwarfs generally have low stellar mass, they are very faint. Our most complete sample of dwarfs is therefore restricted to those that are nearby. These nearby systems are dominated by dwarfs satellite to the Milky Way and M31. However, the evolution of these satellites will be greatly influenced by their massive host. By studying nearby isolated dwarfs, we can try to separate the secular evolutionary processes of dwarfs from the influence of their larger host. Additionally, stellar populations can

be resolved in these nearby galaxies, and so their structures can be probed to much fainter regimes than integrated light studies allow.

The Sagittarius Dwarf Irregular Galaxy (Sag DIG) is one of the most isolated, low mass galaxies, located at the edge of the Local Group. Its isolation from other galaxies coupled with its relative proximity provide an excellent opportunity to study the intrinsic properties of this low mass system. We preform an in-depth analysis of its resolved stellar populations and its structural properties as the first galaxy in the larger dataset, *So*litary *Lo*cal Dwarfs Survey (*Solo*). *Solo* is a wide field photometric study targeting every isolated dwarf galaxy within 3 Mpc of the Milky Way. *Solo* is based on $(u)gi$ multi-band imaging from CFHT/MegaCam for northern targets, and Magellan/Megacam for southern targets. All galaxies fainter than $M_V \simeq -18$ situated beyond the nominal virial radius of the Milky Way and M31 ($\gtrsim 300$ kpc) are included in this volume-limited sample, for a total of 42 targets.

For Sag DIG, we provide updated estimates of its central surface brightness and integrated luminosity, and trace its surface brightness profile to a level fainter than 30 mag./sq.arcsec. Sag DIG is well described by a highly elliptical (disk-like) system following a single component Sersic model. However, a low-level distortion is present at the outer edges of the galaxy that, were Sag DIG not so isolated, would likely be attributed to some kind of previous tidal interaction. Further, we find evidence of an extremely low level, extended distribution of stars beyond ~ 5 arcmins (> 1.5 kpc) that suggests Sag DIG may be embedded in a very low density stellar halo. We compare the stellar and HI structures of Sag DIG, and discuss results for this galaxy in relation to other isolated, dwarf irregular galaxies in the Local Group. Sag DIG, and the similarly isolated dwarf Aquarius, both have HI distributions that are more circular than their stellar components. In contrast, Wolf – Lundmark – Mellote (WLM), another isolated but slightly more massive dwarf, has stellar and HI components that trace each other well. Sag DIG and Aquarius also differ in that there is no signature of rotation in the HI of Sag DIG, while there is clear rotation in both the HI and stellar component for Aquarius. These preliminary comparisons demonstrate some of the potential analysis which will be possible on a much larger scale with the full *Solo* Survey.

Contents

List of Tables

List of Figures

ACKNOWLEDGEMENTS

I would like to thank Alan McConnachie for his plentiful help, support, wisdom and patience. Also Kim Venn for her guidance, help and enthusiasm.

In addition, I would like to thank my friends, family as well as the other students and faculty in the department for their kindness and support.

Based on observations obtained with MegaPrime/MegaCam, a joint project of CFHT and CEA/DAPNIA, at the Canada-France-Hawaii Telescope (CFHT) which is operated by the National Research Council (NRC) of Canada, the Institut National des Science de l'Univers of the Centre National de la Recherche Scientifique (CNRS) of France, and the University of Hawaii. We thank the staff at CFHT for their help in obtaining the observations for the *Solo* sample.

Based on observations made with the NASA/ESA Hubble Space Telescope, and obtained from the Hubble Legacy Archive, which is a collaboration between the Space Telescope Science Institute (STScI/NASA), the Space Telescope European Coordinating Facility (ST-ECF/ESA) and the Canadian Astronomy Data Centre (CADC/NRC/CSA)

To my Grandma Nicky, who said to never let grass grow around my dreams, and to Holly.

Chapter 1

Introduction

We strive to understand galaxy evolution and the faintest known galaxies by studying those nearest to the Milky Way. The mechanisms which shape galaxies and result in their present structure are driven both internally and by external interactions. These internal and external factors are interconnected and work in concert with each other, making it challenging to untangle the secular evolution of dwarf galaxies. Isolated, nearby dwarf galaxies are sensitive probes of these different mechanisms which we can study in great detail, while isolating the internal from external processes.

1.1 The Big Picture

Galaxies are diverse and plentiful, showing a large range of features and characteristics suggestive of complex processes and variables governing both their formation and evolution. Galaxies are thought to form hierarchically through a series of mergers. This model was first supported by Searle & Zinn (1978) who studied the abundances of globular clusters in the Milky Way. They found the lack a metallicity gradient at large distances is more consistent with hierarchical formation than a pressure supported slow collapse (as suggested by Eggen et al. 1962). Beyond initial formation, there are numerous evolutionary processes, both on small scales, like feedback from star formation, to much larger scales, like mergers, which shape and re-shape galaxies.

Using simulations, we can probe the large scale structure of our universe and the processes which form the observable structures. Dark matter simulations trace the overall structures and successfully recreate the general features of our observable universe. From these dark matter only simulations, mapping to the baryonic structure is

more complicated and less constrained. For example, Abadi et al. (2003) successfully simulate a galaxy with hierarchical formation, however, their results are dependent on the stellar feedback recipe applied. These parameters are tuned to match observations but is poorly constrained.

This mapping between dark matter and stars is important as it connects large scale structure to galaxies and galaxy groups, which are critical to test the success of the models. When connecting to observed galaxies, inconsistencies between observations and simulations appear, such as the "missing satellite" problem (see Klypin et al. 1999; Moore et al. 1999) or "the too big to fail" problem (see Boylan-Kolchin et al. 2011). The missing satellite problem is a dearth of small dwarf galaxies observed compared to the number simulated. While many new dwarfs have been discovered in the Local Group (Koposov et al. 2015 for example), there is still at least several orders of magnitude difference. It has been speculated that these missing halos are simply dark, that is, they do not contain stars and gas. The "too big to fail" problem takes the discrepancy a step further by showing that the mass distribution of galaxies predicted in cold dark matter simulations is a poor match with observed galaxies. Simulations predict the existence of halos massive enough that they cannot possibly have remained dark. These two problems highlight the importance of understanding small galaxies to test and advance the large scale dark matter simulations.

We can observe galaxies both nearby and at high redshifts, allowing us to probe their evolution. However, we are restricted to only more massive galaxies at higher redshift. When studying galaxies at the faint limit, we have only the nearest galaxies, in and around the Local Group. We therefore look to the nearest systems to obtain the most detailed view of their stellar structure using resolved stellar analysis and trace the properties of the galaxy to extremely low surface brightness levels, impossible for more distant systems. The overwhelming majority of nearby galaxies are on the dwarfs scale, with the most obvious exception being M31. Dwarf galaxies are the building blocks of larger systems via hierarchical galaxy evolution (again see Searle & Zinn 1978 for some of the first observational evidence). They are also interesting in their own right as sensitive probes to both internal and external galaxy evolution processes, as discussed later.

As the dwarfs are nearby, we can use resolved stars to preform detailed and in depth analysis, as well as being able to observe the whole system. Additionally, there is a variety of dwarfs types, ranging from the comparatively large Magellanic Clouds to dwarfs with just a few thousand stellar masses. While there is not a large

population, there are sufficient numbers of dwarfs, both as satellites to M31 and the Milky Way, and isolated, to survey and characterize their general features.

To understand galaxies, we must determine the dominant drivers of their evolution and determine how these effects shaped them into the systems we observe. We can determine the characteristics of galaxies on the faint end without the unknown influence of a larger host by studying dwarfs that have evolved in isolation.

1.2 A Census of the Closest Galaxies

The Local Group contains an interesting assortment of galaxies, dominated by the two most massive systems, our own Milky Way and M31 (Andromeda). There is a growing list of nearby galaxies (see Koposov et al. 2015 for example) observed in the vicinity of the Milky Way and M31, classified as dwarf galaxies. McConnachie (2012) summarizes the known closest galaxies (within 3 Mpc of the Sun).

The close proximity of these galaxies makes them a unique testbed to study their resolved stars, hence our understanding of stellar populations and substructure is much improved over more distant systems. We can also resolve very faint structures such as tidal tails. Such work is very hard to do based on unresolved light. A new player to the field, Dragonfly (see van Dokkum et al. 2014 for a general description), demonstrates the scale and diversity of faint structures previously missed in the vicinity of more distant galaxies. Dragonfly is optimized to have extremely low internal scattered light, allowing for long integration times, so very faint structures can be observed based on unresolved light. Its magnitude limits are able to probe the luminosity of the extended structures, predicted by simulations but rarely observed outside of the Local Group. As part of their program, Dragonfly has discovered a potentially new class of galaxies, the ultra diffuse galaxies, discovered by van Dokkum et al. (2015) in the Coma Cluster. Shown in Figure 1.1, these new objects have a different effective radius – surface brightness relation in comparison to galaxies identified in the SDSS or Virgo cluster, occupying a new area of parameter space. These new galaxies have stellar masses comparable to dwarfs and effective radii on the order of the Milky Way. They appear red and very round, not disk– like (van Dokkum et al. 2015).

While the sample of galaxies for which we can obtain wide field perspectives of their resolved stellar populations is limited, the power and potential of using these resolved stars to trace the faint structures visible in nearby systems is demonstrated

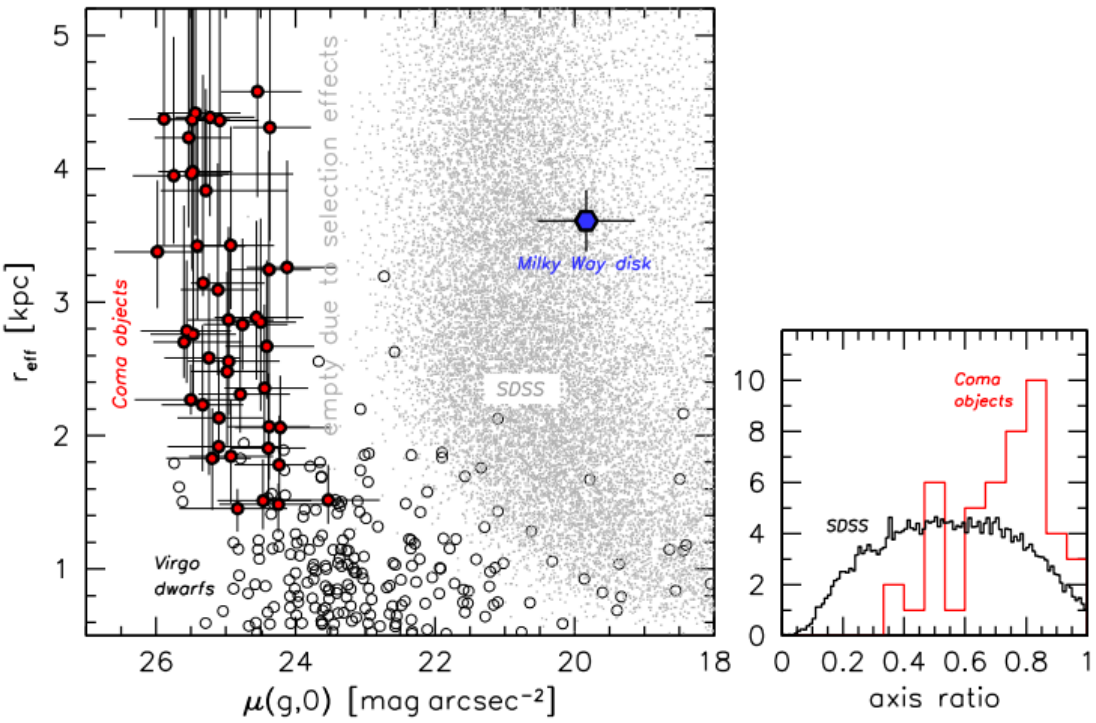

Figure 1.1 From van Dokkum et al. (2015), the new ultra faint galaxies appear to lie in a different size/luminosity regime. The ultra faint galaxies also appear more round than the general SDSS sample.

by the Pan-Andromeda Archaeological Survey (PAndAS; McConnachie et al. 2009). By looking at specific stellar populations of resolved stars, highly extended structures with extremely low surface brightness are revealed, demonstrating the hierarchical nature of galaxy formation (that is, small galaxies merge to form larger galaxies). Such surface brightness limits are unattainable for more distant galaxies, even with Dragonfly. When applied to dwarf galaxies, we are limited to a relatively small sample of galaxies (of order a hundred), predominantly dwarfs. Such a sample does not necessarily cover all possible parameter space for dwarf galaxies, but they are the most detailed examples of their galaxy class that can be achieved.

1.2.1 Nearby Dwarf Galaxies

Before discussing dwarf galaxies nearest to the Milky Way, we must establish what defines a dwarf galaxy. Figure 1.2 from Tolstoy et al. (2009) shows dwarf galaxies in relation to their larger counterparts and smaller structures (like globular clusters) in

terms of their absolute magnitude, scale radius and surface brightness. This figure is several years old and is lacking the most recent discoveries, however it clearly demonstrates the poor distinction between types. The distinction has become even more blurred with the newest discoveries with very low stellar masses, which look increasingly similar to stellar clusters (see Willman & Strader 2012). An updated version of this plot, including the most recently discovered dwarf from the Dark Energy Survey (DES), is shown in Figure 1.3 from Koposov et al. (2015). A significant dark matter component is generally considered to be the major distinguishing factor between clusters and galaxies, usually identified through a high stellar velocity dispersion based on radial velocity measurements of many stars. However, in some cases the data are not conclusive, due either to only a few stars being accessible for measurement (e.g., Simon & Geha 2007; Kirby et al. 2015) or uncertainties on the conversion from a radial velocity dispersion to a dynamical mass (e.g., McConnachie & Côté 2010 and references therein). In some cases without reliable velocity measurements, a spread in iron abundance can be used as indirect evidence of dark matter (with the implication that a deep gravitational potential is required to retain the enrichment products of Type II supernovae; e.g., see Kirby et al. 2015 for a recent example).

At the bright end of the dwarf luminosity distribution, Kormendy (1985) famously demonstrated that "dwarf" galaxies appear to define a scaling relation between surface brightness and magnitude that is nearly orthogonal to"giant" galaxies. A more recent version of this result is shown in Figure 1.6 from Kormendy et al. (2009). This orthogonality is suggestive of a different evolutionary partway for dwarfs, making them distinct from their larger cousins. If this is indeed the case, then the definition of a dwarf galaxy could be based on this physical difference. Recently, however, growing evidence suggests that dwarfs and giants define a single, continuous but non-homologous relation in this parameter space (Ferrarese et al. 2012). Mindful of these considerations, we adopt the generally-accepted definition of a dwarf galaxy as having an absolute magnitude of $M_V > -18$ (e.g., Grebel et al. 2003; McConnachie 2012).

Dwarf galaxies form a surprisingly large morphological menagerie, including (but probably not limited to): blue-compact, elliptical, irregular, low surface brightness, Magellanic-type, spheroidal, spiral, transition-type, ultra-compact, and ultra-faint. The recently discovered ultra-diffuse galaxies (van Dokkum et al. 2015) highlight the variety.

Within the Local Group, there are three major categories of dwarf galaxies, that relies most on gas content and star formation for classification. Dwarf spheroidals

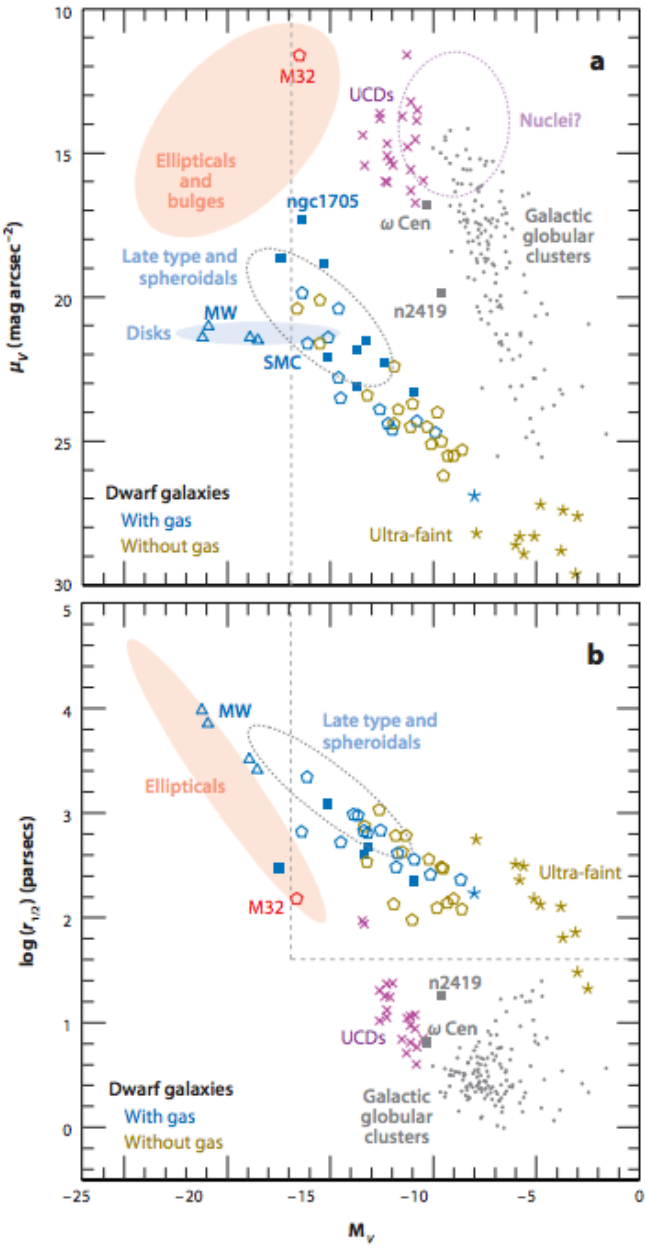

Figure 1.2 From Tolstoy et al. (2009), the different objects, from large elliptical galaxies to small stellar clusters are labeled relative to absolute magnitude - surface brightness in the upper panel and absolute magnitude- scale radius in the lower panel.

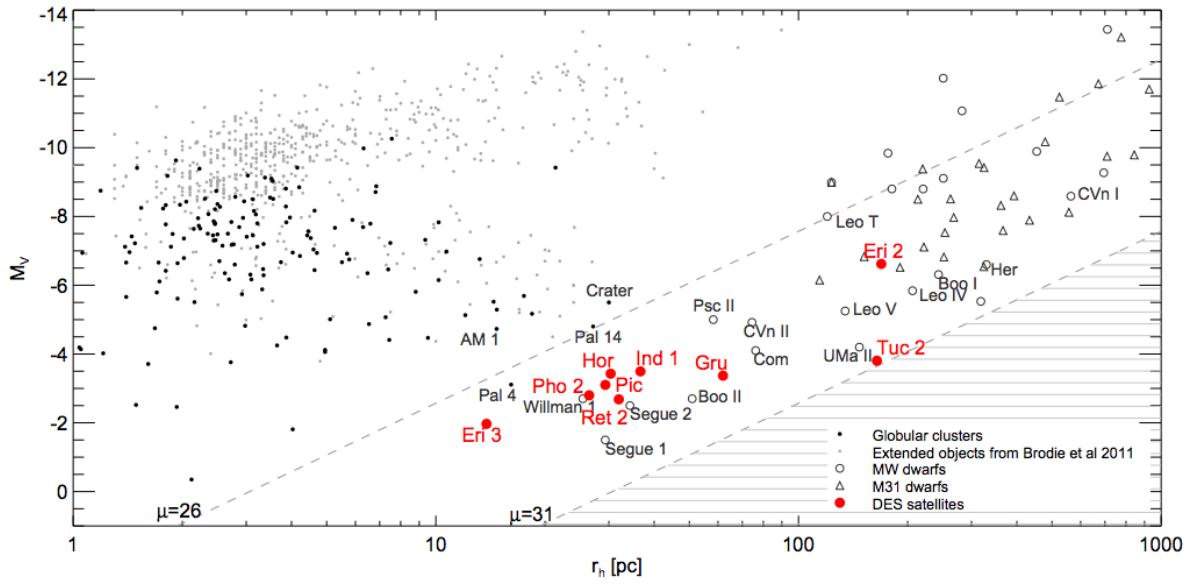

Figure 1.3 From Koposov et al. (2015), an updated version of the previous figure showing the newest dwarfs detected in DES.

(like Cetus) are devoid of gas and as a result, have no ongoing star formation. They are somewhat analogous to ellipticals, just on a smaller scale. In contrast, dwarf irregulars (like Sagittarius dwarf irregular galaxy) do contain gas and have young populations indicative of current star formation. The third type, know as the transition dwarfs, contain gas but no current star formation (like Aquarius). The drivers of this diversity are the focus of much of the literature on these objects. While certainly governed by the same physics as their more massive counterparts, dwarf galaxies are generally expected to be more sensitive to the processes that drive galaxy formation and evolution (for example, see Verbeke et al. 2015). Both internally driven processes, like star formation and stellar feedback, and externally driven processes, like ram pressure or tidal stripping, can greatly impact the structure and morphology of these small systems.

Due to the proximity bias described above for dwarf galaxies, the most detailed studies of dwarfs are heavily biased towards the Milky Way satellites (and, to a lesser extent, the M31 satellites). The nearby dwarf galaxies show some general trends. Figure 1.4 (from McConnachie 2012) shows the nearby dwarfs by their HI gas content and their separation from the Milky Way and Andromeda. With some notable exceptions (like Sculptor and Fornax), these dwarfs are generally devoid of gas and show no sign of ongoing star formation. Therefore, most are classified as dwarf spheroidal (or dwarf elliptical if they are brighter than $M_V \simeq -15$). In contrast, it has long been known (Einasto et al. 1974) that more isolated dwarf galaxies (beyond the virial radius of the Milky Way and Andromeda) are frequently found to be gas rich and have young stellar populations, indicative of ongoing or very recent star formation. The exceptions to this trend are Cetus and Tucana which are isolated but devoid of gas. The position–morphology relation in the Local Group is seen in other groups as well (Bouchard et al. 2009) and suggests a close link between the nearby presence of a large galaxy and the evolution of dwarf galaxies.

The position-morphology relation in the Local Group has recently been clearly demonstrated with new measurements of the HI content of dwarfs within and beyond the virial radius. This is seen in Figure 1.4 from Spekkens et al. (2014). This paper specifically tried to find HI gas in the closest dwarfs, and finding none, placed stronger limits on the gas content. It is interesting to note that there is no obvious gradient with distance from the Milky Way. That is, there is a sharp transition between gas rich and gas poor. The potential mechanisms for the removal of gas are discussed in the following section.

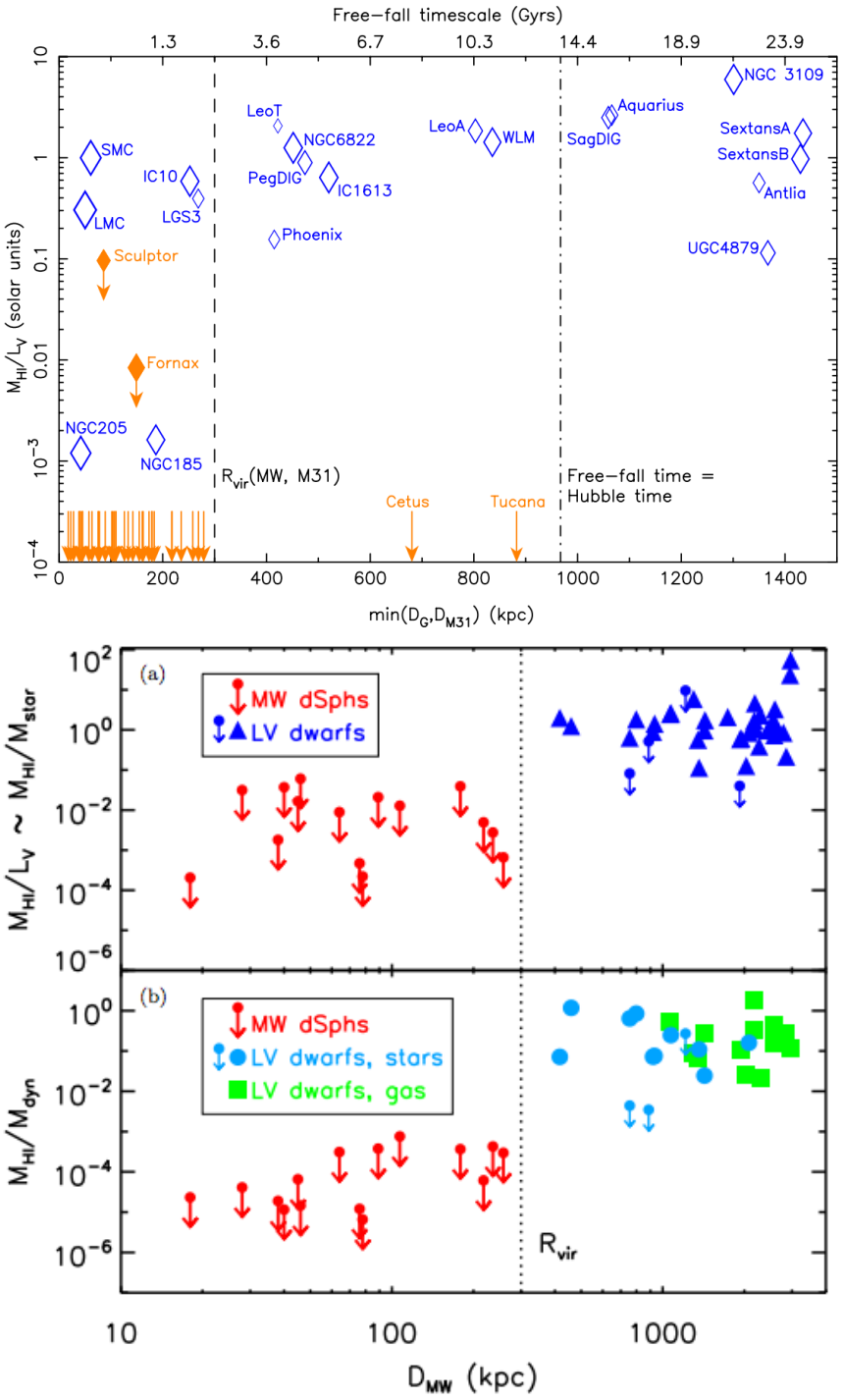

Figure 1.4 *Upper plot*: From McConnachie (2012), the distribution of nearby dwarf galaxies as a function of distance from the nearest large galaxy (Andromeda or the Milky Way). The neutral hydrogen content is shown (blue diamonds) or given as an upper limit for those without a detection (orange arrows). *Lower plot*: From Spekkens et al. (2014), the upper panel shows the HI mass (or upper limit to the HI mass) relative to the V band luminosity. The lower panel shows the HI mass (or limit) relative the the dynamical mass computed using stellar kinematics for the spheroidal and dwarfs shown in blue, or using HI kinematics for the dwarfs shown in green.

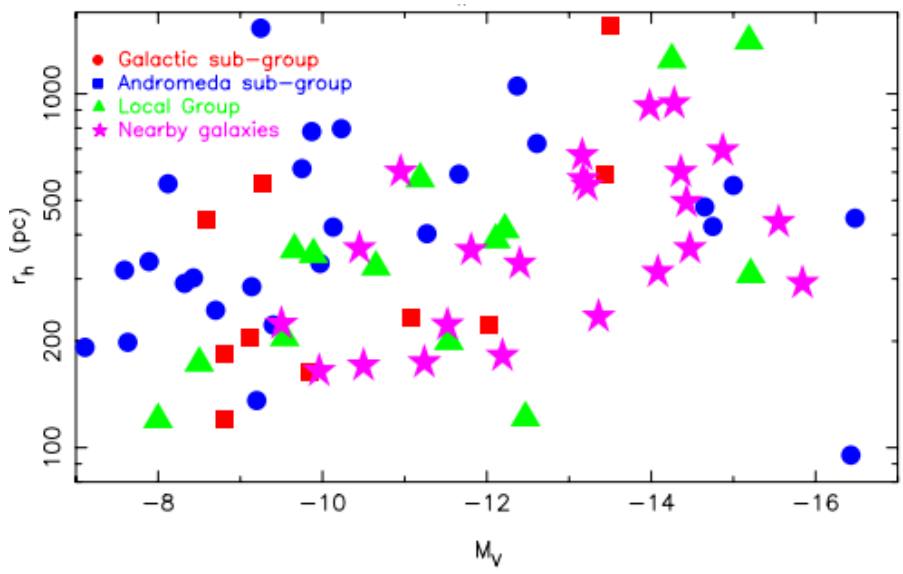

Figure 1.5 From McConnachie (2012), showing the effective radius of nearby dwarfs in comparison to their absolute magnitude. The different populations, Andromeda (M31) satellites, Milky Way satellites and more isolated dwarfs, are distinguished from each other.

As well as differences between dwarfs within and beyond the Milky Way virial radius, there are also potential differences identified between the M31 dwarf population and the Milky Way dwarf population. McConnachie & Irwin (2006), found that for a given mass, the characteristic size of dwarfs around M31 is about twice the size of those around the Milky Way. However, with new observations and discoveries, Brasseur et al. (2011) find that there is no statistical difference between the two populations. McConnachie (2012) summarizes with all new observations in Figure 1.5. While the two populations are not statistically different at a significant level, it is clear that the most extended satellites do generally belong to M31.

It is also interesting to note in 1.5 that there is large scatter in the relation between total absolute magnitude and size. There is a clear correlation between these two parameters for brighter galaxies, noted in Kormendy (1985) as discussed previously. However, for these nearby faint galaxies, there is only a very weak correlation between luminosity and size (at a given luminosity, dwarf could have a large range in scale-size).

Whether dwarfs are in fact distinct from larger galaxies is not clear; Ferrarese et al. (2006) (and references therein) suggest that they are simply different ends of

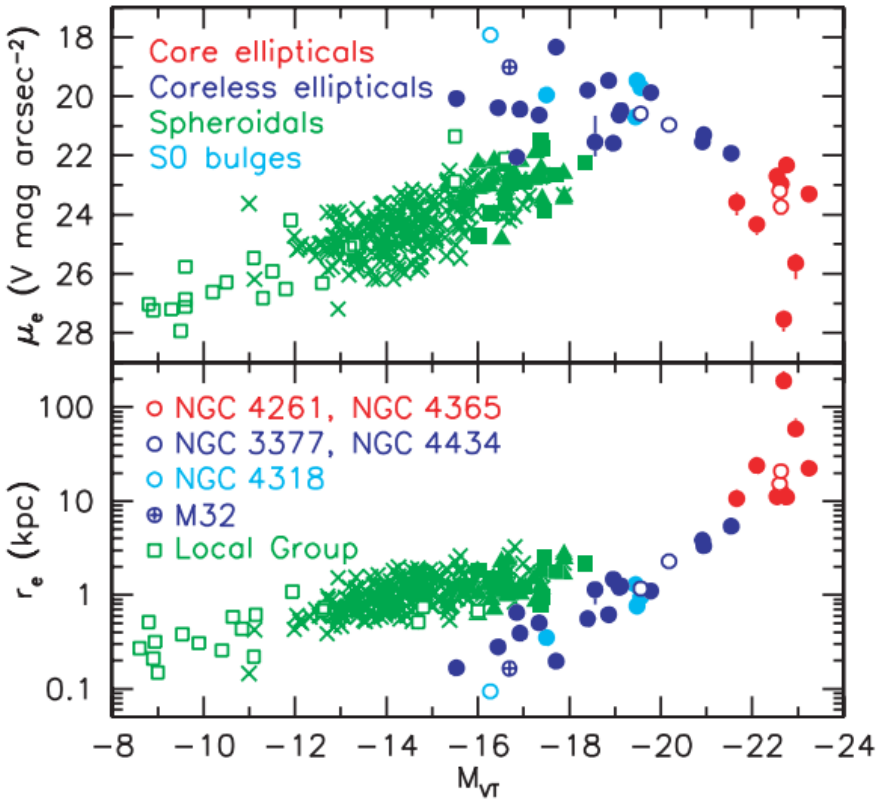

Figure 1.6 From Kormendy et al. (2009), the relationship between total absolute V band magnitude and surface brightness is shown for dwarf spheroidals, and their larger counterparts.

the same sequence. It is certainly true that the evolutionary history of dwarfs may be more varied, they may be the result of galaxy interactions leaving a remnant or a stripped bulge. Furthermore, if we consider hierarchical growth, a dwarf is likely the product of fewer interactions and so each SFH may be more influential, so we might expect to see more scatter within this relationship between scale-size and total luminosity in contrast to larger galaxies. Indeed, in Figure 1.5, we do see substantial scatter.

Overall is clear that the characteristics of the nearby dwarf galaxy population are dependent on multiple variables including intrinsic properties such as their stellar mass and environmental properties such as their location relative to large galaxies. We now discuss these various processes in detail.

1.3 Galaxy Evolution

The evolution of a galaxy is shaped by various factors, some internal, others external. The impact of different factors can vary depending on the size and mass of the galaxy. Due to their small size, dwarf galaxies are particularly sensitive to these factors.

The following sections describe the processes which form and reshape galaxies, divided broadly into internal and external effects. This division is not always definitive (as there is often an external stimulus for an internal process). The two sections are intended to separate those effects which can influence a galaxy in isolation as compared to those which involve interactions with a second galaxy or galaxy group.

1.3.1 External Processes

Galaxy mergers clearly play a large role in re-shaping a galaxy, with galaxy formation occurring via a series of mergers (hierarchical galaxy formation). Interactions are known to increase star formation (e.g. Scudder et al. 2012) which will clearly change stellar populations within the galaxy. Figure 1.7 from Scudder et al. (2012) shows the change in star formation in matched pairs of galaxies in the SDSS. Galaxies with a companion are seen to have enhanced rates of star formation out to large radii. It is interesting to note that even pairs with large separations still show an increase in star formation, and this change is not restricted to presently merging pairs. The impact of star formation is discussed in Subsection 1.3.2.

Dwarf galaxies which are satellites to a larger host galaxy are effected by their close proximity to a larger galaxy. As shown previously in Figure 1.4, the gas content, and hence morphological type of dwarf, is dependent on distance from the host. A key study by Geha et al. (2012) (and a more recent version by Bradford et al. 2015) using dwarfs identified in the SDSS has shown that the influence of a host galaxy can be detected in the average properties of dwarf galaxies out to a distance of some 1.5 Mpc from the host, shown in Figure 1.8. Contrary to the results of Scudder et al. (2012), they find star formation is reduced in dwarfs near a companion. Furthermore, Geha et al. (2012) shows that quenched dwarf galaxies rarely exist in isolation, that is, quenched dwarfs are always satellites. Geha et al. (2012) suggests a minimum mass for which a galaxy can quench itself isolation, with this mass marking the point below which it is unable to maintain a hot gaseous halo. This gaseous halo is necessary to suppress star formation. Isolated dwarf galaxies are unable to maintain this halo, and therefore cannot quench their star formation, which instead requires interactions to

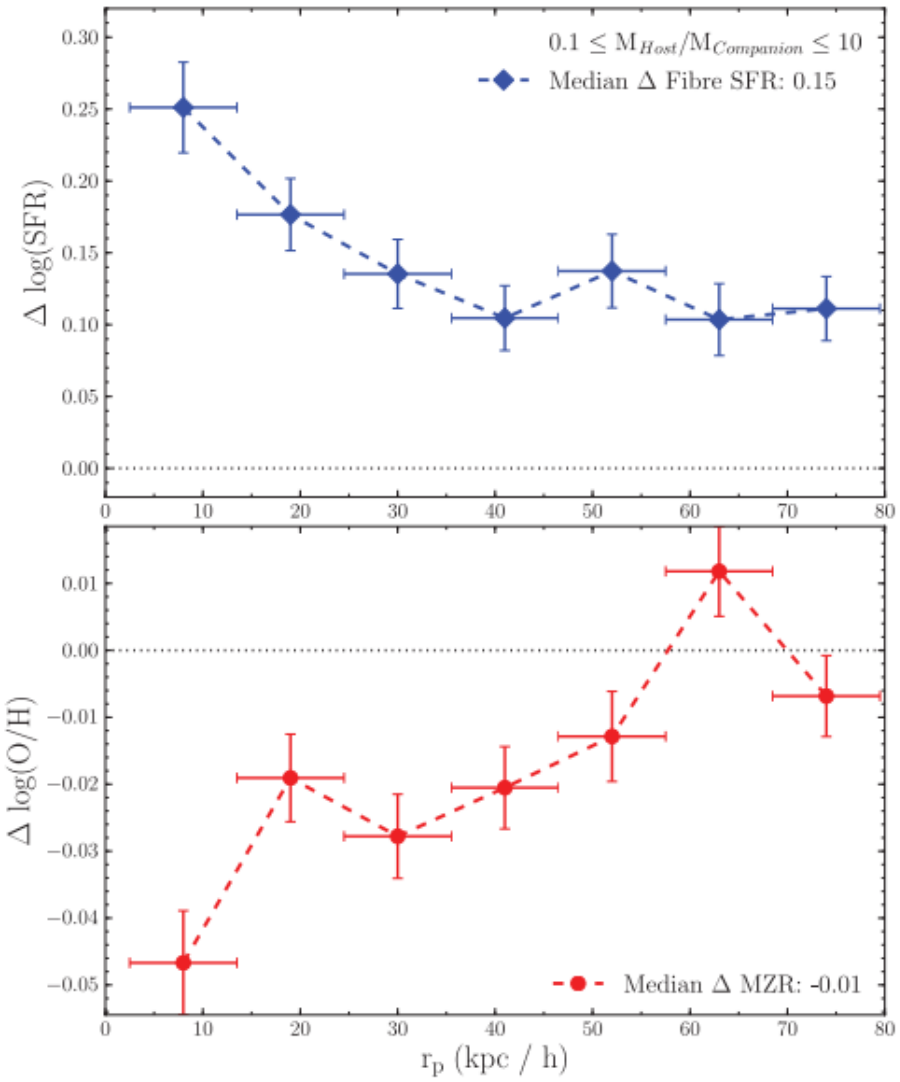

Figure 1.7 From Scudder et al. (2012), the upper panel shows that star formation is enhanced in galaxies with a companion relative to those isolated out to separations of about 80 kpc.

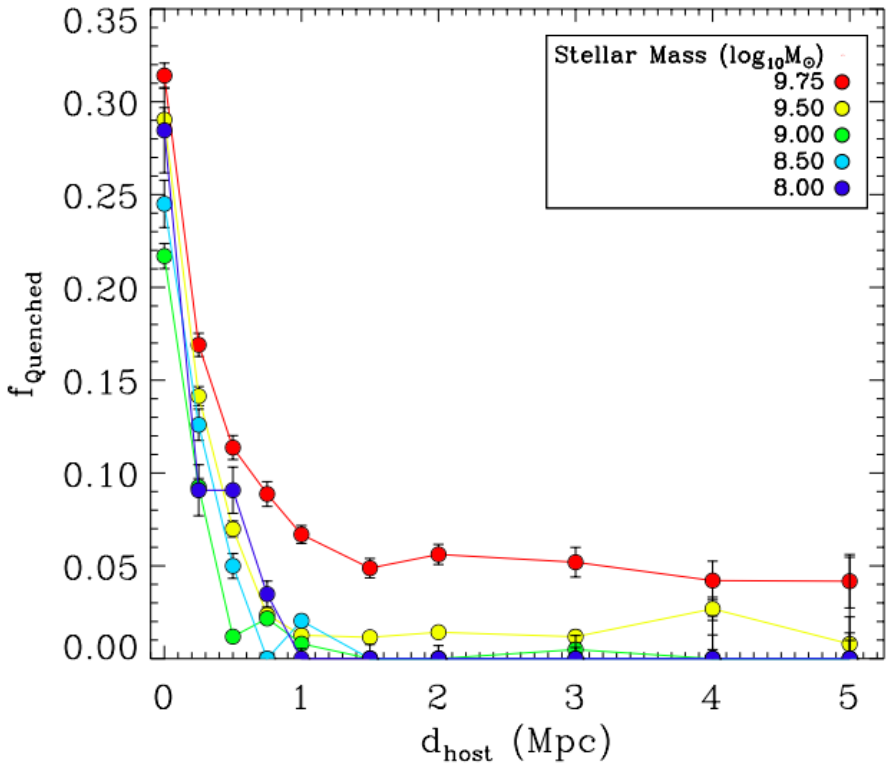

Figure 1.8 From Geha et al. (2012), we see there is quenching of star formations for all galaxies at small separations. At larger separations, no quenched dwarfs are observed below a mass threshold.

remove their gas supply and so stop star formation.

The proximity of a large galaxy can also introduce more subtle effects in the properties of the smaller satellite. For example, interactions could lead to disk instabilities in the satellite and produce warping. In the right circumstances, rotationally supported systems could be transformed into pressure supported systems (Mayer et al., 2006). Interactions may also trigger star formation if there is gas still present in the dwarf (particularly at pericenter), but conversely could also prevent the dwarf from accreting new gas to replenish its supply, thus leading to the eventual termination of star formation, so called "strangulation". Kawata & Mulchaey (2008) demonstrate using simulations that the hot gas can be removed, which limits the future supply of cold gas and effectively halts star formation.

Ram pressure stripping is the removal of gas from a galaxy by hot gas in an intra cluster medium or dense environment. There are numerous examples of galaxies

undergoing ram-pressure stripping due to interactions in cluster-like environments (e.g., NGC4522 in the Virgo cluster, Vollmer et al. 2000; Peg DIG in the Local Group, McConnachie et al. 2007b; see also Boselli & Gavazzi 2014). Gas can also be removed via tidal stripping, for which there are some well known examples. The Sagittarius dwarf spheroidal galaxy (Ibata et al. 1994) which has an enormous stellar stream spanning the entire sky that reveals its interaction history with the Milky Way (Ibata et al. 2001; Majewski et al. 2003 and references therein).

It has been proposed that ram pressure stripping by a hot gaseous halo surrounding a large galaxy, perhaps working in concert with tidal effects such as stripping and stirring, could remove the gas from a dwarf-irregular type galaxy and transform it to a dwarf spheroidal galaxy (in particular, see the models by Mayer et al. 2006 and collaborators). Certainly, the results of Geha et al. (2012) and the Local Group position-morphology relation suggest that stripping processes must occur.

The net result of a large body of work is a demonstration that the morphological, dynamical, star forming and chemical evolutionary status of dwarf galaxies can be severely affected by proximity to large galaxies. However, many of the "symptoms" of interactions are not unique and indeed may also be explained via secular processes, which we now discuss.

1.3.2 Internal Processes

Star formation rate (SFR) obviously changes the stellar populations present in a galaxy. While it is considered an internal process, it is linked to external factors, such as galaxy interaction or mergers, which can trigger a burst of star formation, as discussed above in Subsection 1.3.1. The presence of gas is necessary for star formation, and in turn, gas within a galaxy is heavily influenced by star formation.

The existence of feedback from supernovae in all galaxies is clear from abundance studies; that is, younger population are, in general, more metal rich as the interstellar medium is enriched by previous generations of stars. The coupling between the energy released in a supernova and the surrounding gas is not well defined, as discussed in Abadi et al. (2003) for example. In a dwarf galaxy, which has shallower potential well, gas could be lost from a low mass galaxy due to feedback from supernovae (Dekel & Silk 1986; Dekel & Woo 2003). A clear understanding of the gas content of a dwarf along with its star formation history can therefore aid in defining the effectiveness of feedback. It should also be noted that stellar feedback has recently been proposed as

a means to turn a cuspy dark matter halo profile into a cored profile (Teyssier et al. 2013). Work by Di Cintio et al. (2014) suggests that there is an ideal mass range for which stellar feedback can reshape the halo profile (see Di Cintio et al. 2014). If the galaxy is more massive, stellar feedback is not capable of significantly reshaping the dark matter halo. Dwarfs, like Aquarius and Sag DIG, lie in the mass range for which cusps are expected to survive, as seen in simulations like those of Governato et al. (2012).

Feedback for active galactic nuclei (AGN) can also significantly reshape a galaxy. For example, Ishibashi & Fabian (2012) simulate how AGN may change the star formation rate within a galaxy, causing star formation at larger radii due to an expanding feedback driven shell. While important for larger galaxies, AGN are not a consideration for the dwarf population since there is no evidence that dwarfs host supermassive black holes.

1.4 Summary

The vast majority of our nearest, neighbouring galaxies that are accessible for resolved stellar analysis are dwarf galaxies. These small galaxies are thought to be the building blocks of our own through hierarchical galaxy formation. Dwarf galaxies are a challenging regime for dark matter simulations and provide a unique test of the prevailing cosmological paradigm on small scales. It is therefore important to characterize the nearby populations of dwarfs, including both satellites and isolated dwarfs, to better understand their properties and so start to untangle the evolutionary processes governing galaxy formation by separating secular processes from environmentally-driven ones. Whereas the satellite populations of the Milky Way and M31 have been well studied, this is not the case for the nearby isolated dwarf galaxies.

Here, we present the first result from the *So*litary *Lo*cal Dwarfs Survey (*Solo*) which will cohesively study all isolated nearby (within 3Mpc) dwarfs for comparison to the satellite populations of the Milky Way and M31.

1.5 Agenda

Chapter 2 introduces the general *Solo* survey and explains the data acquisition and preliminary processing steps.

Chapter 3 summarizes the literature for the focus of this work, Sag DIG.

Chapter 4 examines the stellar populations of Sag DIG.

Chapter 5 goes in to detail about the low surface brightness structure of this dwarf.

Chapter 6 summarizes the results and discusses them in the context of other nearby dwarfs, as well as incorporating HI data and expanding on future work.

Chapter 7 concludes and discusses future work.

Chapter 2

The *Solo* Dwarfs

We have constructed the *Solo* (*So*litary *Loc*al) Dwarf Survey with the intent to provide homogeneous, high quality, wide field optical characterization of the closest, isolated dwarf galaxies whose resolved stellar content is accessible, at least in part, using current ground based facilities. Specifically, this survey uses wide field imaging from the Canada France Hawaii Telescope (CFHT) for northern targets, and the Magellan Telescope for southern targets. This sample constitutes all known isolated dwarf galaxies for which we can expect to obtain, now or in the near future, the most detailed perspectives on their structures, dynamics, star formation and chemical evolution that is of a comparable nature and quality to the Milky Way and M31 satellite galaxies. When viewed as a population, the *Solo* dwarfs are potentially a powerful benchmark for studies of the interplay between secular and environment-driven galaxy evolution at the low mass end. The *Solo* dwarfs are introduced in the following section, followed by details on the data acquisition and preliminary processing.

2.1 The Nearest Dwarfs

The *Solo* dwarf galaxies are selected from the compilation of dwarf galaxies presented in McConnachie (2012). Briefly, McConnachie (2012) presents all dwarf galaxies that have distance estimates based on measurements of resolved stellar populations (i.e., Cepheids, RR Lyrae, tip of the red giant branch, main sequence fitting) that place them within 3 Mpc of the Sun. A regularly updated version of this catalog is available online[1]. The distance threshold of 3 Mpc corresponds to the approximate distance

[1] http://www.astro.uvic.ca/∼alan/Nearby_Dwarf_Database.html

to the next nearest galaxy groups to the Local Group (Karachentsev 2005). More than 100 galaxies are known within 3 Mpc, with several discovered since the original publication of McConnachie (2012). The majority of these new discoveries are Milky Way satellites. However, two new isolated galaxies - KK258 and KKs3 - have also been "discovered" in the neighbourhood of the Local Group, as updated distances from HST have shown them to be closer than previously estimated (Karachentsev et al. 2014, 2015). This brings the total number of galaxies within 3 Mpc and lying beyond the nominal virial radii of the Milky Way and M31 (adopted to be 300 kpc, e.g., Klypin et al. 2002) to 42. Very recently, Eridanus 2 has been discovered in the Dark Energy Survey data (Koposov et al. 2015; Bechtol et al. 2015). Its distance is estimated to be $\sim$ 380 kpc using horizontal branch stars. These horizontal branch stars are near the magnitude limit of the observations, hence this distance is uncertain. Moreover DES identified 7 other candidates in Koposov et al. (2015) (also see Bechtol et al. 2015). Their distances, estimated by fitting the horizontal branch again, all put them much closer to the Milky Way, such that they'd be considered satellites rather than isolated dwarfs. However, with follow up observations, their locations may be revised and they may actually be more isolated. Also in DES data, Sand et al. (2015) find Antlia B, a new dwarf irregular located at a distance of 1.28 ± 0.02 Mpc, probably associated with NGC 3109. These new discoveries by Koposov et al. (2015); Karachentsev et al. (2014, 2015) and others highlight the incomplete nature of the faint end for galaxies and the challenges identifying these very low mass systems.

Figure 2.1 shows a projection of all the dwarf galaxies within 3 Mpc using the positions and distances given in McConnachie (2012). The isolated *Solo* sample (black points) is shown along with the satellites of M31 and the Milky Way (grey points).

For the purposes of this work, we consider any dwarf located within 300 kpc of either the Milky Way or M31 as a satellite, and any dwarf located beyond this threshold as isolated. All dwarfs meeting this latter criterion are considered part of the *Solo* survey. Considering Figure 1.4, this criteria is consistent with the separation from a host where the gas content and type of dwarf dramatically shifts. We recognize that this (semi-arbitrary) cut will not uniquely select galaxies that have never interacted with either the Milky Way or M31 (for example, see the study by Geha et al. 2012). It may include some dwarfs that are on very long period orbits, or "backsplash" galaxies that are at very large distances but which have had a previous pericentric passage with one of the two large bodies (e.g., Gill et al. 2005). Numerical simulations of Local Group environments are a particularly useful comparison to observational datasets in

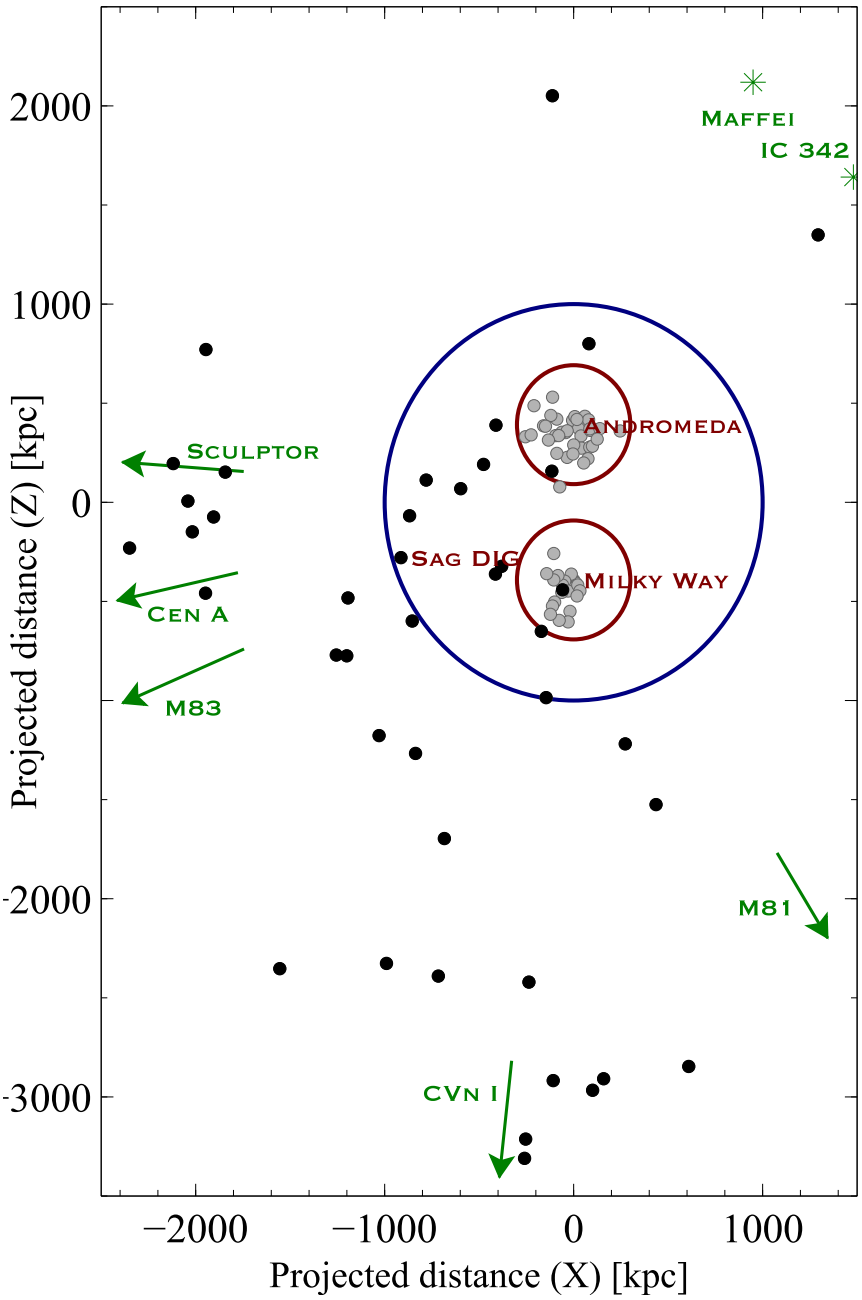

Figure 2.1 Projected distribution of dwarf galaxies within 3 Mpc, with M31 (Andromeda) and the Milky Way labelled. The projection is centered on the point halfway between the Milky Way and M31, with the y axis aligned with the M31 - Milky Way direction. Black points indicated isolated dwarfs in the *Solo* sample. Grey points are M31 and Milky Way satellites (defined to lie within 300 kpc of their host, indicated by the red circles). Green symbols indicate the positions or directions of the nearest galaxy groups to the Milky Way. The blue circle indicates the zero velocity surface (as determined by McConnachie 2012) of the Local Group.

understanding the orbital diversity of the dwarf population (e.g., Barber et al. 2014; Garrison-Kimmel et al. 2014). Timing arguments suggest that most galaxies located near the periphery of the Local Group or more distant will not have had time to have had a close interaction at any point in their history (McConnachie 2012). Table 2.1 lists all the dwarf galaxies in the *Solo* survey, along with their positions, current distance estimates, and relevant observational details.

All the galaxies listed in Table 2.1 are close enough to resolve their brighter stellar populations (at least in their outskirts) from the ground. Many of the closest targets in this list are reasonably well studied, particularly the members of the Local Group. However, a systematic, modern survey including more distant dwarfs is lacking. Arguably the most systematic study of a subset of these galaxies is Massey et al. (2006), who surveyed ten star forming galaxies to determine certain properties relating to star formation activity. Many of the more distant dwarfs listed in Table 2.1 are relatively poorly studied in the era of modern wide field CCD studies. An examination of the data tables in McConnachie (2012) reveal that many of the dwarfs' basic properties are derived from the Third Reference Catalog survey by de Vaucouleurs et al. (1991), and a homogeneous wide field study of the entire sample has not occurred recently. Of course, there are notable programs that have focused on other aspects of the properties of these systems. For example, Dalcanton et al. (2009) have studied many nearby targets using HST/ACS and WFPC2. Alternatively, Local Cosmology from Isolated Dwarfs (LCID) survey studied six isolate dwarfs with HST as well, as outlined in Bernard et al. (2008) among others. HST is ideal for studying the resolved stars in the centers of the galaxies, but its limited field of view makes it less ideal for wide-field structural and stellar content studies. *Solo* is clearly complementary to this space-based program due its wide field imaging. Overall, the lack of a systematic, homogeneous wide field study of these galaxies means that their basic data may still be uncertain. For example, the total luminosity of the nearby Phoenix dwarf (van de Rydt et al. 1991) is based on imaging that covers only part of the galaxy, and no direct measurement was ever made of the integrated light in the image.

2.2 Data Acquisition

The *Solo* dwarfs have been observed with CFHT/MegaCam for mostly (but not exclusively) northern targets, and Magellan/Megacam for (most of) the southern targets, detailed in Table 2.1. CFHT/MegaCam is an array of 40 individual 2048 $\times$ 4612

Table 2.1 The *Solo* dwarfs. In the "Tel." (Telescope) column, "C" indicates observations with CFHT/MegaCam, and "M" indicates observations with Magellan/Megacam. Distance estimates are from the updated compilation by McConnachie (2012). $E(B-V)$ estimates are from the Schlafly & Finkbeiner (2011) dust maps along the line of sight to the center of the galaxy.

Name	RA	Dec.	Distance [kpc]	$E(B-V)$ [Mags.]	Tel.	Filters	Notes
Complete data							
WLM	$00^h01^m58.2^s$	$-15^o27'39"$	933 ± 34	0.04	M	*gi*	2014B
					C	*g*	2013B
AndXVIII	$00^h02^m14.5^s$	$+45^o05'20"$	1355 ± 81	0.10	C	*gi*	PAndAS data
ESO410-G005	$00^h15^m31.6^s$	$-32^o10'48"$	1923 ± 35	0.01	M	*ugi*	2012B
Cetus	$00^h26^m11.0^s$	$-11^o02'40"$	755 ± 24	0.03	M	*gi*	2014B
ESO294-G010	$00^h26^m33.4^s$	$-41^o51'19"$	2032 ± 37	0.01	M	g i	2014B
IC1613	$01^h04^m47.8^s$	$+02^o07'04"$	755 ± 42	0.03	M	*ugi*	2012B
HIZSS3A(B)	$07^h00^m29.3^s$	$-04^o12'30"$	1675 ± 108	0.69	M	*ugi*	2012A
					C	*g*	2012A
NGC3109	$10^h03^m06.9^s$	$-26^o09'35"$	1300 ± 48	0.07	M	*ugi*	2012A
Antlia	$10^h04^m04.1^s$	$-27^o19'52"$	1349 ± 62	0.08	M	*gi*	2015A, IMACS
SextansA	$10^h11^m00.8^s$	$-04^o41'34"$	1432 ± 53	0.05	M	*ugi*	2012A
LeoP	$10^h21^m45.1^s$	$+18^o05'17"$	1620 ± 150	0.03	C	*gi*	2014A
IC3104	$12^h18^m46.0^s$	$-79^o43'34"$	2270 ± 188	0.30	M	*ugi*	2012A
GR8	$12^h58^m40.4^s$	$+14^o13'03"$	2178 ± 120	0.03	M	*gi*	2015A, IMACS
KKH86	$13^h54^m33.5^s$	$+04^o14'35"$	2590 ± 190	0.03	M	*ugi*	2012A
DDO190	$14^h24^m43.4^s$	$+44^o31'33"$	2790 ± 93	0.01	C	*gi*	2014A
KKR25	$16^h13^m48.0^s$	$+54^o22'16"$	1905 ± 61	0.01	C	*gi*	2014A
Sag DIG	$19^h29^m59.0^s$	$-17^o40'41"$	1067 ± 88	0.12	C	*ugi*	2012B, 2013A
NGC6822	$19^h44^m56.6^s$	$-14^o47'21"$	459 ± 17	0.19	C	*ugi*	2013A
Phoenix	$19^h44^m56.6^s$	$-14^o47'21"$	415 ± 19	0.02	M	*ugi*	2012B
DDO210	$20^h46^m51.8^s$	$-12^o50'53"$	1072 ± 39	0.05	M	*ugi*	2012B
					C	*ugi*	2013A
IC5152	$22^h02^m41.5^s$	$-51^o17'47"$	1950 ± 45	0.03	M	*ugi*	2012B
AndXXVIII	$22^h32^m41.2^s$	$+31^o12'58"$	661^{+152}_{-61}	0.09	C	*ugi*	2012A, 2013A
Tucana	$22^h41^m49.6^s$	$-64^o25'10"$	887 ± 49	0.03	M	*ugi*	2012B
UKS2323-326	$23^h26^m27.5^s$	$-32^o23'20"$	2208 ± 92	0.01	M	*ugi*	2012B
Peg DIG	$23^h28^m36.3^s$	$+14^o44'35"$	920 ± 30	0.07	C	*ugi*	2012B, 2013A
KKH98	$23^h45^m34.0^s$	$+38^o43'04"$	2523 ± 105	0.12	C	*ugi*	2013A
Incomplete data							
UGCA86	$03^h59^m48.3^s$	$+67^o08'19"$	2960 ± 232	0.65	C	*g*	2012B
DDO99	$11^h50^m53.0^s$	$+38^o52'49"$	2590 ± 167	0.03	C	*i*	2014A
DDO113	$12^h14^m57.9^s$	$+36^o13'08"$	2950 ± 82	0.02	C	*g*	2014A
UGC8508	$13^h30^m44.4^s$	$+54^o54'36"$	2580 ± 36	0.02	C	*g*	2014A
KKR3	$14^h07^m10.5^s$	$+35^o03'37"$	2188 ± 121	0.01	C	*g*	2014A
UGC9128	$14^h25^m56.5^s$	$+23^o03'19"$	2291 ± 42	0.02	C	*g*	2014A
Data pending							
KKs3	$02^h24^m44.4^s$	$-73^o30'51"$	2120 ± 70	0.05			
Perseus	$03^h01^m22.8^s$	$+40^o59'17"$	785 ± 65	0.12			
UGC4879	$09^h16^m02.2^s$	$+52^o50'24"$	1361 ± 25	0.02			
LeoT	$09^h34^m53.4^s$	$+17^o03'05"$	417 ± 19	0.03			
LeoA	$09^h59^m26.5^s$	$+30^o44'47"$	798 ± 44	0.02			
SextansB	$10^h00^m00.1^s$	$+05^o19'56"$	1426 ± 20	0.03			
NGC4163	$12^h12^m09.1^s$	$+36^o10'09"$	2860 ± 39	0.02			
DDO125	$12^h27^m40.9^s$	$+43^o29'44"$	2580 ± 59	0.02			
IC4662	$17^h47^m08.8^s$	$-64^o38'30"$	2440 ± 191	0.07			
KK258	$22^h40^m43.9^s$	$-30^o47'59"$	2230 ± 50	0.01			

pixel CCDs arranged in a $9(11) \times 4$ grid (where the middle 2 rows have 11 CCDs, and the outer 2 rows have 9 CCDs) with a pixel scale of 0.187 arcsecs/pixel, mounted at the prime focus of the 3.6m CFHT on the summit of Mauna Kea. Prior to the 2015A semester, only the central 36 CCDs were in use for science observations, resulting in a rectangular, 0.96×0.94 degree field of view. Magellan/Megacam is an array of 36 individual 2048×4608 pixel CCDs arranged in a 9×4 grid with a pixel scale of 0.08 arcsecs/pixel, mounted at the Cassegrain focus of the 6.5m Clay telescope at the Las Campanas Observatory. The resulting field of view is 25×25 arcmins. In general, we usually observe a single field with CFHT/MegaCam centered on the target, whereas we try to observe multiple (usually 4) fields to tile the target with Magellan/Megacam to compensate for the smaller field of view. We note that it is a convenient coincidence that the difference in apertures between the telescopes roughly compensates for the difference in field of view between the cameras.

Observations were primarily made in the g and i filters in both hemispheres, with some targets also observed in u with lower priority. Some equatorial targets are observed with both telescopes in order to provide transformations between the CFHT and Magellan photometric systems and to ensure a uniform calibration of the dataset, as indicated in Table 2.1.

CFHT/MegaCam is a queue scheduled instrument, and therefore our observing conditions and strategy are very uniform. We observe for $\sim$ 450s in g and $\sim$ 900s in i per field, usually with $\sim$ 4 fields per target. For those targets that have u band data, our exposures were generally of order 360s. The uniform exposure time adopted for targets at considerably different distances results in varying depths of resolved star analysis. Considerably fainter stellar populations will be reached for the closest galaxies than for the most distant galaxies. This approach is optimal given the very large amount of time that is otherwise required to push to fainter stellar populations for the most distant targets, where crowding will limit the regions in which we can conduct the resolved star analysis anyway. Magellan/MegaCam is a classically-scheduled instrument, and as such our targets were observed over a broader range of conditions and with some variation in observing time. Generally, we observe in dark time and typically have better than 1 arcsecond image quality. Our data processing is generally the same for each galaxy, with some slight modifications depending on any individual peculiarities of the target, pointing or conditions. For the Sagittarius dwarf irregular galaxy (Sag DIG) CFHT/MegaCam data analyzed here, the image processing steps were similar to those followed by Richardson et al.

(2011). Data were preprocessed by the Elixir system at CFHT, including de-biasing, flat-fielding and fringe-correcting the i band data in addition to determining the photometric zero-points. The data were then transferred to Cambridge Astronomical Survey Unit where the overscan region was first trimmed off, then all images and calibration frames were run through a variant of the data reduction pipeline originally developed for processing Wide Field Camera (WFC) data from the Isaac Newton Telescope (INT). For further details, see Irwin (1985, 1997), Irwin & Lewis (2001) and Irwin et al. (2004).

Prior to deep stacking, catalogues were generated for each individual processed science image to further refine the astrometric calibration and also to assess the data quality. For astrometric calibration, a Zenithal polynomial projection (Greisen & Calabretta 2002) was used to define the World Coordinate System (WCS). A fifth-order polynomial includes all the significant telescope radial field distortions leaving just a six-parameter linear model per detector to completely define the required astrometric transformations. The Two Micron All Sky Survey (2MASS) point-source catalogue (Cutri et al. 2003) was used for the astrometric reference system.

Quality control assessment for each exposure was based on the average seeing and ellipticity of stellar images, together with the sky level and sky noise, all determined from the object catalogues. During the stacking process, the individual catalogues from each MegaCam image were used, in addition to the standard WCS solution. The images were aligned with to a sub-pixel level for the stacked images. The common background regions in the overlap area from each image in the stack were used to compensate for sky variations during the exposure sequence and the final stacks for each band included seeing weighting, confidence (i.e. variance) map weighting and clipping of cosmic rays.

As a final image processing step, catalogues were derived from the deep stacks for each detector and their WCS astrometry was updated. All objects detected in the catalogues are morphologically classified (stellar, non-stellar, noise-like) before creating the final band-merged g and i products. The classification is done using a ratio of fluxes within apertures around each source. This ratio determines how point like or extended the source appears. Using the ratio, stellar (point like) sources are distinguished from background extended sources or cosmic rays. In the final catalogue, each source is classified, with stellar objects in two classes (1σ and 2σ) on how star-like they are. The catalogues provide additional quality control information and the classification step also computes the aperture corrections required to place

the photometry on an absolute scale. The g and i catalogues for each field are then combined to form an overall single entry g, i catalogue for each detected object. In this process, objects lying within 1 arcsec of each other are taken to be the same and the entry with the higher signal-to-noise measure is retained. Objects present only on g or i are retained throughout this process.

In the following, unless otherwise stated, the magnitudes are presented in their natural instrumental (AB) system with reddening corrections derived star by star from the Schlegel et al. (1998) dust extinction maps combined with the Schlafly & Finkbeiner (2011) extinction coefficients for the g,i bands. We use the following correction coefficients: $g_o = g - 3.793E(B-V)$ and $i_o = i - 2.086E(B-V)$ (Schlegel et al. 1998).

2.3 Summary

The *Solo* Dwarf Survey has been designed to untangle internal and external factors in galaxy evolution. The dwarfs are selected to be near enough such that individual stars can be resolved in the majority of the galaxy, while the dwarfs are required to be far enough away from both the Milky Way and M31 such that an interaction is unlikely. This sample uses g and i (and some with u) band imaging from CFHT MegaCam and Magellan Megacam, both with approximately 1 square degree field of view. In the next section, we will focus on one specific dwarf from the survey, the Sagittarius Dwarf Irregular Galaxy.

Chapter 3

The Sagittarius Dwarf Irregular Galaxy

We now turn our attention to the first galaxy analyzed as part of this program, the Sagittarius Dwarf Irregular Galaxy (Sag DIG). Sag DIG is located near the zero velocity surface of the Local Group, where the gravitational attraction of the Local Group is balanced by the local Hubble flow. McConnachie (2012) estimate that its free-fall timescale to either the MW or M31 is of order the age of the Universe, hence interactions with these systems seem improbable. The free-fall time scale is the estimated time for a dwarf to reach its host galaxy if it starts at rest from its current separation and the only force acting upon it is the gravitational attraction from the host. If this time scale is short, a dwarf would likely have interacted with the host previously. In Sag DIG's case, the long time scale makes it highly unlikely to have had a previous encounter with its host.

The closest known galaxy to Sag DIG is the low mass Aquarius dwarf galaxy (DDO210), still some 300 – 400 Kpc away from Sag DIG. We compare the characteristics of theses two isolated dwarfs, Aquarius and Sag DIG, in Chapter 6.

Sag DIG (also known as UKS 1927-177) is an ideal candidate for the primary target to study from the *Solo* Survey. Relative to other dwarfs in the survey, it is quite large and bright, with a distinct old population, making our analysis more simple. As summarized in this chapter, previous work on this dwarf provides a solid comparison to validate and confirm analysis methods used. Despite its proximity, we are limited to only the brighter stars within the dwarf, as we will be with majority of the *Solo* dwarfs. We will not be able to observe features such as the main sequence turn off

for any of these isolated dwarfs. Like most dwarfs in the survey, Sag DIG is a dwarf irregular galaxy, containing a variety of stellar populations and a significant gaseous component, like the majority of isolated dwarfs. Sag DIG does have some more challenging aspects compared to other targets due to heavy foreground contamination as it lies at a low galactic latitude.

3.1 Introducing Sag DIG

The CFHT/ MegaCam of Sag DIG was processed as described in the previous section, and Figure 3.1 shows the processed i band MegaCam image. An enlarged g, i composite image of the central 6' by 6' region is also shown. Also overlaid in Figure 3.1 are HI gas contours from the LITTLE THINGS survey (Hunter et al. 2012). The green dashed line indicates the HST ACS field of view studied by Momany et al. (2005) and discussed later.

Figure 3.1 clearly shows blue stars visible in the center of the object, with fainter, redder stars more widely distributed. The HI contours show that there is extensive gas present within this dwarf, and the blue stars are indicative of recent star formation. As a result, Sag DIG is classified as a dwarf irregular system. Numerous, often saturated, foreground Milky Way stars are obvious across the entire field of view, and reflects that fact that Sag DIG is located at moderately low Galactic latitude ($b = -16.3°$). Saturation spikes and "halos" generated by internal reflections within the MegaCam instrument are also visible around the brightest stars.

3.2 Previous Observations of Sag DIG

3.2.1 Discovery

It was discovered by Cesarsky et al. (1977) on photographic plates obtained with the ESO Schdmidt telescope, and then studied further with the ESO 3.6m and the Nançay radio telescope. Young blue stars were observed, as well as 21cm detections of neutral hydrogen, leading to its classification as a dwarf irregular. The optical body of Sag DIG was noted to have a roughly elliptical shape, with approximate dimensions of 2.5' by 5'. Cesarsky et al. (1977) estimated its distance to be similar to that of NGC 6822 due to their close angular separation on the sky and similar heliocentric velocities (-58 $\pm$ 5 km s^{-1} for Sag DIG as compared to 57 km s^{-1} for

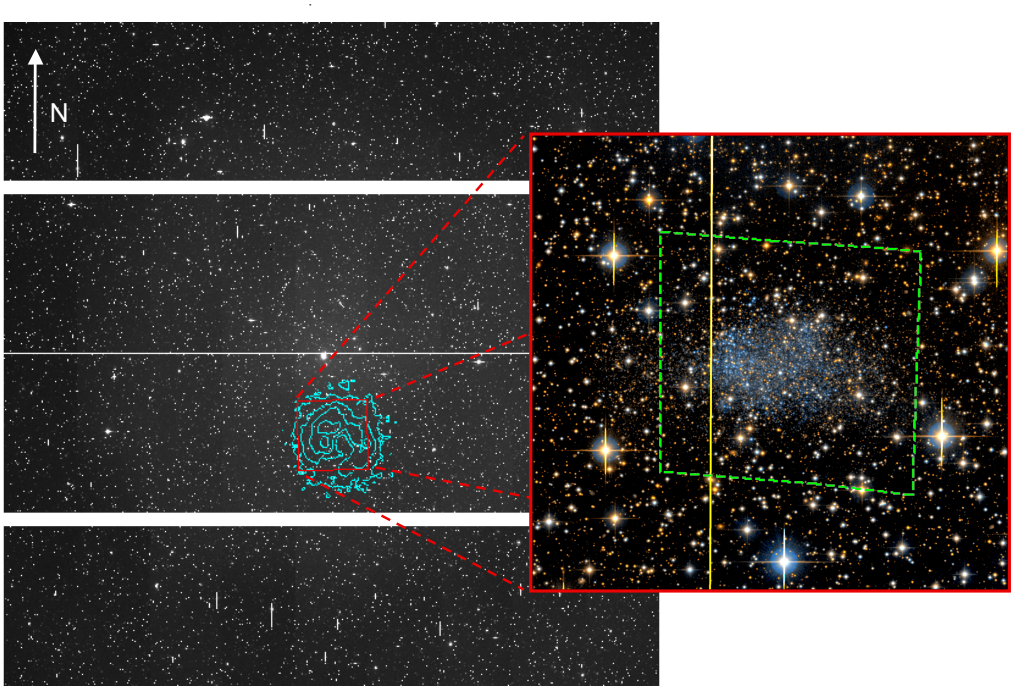

Figure 3.1 Processed i band CFHT/MegaCam image, showing the full 1° by 1° field of view, oriented with north upward, east left. Overlaid blue contours show the HI distribution from LITTLE THINGS (Hunter et al. 2012), with contours at 10, 50, 100, 250, 500 (Jy/beam)(m/s). The inner 6' by 6' region is shown in the composite g and i band image, with the green dashed box indicating the HST ACS observations analyzed by Momany et al. (2005).

NGC 6822). A more precise estimate of its distance modulus was made by comparison of its brightest blue stars to those in Sculptor and Phoenix, resulting in an estimate of $(m - M)_{AB} = 25 \pm 1$. With this estimate distance, $M(HI)/L_B = 4.5 M_\odot/L_\odot$, noted to be very high, particularly since, at the time of its discovery, Sag DIG was one of the smallest and faintest galaxies.

3.2.2 Gas in Sag DIG

Subsequent observations by Longmore et al. (1978) observed the neutral hydrogen with the Parkes 64m Telescope and broadly confirmed the findings of Cesarsky et al. (1977). The distance was estimated to be 1.1 ± 0.5 Mpc from the method outlined in Sandage & Tammann (1976), which uses the three brightest stars and the total apparent luminosity. No resolved HII regions were detected, and the high $M(HI)/L_B$ ratio was confirmed. Longmore et al. (1978), in agreement with Cesarsky et al. (1977), described this dwarf as a very low mass system which has undergone a recent burst of star formation.

Although Longmore et al. (1978) was originally unable to detect any HII, Skillman et al. (1989) obtained optical long slit spectra of two compact and one extended HII source. These observations were based on an Hα map obtain while Hodge et al. (1988) observed the nearby galaxy NGC 6822. The compact sources were Galactic in origin while the extended source belongs to Sag DIG. The oxygen abundance was determined to be about 3% of Solar. This value in in general agreement with the luminosity – abundance relationship for such a faint system. At the time, Sag DIG was the lowest luminosity irregular galaxy with a measured abundance. Strobel et al. (1991) extend on the HII regions in Sag DIG and other dwarf irregulars using CCD Hα observations from the Kitt Peak National Observatory. Across their sample of seven dwarf irregulars, there is a similar morphology for all the HII regions. Strobel et al. (1991) go on to use Sag DIG and the other galaxies in their sample to tentatively suggest a relationship between the size of HII region and the absolute magnitude of the parent galaxy (with the characteristic size of the regions being larger in fainter galaxies). More recently Saviane et al. (2002) study O, N, Ne abundances in the brightest HII region of Sag DIG, finding $12+log(O/H) = 7.26$ to 7.50 and establishing Sag DIG's very low oxygen abundance. The aim of this paper was to show that Sag DIG, with an old population, can be metal poor, even with on going star formation. That is, metal poor systems are not necessarily "young". Sag DIG is extremely metal

poor, but the presence of a very old population was not confirmed.

A more recent study of the HI content of Sag DIG was conducted by Lo et al. (1993) using VLA observations to study in detail a total of 9 dwarf irregulars including Sag DIG. The HI was noted as being more extended than the stars and having a large crescent shape, in contrast to the very regular, elliptical, optical image of Sag DIG. In all the dwarves studied by Lo et al. (1993) including Sag DIG, the HI is clumpy and not well described as belong to a thin, disk-like structure as is often found in more luminous galaxies; pressure support is generally more important than rotational support for these low mass systems. These observations are supported by Young & Lo (1997), which obtains VLA and single dish observations of Sag DIG. No systematic rotation is observed, making it hard to estimate the mass of the galaxy. The HI gas is found to have two components, one with a broad velocity dispersion of 10 km s^{-1} distributed throughout the galaxy and a narrow component with a velocity dispersion of 5 km s^{-1} found in clumps with masses on the order of $8\times10^5 M_\odot$. Young & Lo (1997) also present a more detailed comparison between the stellar and HI features. They estimate that the HI is about three times more extended than the stellar component, and that the HI clumps do not correlate with any features in the stellar distribution. However, the position of one of the HI clumps correlates well with the previously identified HII region, suggesting it is potentially a star forming region. Young & Lo (1997) also considers timescales for the collapse of the HI gas, considering that it is not rotationally supported, and suggest that magnetized turbulence is a plausible explanation to help support the gas and prevent more rapid collapse. Much of the structure of the gas discussed by these authors is visible in the LITTLE THINGS HI map (Hunter et al. 2012) of Sag DIG overlaid on Figure 3.1.

3.2.3 Photometric Analysis

Karachentsev et al. (1999) obtained resolved stellar photometry in the V and I bands for Sag DIG. An updated distance modulus is found using the tip of the RGB to be $(m-M)_o = 25.13 \pm 0.2$, corresponding to 1.06 ± 0.10 Mpc and placing Sag DIG on the edge of the Local Group. Sag DIG's low metallicity is confirmed by Karachentsev et al. (1999) using the calibration of the RGB color as done for globular clusters. They find a mean metallicity is [Fe/H]$=-2.45 \pm 0.25$ dex. which is more metal poor than the estimate of 3% of Solar from Skillman et al. (1989), but is consistent given that the two estimates are probing different ages in the galaxy. Karachentsev et al. (1999)

find an exponential scale length of 27."1, a central surface brightness of $\mu_V = 23.9$ mag. arcsec^{-2} and an absolute magnitude of $M_V = -11.74$. The star formation history is estimated by generating a synthetic CMD, showing that Sag DIG's current star formation rate is high relative to its mean. Overall, Karachentsev et al. (1999) note that Sag DIG appears to be a "normal" gas rich, low metallicity dwarf irregular. Lee & Kim (2000) conduct a similar analysis to that of Karachentsev et al. (1999) using BVRI photometry from the 2.2m University of Hawaii Telescope on Mauna Kea and broadly confirm the results of Karachentsev et al. (1999), although they derive a larger exponential scale radius of $r_e = 37" \pm 2"$. They also note that the youngest stars in their CMD – some consistent with forming as recently as 10 Myrs ago – are very much more centrally concentrated than the other stellar populations.

Momany et al. (2002) studied the stellar populations of Sag DIG using deep BVI observations, and identify an AGB population as well as the RGB and blue loop stars, consistent with the observations of Carbon stars. A follow-up study of Sag DIG using the Hubble Space Telescope (HST) by Momany et al. (2005) presents a much deeper CMD, albeit in a more restrictive field of view (see Figure 3.1). They estimate a metallicity for the galaxy between [Fe/H]=-2.2 to -1.9 dex. Within the CMD, they are able to identify a very old population (>10 Gyrs) as well as a red clump indicative of intermediate ages. They also compare the locations of the stars to the HI gas, and find that the youngest stars are found near to, but not coincident with, the HI clumps.

The most recent study of Sag DIG - published during the preparation of this manuscript - is by Beccari et al. (2014). They, like us, examine the extended structure of Sag DIG from wide field photometry by using resolved stars to trace the faintest features, and find that it is well described by a single exponential curve with a scale radius of order 340 pc, with no evidence of disturbances or breaks in the profile. We will return to discussion of this paper and compare it to our findings for Sag DIG.

3.2.4 Star Formation History

As well as the presence of very young stars, an extended star formation history of Sag DIG is implied by the present of carbon stars, first photometrically identified by Cook (1987). These authors identify two populations of carbon stars, one which is brighter and redder, the other is fainter and bluer. The redder population area younger, higher metallicity carbon stars like those observed in the Large and Small Magellanic Clouds.

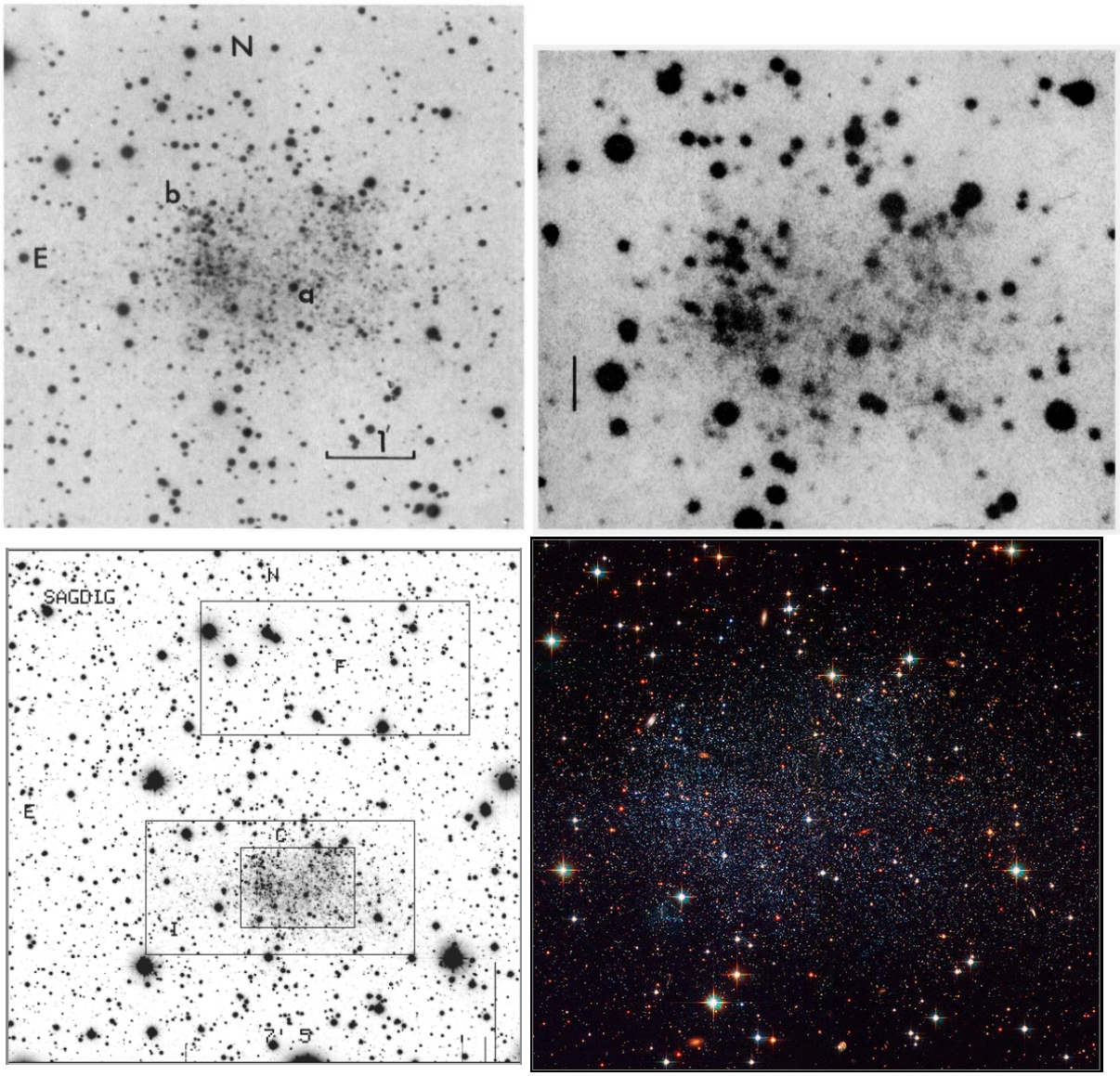

Figure 3.2 A compilation of images of Sag DIG though time. *Top Left:* Discovery image from Cesarsky et al. (1977) with a 90 min exposure with a $GG385$ filter. *Top Right:* ESO/SRC Southern Sky Survey image from Longmore et al. (1978). Bar is one arcminute for scale. *Bottom Left:* 7.5' x 7.5' V band image from Lee & Kim (2000) with regions used in their analysis identified. *Bottom Right:* HST composite image from Momany et al. (2005).

The bluer population is more like carbon stars in the dwarfs spheroidals, older and with a lower metallicity. The presence of both these populations suggest that Sag DIG has had multiple episodes of star formation (or prolonged star formation) at intermediate ages.

Weisz et al. (2014) determines a star formation history for Sag DIG by generating synthetic CMDs for a given stellar population and matching them to features observed in the HST CMD obtained by Momany et al. (2005). However, the data does not reach as deep as the oldest main sequence turn-offs, and so there are very large uncertainties as to the fraction of stars formed at the oldest times. Nevertheless, it is clear that Sag DIG has had on going star formation continuing up until present, with about half its stellar mass formed by ~ 6 Gyrs ago.

3.3 Summary

The dwarf irregular galaxy Sag DIG has been studied previously, characterizing its structure and stellar populations. This dwarf is one of the most metal poor galaxies known, while still containing an old population as well as on-going star formation. There is an HII region identified in this dwarf, and the HI is known to be extended in a general "crescent" shape.

This work presents deep and wide field imaging of this dwarf, giving us a more complete picture and is complementary to previous work.

Chapter 4

Stellar Population Analysis

The wide-field, deep CFHT imaging of the *Solo* survey in the g and i bands provides a detailed look at stellar populations. Individual stars are resolved within Sag DIG, excluding the centre of the dwarf due to high stellar densities. Using a color magnitude diagram (CMD), we can identify the major stellar populations, and examine the influence of background and foreground contamination. The red giant branch (RGB) stars can be selected, from which we can estimate the distance of Sag DIG using the tip of the RGB (TRGB) as a standard candle. We use isochrones to approximate the metallicity of these stars. We can also probe the radial structure to look for metallicity gradients. These RGB stars are also used in the next chapter to trace the extended structure.

4.1 The Color Magnitude Diagram

The outskirts of Sag DIG are resolved into stars in our CFHT/MegaCam imaging and we construct a CMD of these sources, shown in Figure 4.1. The left hand panel is a Hess diagram of the Sag DIG CMD, using the full 1° by 1° field of view. The Hess diagram shows the CMD as a density of stars, rather than individual points for each star, which is necessary due to the large number of stars (over 172 000) in the full field.

Sag DIG is at relatively low Galactic declination, and so the field is polluted with a large number of foreground Milky Way stars as well as heavily influenced by Galactic dust. From the Hess diagram, we can identify the major sources of contamination. Clearly, the foreground stars are not uniform across the CMD. Stars near the main

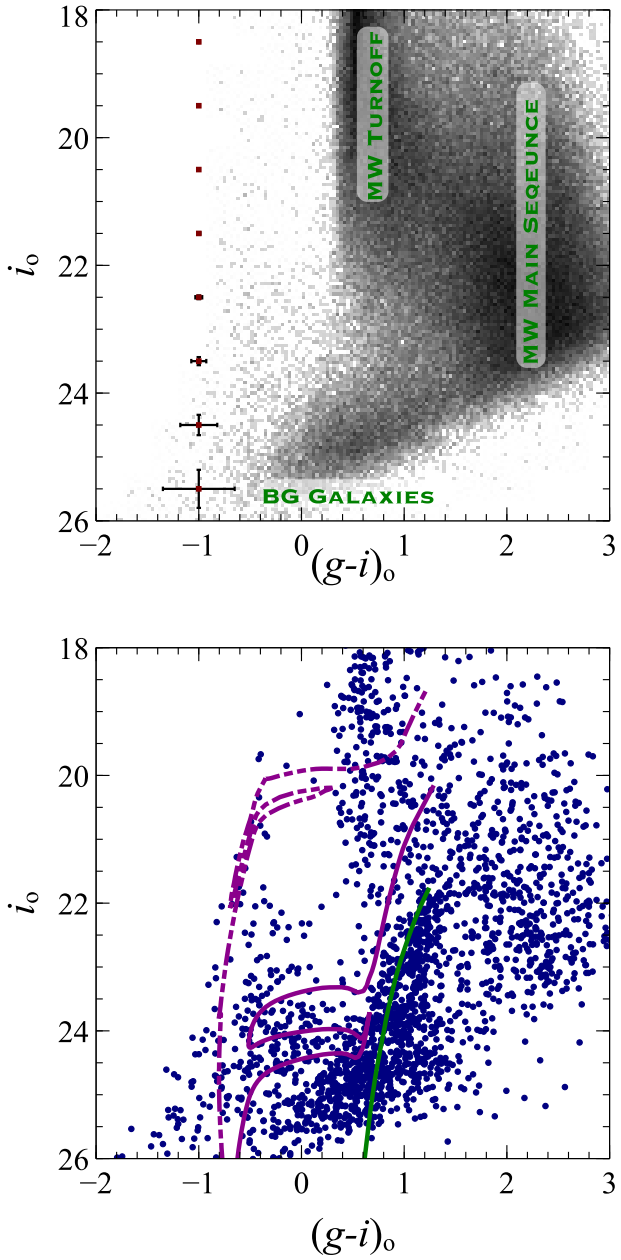

Figure 4.1 *Left Panel:* A Hess diagram (logarithmically scaled) of the CMD for all stars in the CFHT/MegaCam field. Mean errors as a function of magnitude are shown. Regions of significant foreground and background contamination are labelled with the source of contamination. *Right Panel:* Blue points show the CMD of all stars within 4 r_s from the center of Sag DIG. The green isochrone from Dartmouth (Dotter et al., 2008) traces a RGB, with an age of 6 Gyrs and [Fe/H]=-2.2 dex. The purple isochrones are for younger populations with ages 50 Myrs (dashed) and 500 Myrs (solid) and a metallicity of [M/H]=-2.0 dex, from the PARSEC isochrone set (Bressan et al., 2012). All isochrones have been adjusted to the distance of Sag DIG as determined in Section 4.3.

sequence turnoff in the Milky Way halo, located at a range of distances, produce the vertical sequence with a color near $(g-i)_0$= 0.5, labelled in the left panel of Figure 4.1. Low mass stars in the Milky Way disk at varying distances appear in the cloud of objects around $(g-i)_o$= 2, and are also labelled. An additional source of contamination of the CMD are distant (elliptical) galaxies misidentified as stars at faint magnitudes, and these dominate the CMD at the faintest magnitudes.

We can also study the "non-stellar" objects within the square degree field of view. These objects, as explained in Section 2.2, have PSF's that are inconsistent with point sources. Figure 4.2 shows a Hess diagram of these object in the upper panel. Clearly, as the photometry errors in both bands increases towards fainter magnitudes, so does the number of non-stellar objects. At the brighter limit, the distribution more closely resembles the field CMD shown in the left panel of Figure 4.1, but is more uniform. There are no obvious over-densities for the Milky Way main sequence and turnoff stars.

The lower panel of Figure 4.2 shows the relative fraction of stellar to non stellar objects (N_s/N_{ns}). At bright i band magnitudes, there are many more objects classified as stellar, with more than five times as many stellar objects. As the sources become fainter, this ratio decreases dramatically. Below $i_o \approx 22$, stellar sources are outnumbered by non stellar by more than two to one. In the full field of view, there are 172 031 stellar sources identified compared to 304 153 non-stellar sources.

To remove the overwhelming majority of contamination, the CMD is restricted to stars within 4 r_s of the center of Sag DIG (where r_s is the characteristic radius from the Sersic fit to the radial profile, described in detail in Section 5.4). The CMD is dominated by stars native to Sag DIG, shown in the right hand panel of Figure 4.1.

The effects of dust within the Milky Way are reduced using the Schlafly & Finkbeiner (2011) update of the Schlegel et al. (1998) dust maps. The dust maps give an estimate of the extinction ($E(B-V)$) along lines of sight, based on 100 μm emission. A magnitude correction is determined from the $E(B-V)$ for both the g and i band using $g_{corr} = 3.793E(B_V)$ and $i_{corr} = 2.086E(B_V)$ from Schlegel et al. (1998). The dust maps are interpolated for each identified star; the average correction in the (g,i) bands is (0.45,0.25) mags. This dust correction only applies to Milky Way dust and does not include dust within Sag DIG. As such, it is a minimum value for the possible true dust extinction. Figure 4.1 also shows the average error in both i_0 and $(g-i)_0$ is shown. Below a magnitude of $i_0 \simeq 25$, the uncertainty in the photometry becomes very large, contributing to the apparent width of the RGB.

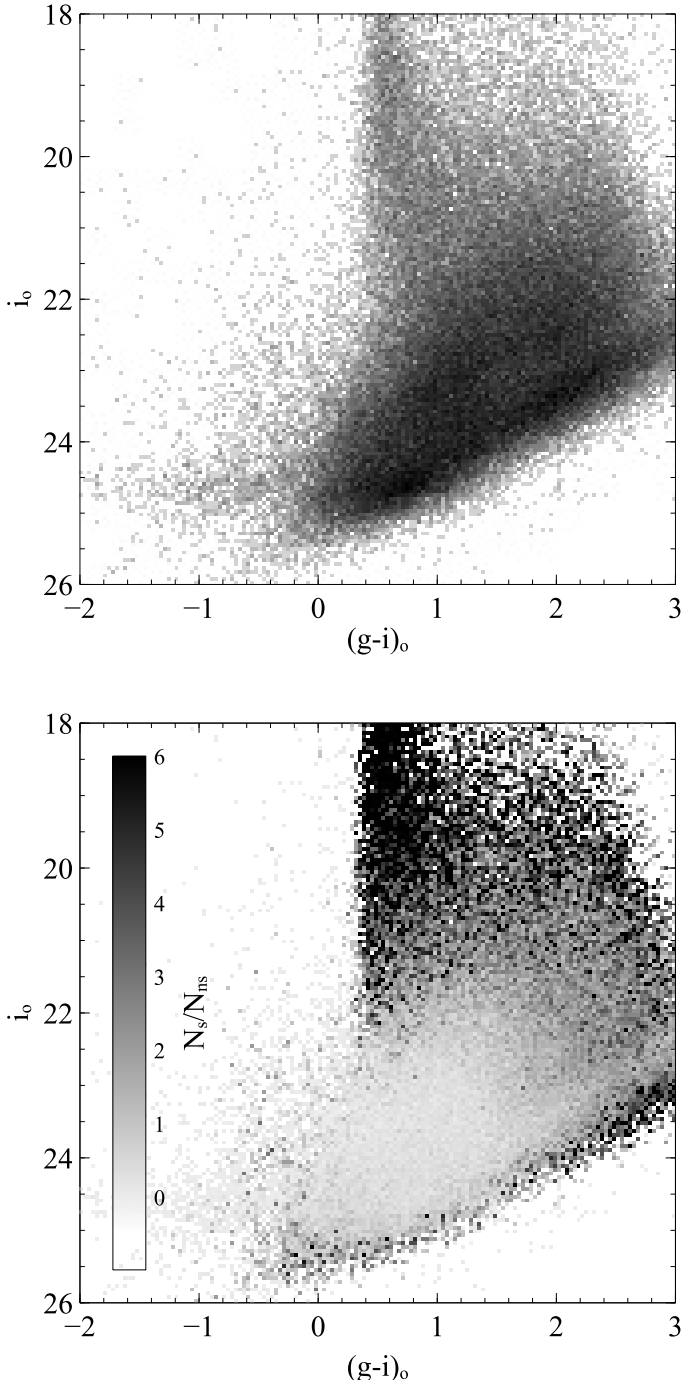

Figure 4.2 *Upper Panel:* A logarithmically scaled Hess diagram CMD of the "non-stellar objects" identified in the image. *Left Panel:* Here, the fraction of stellar to non stellar object is shown as Hess diagram.

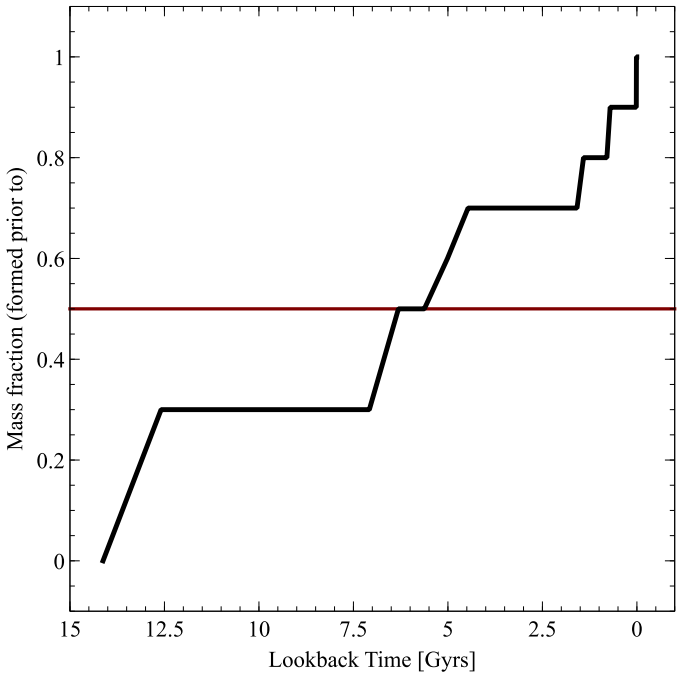

Figure 4.3 The star formation history regenerated from Weisz et al. (2014). The error bars are not reproduced here but are substantial (see original paper).

As discussed previously, the SFH derived by Weisz et al. (2014) shows an extended period of star formation and appears that Sag DIG has a fairly "typical" SFH as compared to other field dwarf irregulars. These galaxies generally form 30% of their mass prior to z $\sim$2 and show an increase in star formation after z $\sim$ 1. This SFH history from Weisz et al. (2014) is reproduced in Figure 4.3.

Qualitatively, we can see various features with the CMD suggesting an extended period of star formation; the prominent RGB suggests an old (at least >2 Gyrs) population while the bright blue stars indicate recent star formation on the timescale of <1 Gyr. Both features are clearly visible in the CMD as there are few Galactic blue stars and the RGB branch is a distinct over density in comparison to the field. Dartmouth (Dotter et al., 2008) and PARSEC (Bressan et al., 2012) isochrones are shown in Figure 4.1 shifted to the distance of Sag DIG (this distance is determined in the following section). These two sets of isochrones are necessary as the Dartmouth isochrones are known to describe the RGB well in the CFHT/MegaCam filter system (McConnachie et al., 2010), and the RGB is the focus of the following analysis. However these isochrones do not include ages less than 1 Gyr hence the PARSEC

isochrones are used to fit the more massive stars. The isochrone overlaid on the RGB is 6 Gyrs – corresponding to the mean age of Sag DIG based on the analysis by Weisz et al. (2014) – and metal poor, [Fe/H]=-2.2 dex. The fact that we see a significant number of RGB stars lying blue-ward of this isochrone are indicative of either an even more metal poor population or a younger component to the RGB; the degeneracy between age and metallicity makes interpreting the colour distribution of RGB stars uncertain (we return to this point in Section 4.4). While we account for reddening due to Galactic dust, no correction for internal extinction is included; however, this effect would make stars appear redder and so would not explain the position of the RGB stars to the blue side of the isochrone in Figure 4.1. Clearly, Sag DIG has a metal poor component and has had multiple, extended periods of star formation, consistent with previous studies (e.g. Weisz et al. 2014 and Momany et al. 2005). The CMD from Momany et al. (2005) is shown for comparison, based on HST ACS imaging. HST has superior resolution but a limited field of view, demonstrated in 3.1. Sag DIG was observed in three wavelengths by Momany et al. (2005). We select the most red (F814W) and most blue (F475W) and generate a CMD. Figure 4.4 shows the CMD for the HST data in the upper panel along side the CFHT CMD in the lower panel. In both panels, the red lines indicate the tramlines used to select RGB stars, used in the following analysis.

4.2 Structure in the Foreground

We now look at the CMD for evidence of structures closer than Sag DIG, namely the tidal stream from the Sagittarius dwarf spheroidal galaxy. In the CMD of Sag DIG in Figure 4.1, there is a suggestion of structure brighter than $i_o = 22$ ranging from $(g-i)_o$=0.5 to 2.5. Considering the location of Sag DIG, we know that within the Milky Way halo, there is known structure, namely the Sagittarius steam. This stream is the stripped tidal remnants of a dwarf galaxy (Ibata et al. 1994). By fitting the observed structure with an isochrone, as shown in Figure 4.5, we can determine if this faint CMD feature is indeed physical or just due to Milky Way structure.

From the fitted isochrone, we obtain an approximate distance to the over density. In addition, we use the updated Besançon Model (as described in Robin et al. (2003) and update described in Czekaj et al. (2014)) to quantify the expected Milky Way structure in the direction of Sag DIG. This model predicts the distribution of stellar types in a given region using the known Milky Way structure, matched with kinemat-

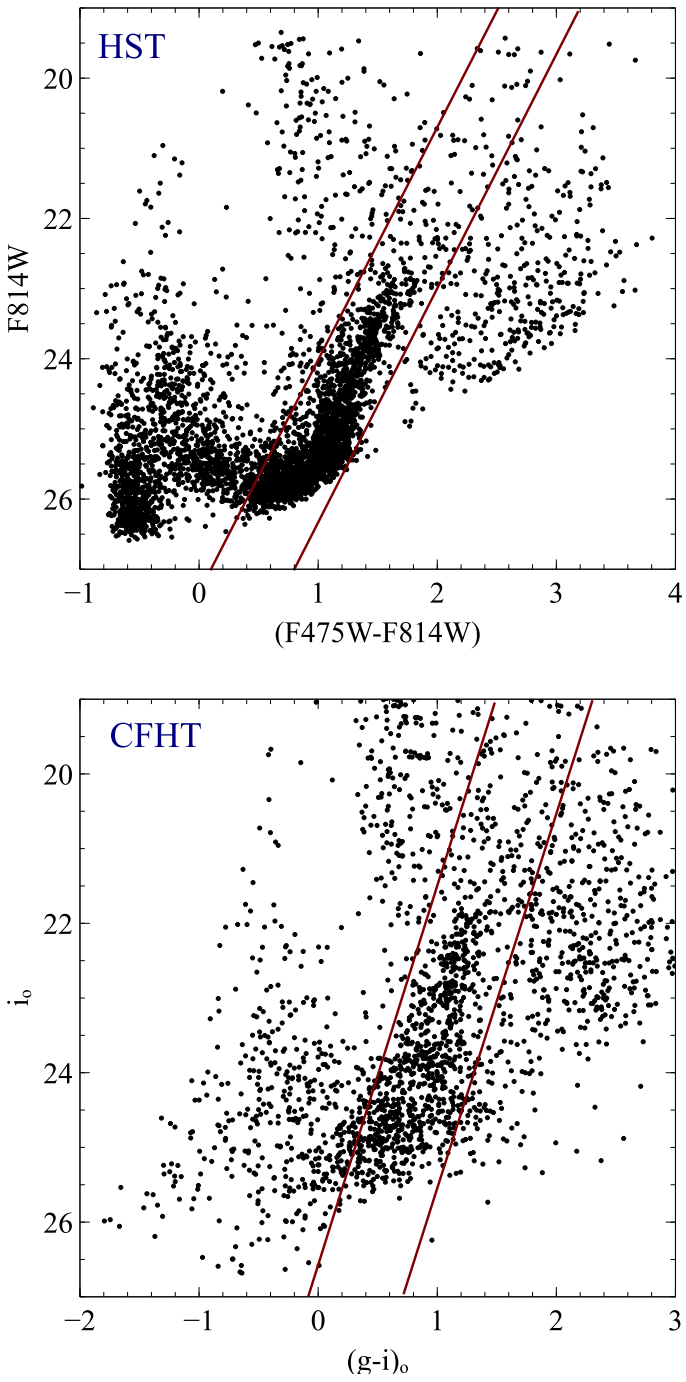

Figure 4.4 *Upper Panel:* A CMD for the HST data, with red tramlines used to select the RGB stars. *Left Panel:* A CMD for the CFHT data, again with tramlines indicating the stars selected for the RGB.

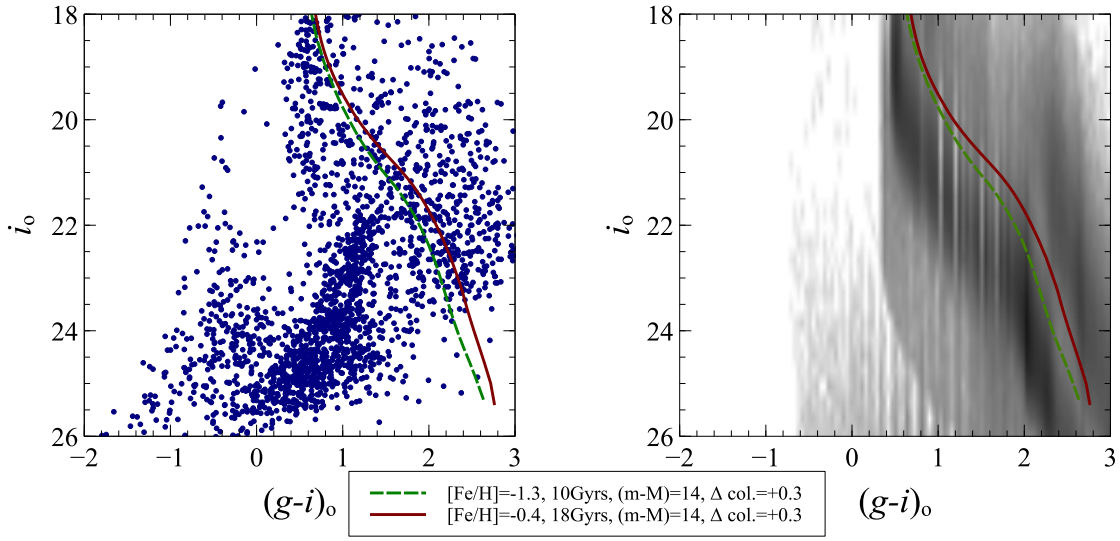

Figure 4.5 The *Left Panel:* Similar to Figure 4.1, the CMD of the Sag DIG. Overlaid are two Dartmouth isochrones with the age and metallicity of the old (green dashed) and intermediate (red solid) populations, shifted to match the observed stars both in distance and color. *Left Panel:* A smoothed Hess Diagram from the Besançon Model (Robin et al., 2003; Czekaj et al., 2014), with the same Dartmouth isochrones overlaid.

ics and stellar populations. The model generates a probable stellar catalogue from which we generate a CMD. We then can compare this CMD, shown as a Hess diagram in the right panel of Figure 4.5, and qualitatively compare the observed CMD structure.

After visually aligning an appropriate isochrone with the tentative structure, the resulting distance modulus is 14, corresponds to a distance of 6.3 Kpc.

The Sagittarius Stream is modelled by Law & Majewski (2010) and we can use this model to check whether the observed distance is consistent. Shown in Figure 4.6, we can see that most stars belonging to the Sagittarius Stream lie at distances around 10 Kpc in the direction of Sag DIG. We can also use the magnitude of the color correction (+0.3 mags.) to estimate the effects of Galactic dust. We have used the relation to correct for Galactic dust $g_o = g - 3.793E(B-V)$ and $i_o = i - 2.086E(B-V)$ from Schlegel et al. (1998). This generates a correction to the i band magnitude of 0.36 mags. Given the qualitative accuracy of this fit, this correction will not change the estimate distance dramatically.

While not in good agreement with the distance found using isochrone fitting, it

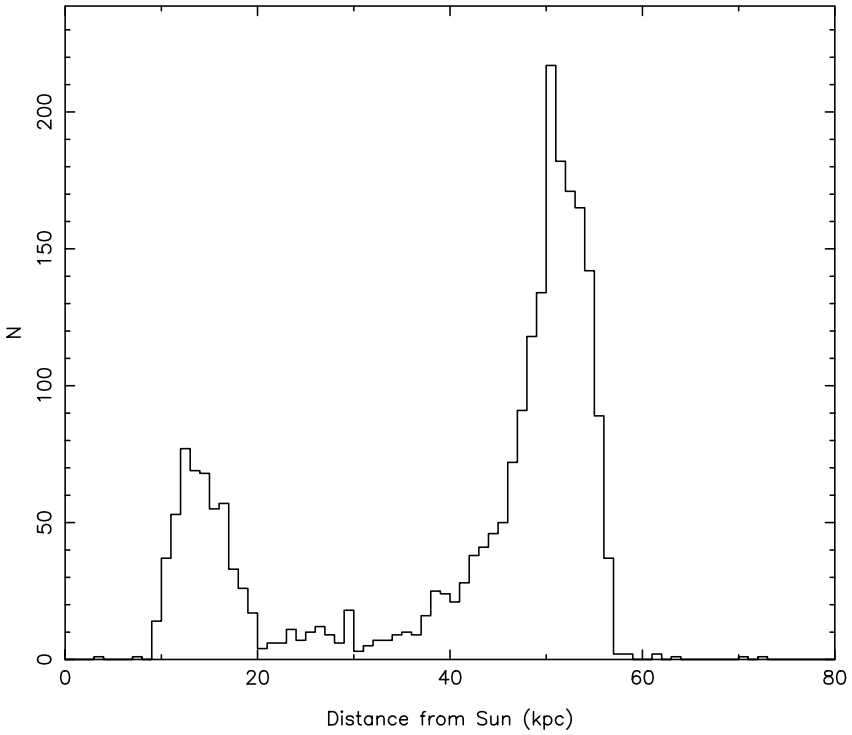

Figure 4.6 From Law & Majewski (2010), the observed distribution of particles within 10 degrees of the center of Sag DIG.

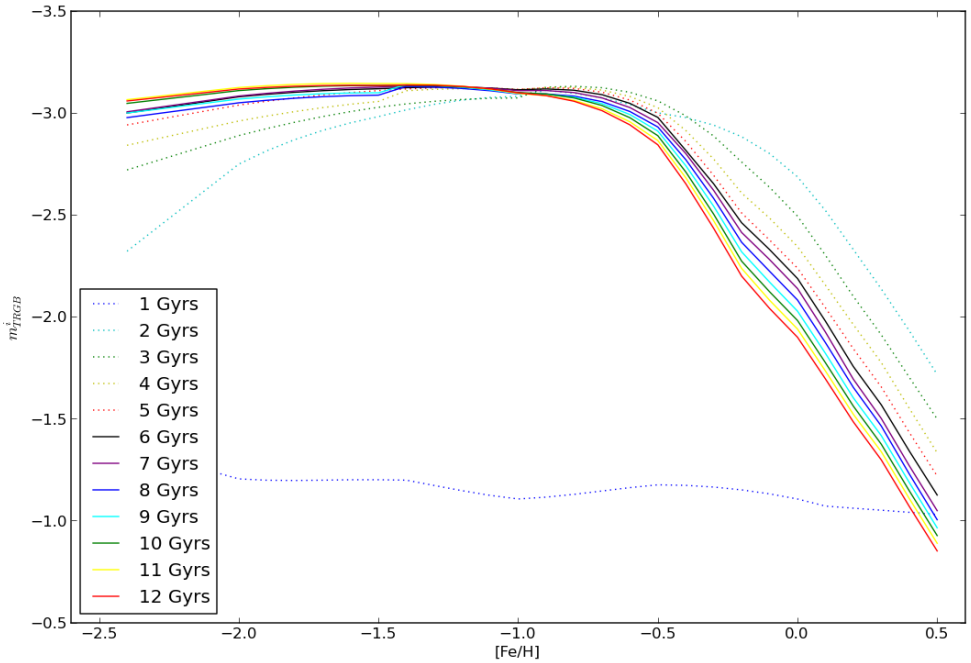

Figure 4.7 The TRGB is identified as the peak brightness from the Dartmouth Isochrones, over range of ages(1-12 Gyrs) and metallicities ([Fe/H]= -2.5 to +0.5). The plateau near m^i_{TRGB} illustrates the age and metallicity ranges for which it can be used as a reliable standard candle.

is still plausible that the structure seen in the CMD belongs to the stream however the observed over density is more likely to be simply the Milky Way. Comparing the CMD from the Besançon Model to the over density, we see clear structure in the same space. This structure is not perfectly coincident with the over density observed but highlights the inhomogeneity of the Milky Way in the CMD. Comparing the model and observed CMD, it is ambiguous whether the potential structure is simply the Milky Way or the Sagittarius Stream.

4.3 Distance Estimate

We use the tip of the red giant branch (TRGB) as a standard candle to determine the distance to Sag DIG. The luminosity of RGB stars as they undergo the helium flash and begin fusing helium in their cores is approximately constant, largely independent

of stellar age and metallicity, at least for ages greater than ~ 2 Gyrs and a metallicity of [Fe/H]$\simeq -1$ dex (see Lee et al. 1993, Bellazzini et al. 2001, Madore et al. 2009 and Salaris & Cassisi 1997 among others). Using the Dartmouth isochrones, Figure 4.7 shows the peak RGB luminosity (TRGB) for age 1-12 Gyrs across metallicities from [Fe/H]=-2.5 to 0.5. The older (>6 Gyrs) and more metal poor ([Fe/H] <-1.0) are almost uniform. For more metal rich stars, there is a clear age dependent turn over, where as for more metal poor stars there is a gradual age dependent increase in luminosity for younger stars. Using the fact that the RGB is old (>6Gyrs) and relatively metal poor(<[Fe/H]=-2.2), the TRGB brightness is known to be $i_o = 3.53$ mags. for the old (12 Gyrs) isochrones (note that plot is in the Vega magnitude system and where as the data is in the AB system so there is a 0.401 mags. correction in the i between these two systems.)

Given a well populated RGB, the maximum luminosity of the RGB stars is characteristic of the helium flash and can be identified by looking for a large discontinuity in the luminosity function (Sakai et al. 1996). A significant AGB population can have a small effect on the accuracy of this distance estimate, since, if present, this population may mask the discontinuity. We look in detail for a faint AGB population at the end of this section and are unable to find evidence of one. Sag DIG has a well populated, intermediate or old RGB without a strong, bright AGB population, hence the TRGB should be a good distance estimator for this dwarf.

The luminosity function for the RGB stars in Sag DIG is shown in the top panel of Figure 4.8, constructed from stars that were bounded by a set of "tramlines" that were drawn around the RGB in the right panel of Figure 4.1. The luminosity function is corrected for foreground/background contamination by constructing a similar luminosity function for stars within the same region of the CMD but that are located at least 10 r_s from the center of Sag DIG (where the foreground/background dominates). The resulting luminosity function is scaled by area and also shown in the top panel of Figure 4.8. The corrected, subtracted luminosity function is shown in the middle panel of Figure 4.8.

The TRGB is clearly visible in the middle panel of Figure 4.8 as the large jump in star counts at $i_0 \sim 21.8$. To more precisely determine the TRGB magnitude and uncertainties, we follow Sakai et al. (1996) and use a 5 point Sobel filter on the luminosity function in Figure 4.8. A Sobel filter works by identifying the local slope and finding the largest value, which will correspond to the jump in star counts observed. For the 5 point filter, the kernel is [-1,-2,0,2,1], so we essentially smooth

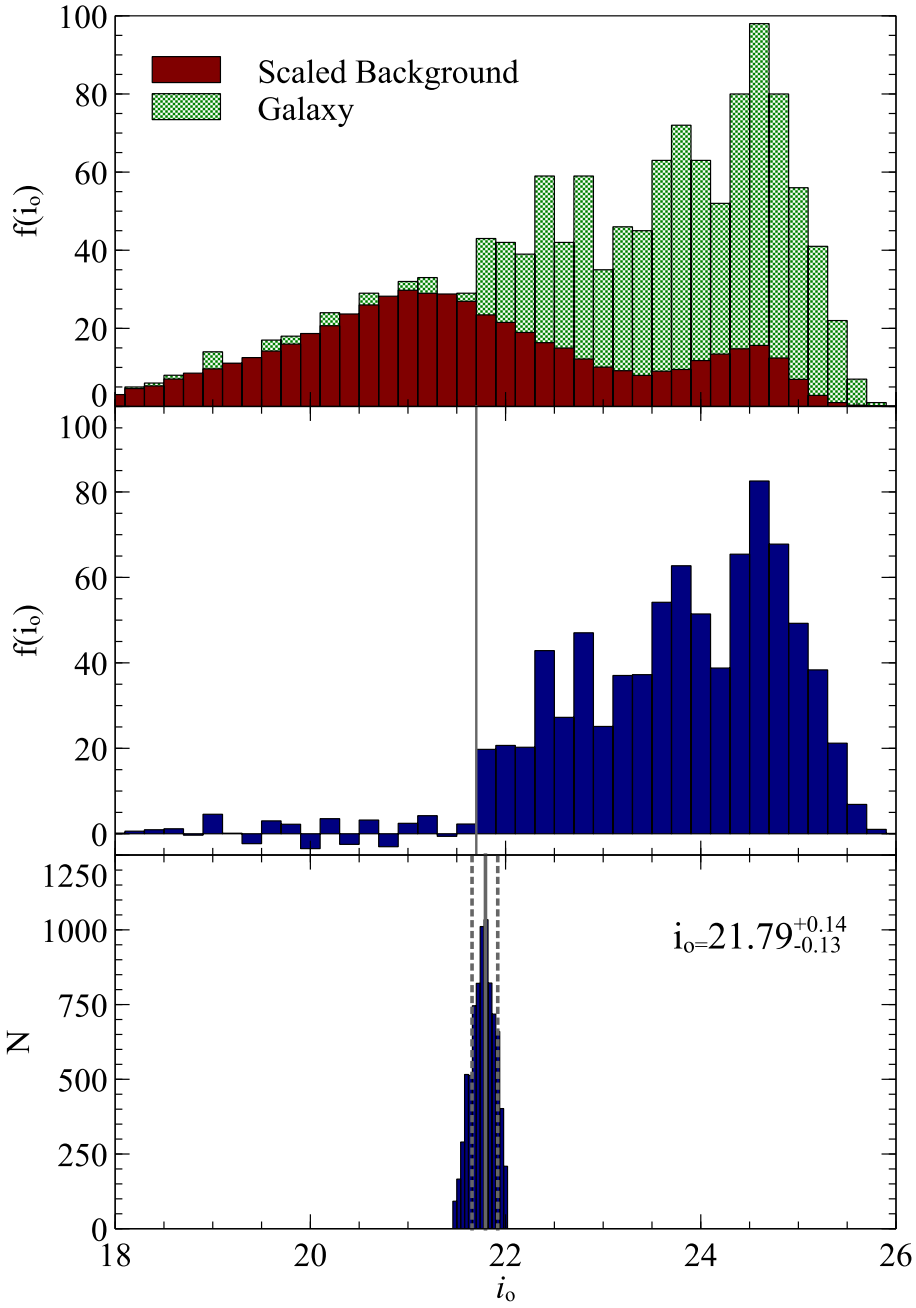

Figure 4.8 The upper panel shows the luminosity function for both Sag DIG (selected to be within $6r_s$ from the galaxy center) and the field (selected to be $> 10r_e$ from the galaxy center), scaled by area. The middle panel shows the background subtracted luminosity function. The distribution of values calculated for the TRGB is shown in the lower panel, derived using the method described in the text.

the slope over four points, making this filter somewhat robust against noise. We also repeated our analysis with a three point Sobel filter (kernel: [-1,0,1]) with no change in the result.

To remove the dependency on choice of bin edges and bin sizes, we conduct this analysis on multiple realizations of the luminosity function: the bright magnitude end was varied from $i_0 = 20$ to $i_0 = 21$ in 2000 steps, and for each of these realizations the bin width was varied from 0.17 to 0.25 mags in 5 steps. This combination resulted in 10 000 luminosity functions on which the Sobel filter was applied to find the TRGB. The distribution of results is shown in the lower panel of Figure 4.8. The mean value from this distribution and bounds containing 68% of the results are used as the luminosity of the TRGB and associated uncertainties, such that $i_{TRGB} = 21.79^{+0.14}_{-0.13}$ mag.

Using the Dartmouth isochrones (Dotter et al., 2008) in the CFHT filter system, the luminosity of the TRGB is i_0=3.53 mag. for an old (approximately 12 Gyrs) and metal poor population. The resulting distance modulus of Sag DIG is therefore $(m-M)_0$=$25.32^{+0.14}_{-0.13}$, corresponding to a distance of $1.16^{+0.08}_{-0.07}$ Mpc. This result is in agreement with recent estimates by Momany et al. (2002) ($(m-M)_0 = 25.14 \pm 0.18$) and Momany et al. (2005) ($(m-M)_0 = 25.10 \pm 0.11$), which implement different reddening corrections, also including internal extinction. It is also in agreement with the most recent estimate by Beccari et al. (2014), finding $(m-M)_0$=25.56±0.11.

Now, we closely reexamine the luminosity function, along with the CMD, for evidence of an AGB population. Both the carbon stars identified by Cook (1987) and the later analysis by Momany et al. (2002) establish that Sag DIG has a AGB population. However, a bright AGB population, which would appear above the TRGB, is not clearly visible in the CMD of Figure 3 or in the luminosity function in Figure 4. As such, we zoom in to the region of the luminosity function immediately brighter than the TRGB by counting the number of stars in $\Delta i_o = 0.17$ mag. bins above the TRGB within the tramlines that were used in Section 3.1, in both the CMD of Sag DIG and the reference CMD. The number of stars in these bins as a function of magnitude is shown in the top panel of Figure 5, along with their Poisson uncertainty. The subtracted counts are shown in the lower panel, again with the uncertainties. We can see that there is essentially no excess of stars in the Sag DIG CMD brighter than the TRGB relative to the reference field. The two faintest bins both show an excess, potentially indicative of an AGB population but, as the error bars demonstrate, it is a weak population if it is in fact real. Given the low number of bright AGB stars that

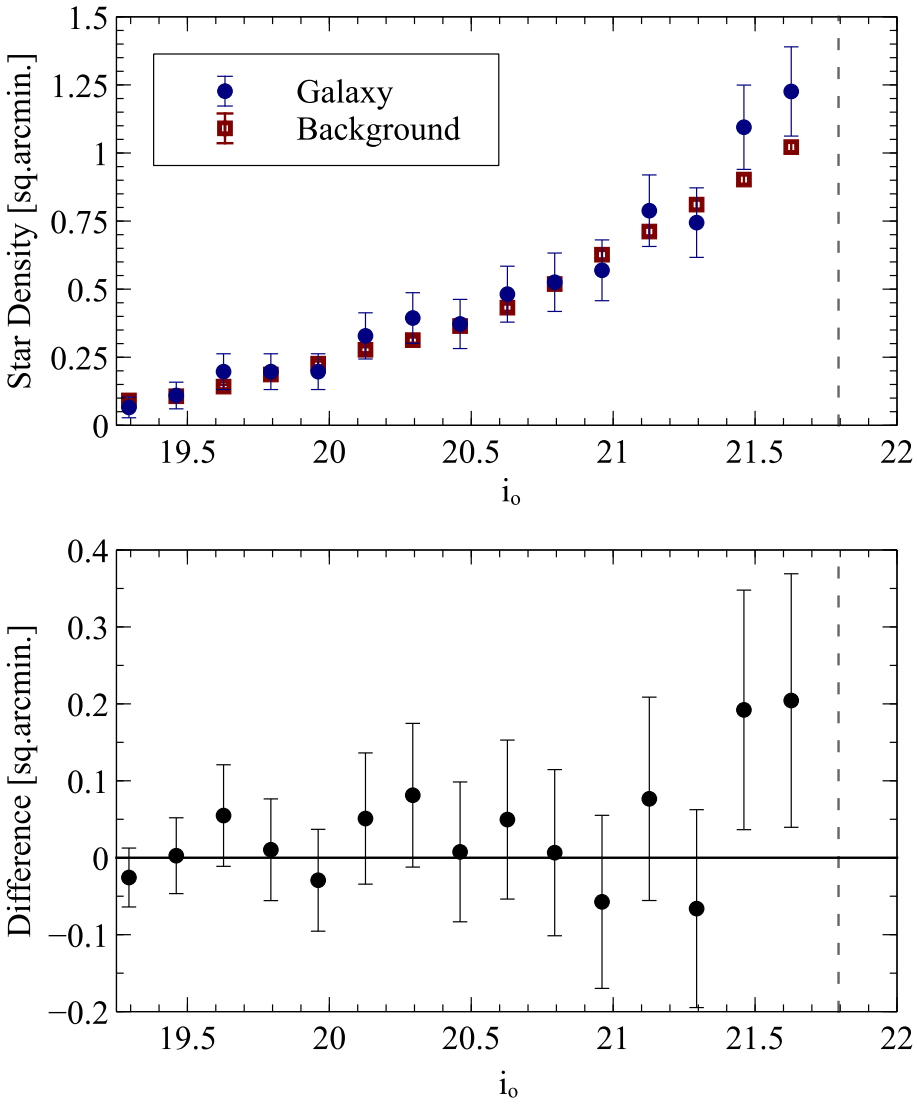

Figure 4.9 The upper panel shows the luminosity function of stars above the TRGB within the tramlines used earlier, for objects within the Sag DIG field and the (scaled) reference field (blue and red, respectively), in $\Delta i_o = 0.17$ mag. bins. The lower panel shows the corrected luminosity function, where an excess of stars in the Sag DIG field would be an AGB population, however no clear excess is visible. The dashed line indicates the location of the TRGB.

we can detect in our luminosity function, particularly in comparison to the RGB, the TRGB remains a reliable distance indicator.

4.4 Metallicity Estimates

Due to the age-metallicity degeneracy introduced at the beginning of this chapter, determining the metallicity of the RGB branch is challenging. However, by making some general simplifying assumptions, we can estimate a metallicity for the RGB using the isochrones and better quantify the spread in metallicity. The metallicity distribution function (MDF) for the red giant branch of Sag DIG, shown in Figure 4.10, is determined using a bilinear interpolation of stellar position in the CMD between a set of Dartmouth isochrones with a fixed age (e.g. Bellazzini et al. 2003, Sarajedini & Jablonka 2005, or Ordoñez & Sarajedini 2015). A set of 12 Gyrs isochrones with metallicities ranging from [Fe/H]=-2.4 to 0 dex were used as well as a 6 Gyr set (corresponding to the approximate mean age of Sag DIG derived by Weisz et al. (2014) as discussed previously). For simplicity, all isochrones used have [α/Fe]=0.0 dex.

To minimize uncertainties in the MDF caused by stellar photometric errors, and also to reduce the contamination due to misidentified galaxies (that becomes more common at fainter magnitudes), only stars brighter than i_o=24 are used. In the same way as for the luminosity function in the previous section, a Sag DIG MDF and a reference field MDF is created are by selecting stars within $4r_s$, and further away than $10r_s$, respectively. The solid line in Figure 4.10 indicates the median metallicity for each set of isochrones, while the dashed lines denote a percentile range from 16% to 84%, approximating one sigma deviation from the median value. For the 6 Gyr isochrones, the median metallicity is [Fe/H]=-1.4$\pm$0.5 dex while for the 12 Gyr set the median metallicity is [Fe/H]=$-1.6^{+0.7}_{-0.4}$ dex.

As previously discussed, Sag DIG is not well described by a stellar population with a single age, and so the basic assumption that goes into the derivation of the MDFs is flawed. However, the adoption of a few different age assumptions helps to estimate the systematic uncertainty produced by this assumption, and it appears to be of order a few tenths of a dex. Also of particular note, there are a significant number of stars that appear bluer than the most metal-poor isochrone ($[Fe/H] = -2.4$ dex) for both age assumptions. Due to the way in which we conduct the bilinear interpolation to estimate metallicities, these blue stars are not included in the analysis, thus we are clearly overestimating the metallicity for Sag DIG. Hence, the metallicity

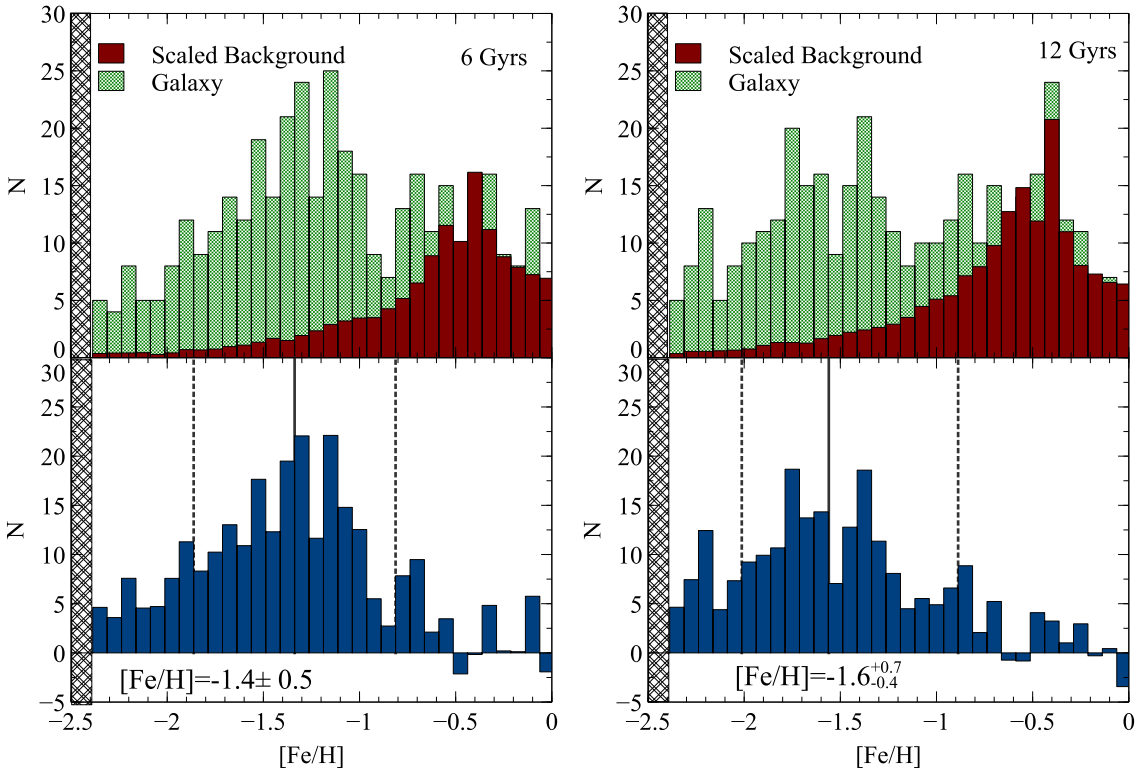

Figure 4.10 The MDF for the galaxy based on stars within $4r_s$ from the center of Sag DIG is shown in the top panels in green. The scaled MDF for the background field, consisting mostly of foreground Milky Way stars, is shown in red. The subtracted MDF is shown in the bottom panels. On the left, the analysis is conducted using 6Gyr isochrones, whereas on the right, a 12 Gyrs set of isochrones is used. The solid line indicates the median value, while the dashed lines represent interquartile range between 16% and 84%, approximating one sigma. The shaded regions indicate a lack of knowledge of the distribution in this region, since it corresponds to the presence of significant numbers of stars with colors bluer than the bluest isochrone ([Fe/H]=-2.4 dex).

estimate is, at best, an upper limit and explains why the derived mean metallicity is of order $[Fe/H] \sim -1.5$ dex, considerably more metal rich than previous estimates by Karachentsev et al. (1999) and Lee & Kim (2000). From comparing the mean color of the RGB to the isochrones in the Dartmouth isochrone set, it appears a more realistic metallicity estimate for Sag DIG is of order [Fe/H] $\simeq -2.2$ dex (for example, see the isochrone in Figure 4.1).

The presence of so many very blue RGB stars in Sag DIG is curious. In particular, while it is possible that their color is a result of a very low metallicity, the color-metallicity relation for RGB stars at these metal-poor values quickly "saturates", and more metal poor stars are not notably much bluer under normal circumstances. Therefore, the RGB possibly contains giants that are not well described by intermediate or old RGB isochrones, for example either young giants or AGB stars. Both types of giants are possible for a galaxy that has ongoing star formation (supported by Weisz et al. 2014), and may suggest that the metallicity is therefore not as low, on average, as the RGB color would seem to suggest. Clearly, spectroscopic estimates of stellar metallicities in this galaxy would be particularly interesting to obtain (for example, see the work on WLM by Leaman et al. 2012).

4.5 Stellar Populations Gradients

Thus far, our analyses assume that there is no variation in the stellar populations of Sag DIG over its spatial extent. However, a large body of work has demonstrated that there can be significant variation in the stellar populations of dwarf galaxies over their spatial extent (e.g. Harbeck et al. 2001, Tolstoy et al. 2004, Rizzi et al. 2004, Battaglia et al. 2006, Lianou et al. 2013, Monelli et al. 2012, McMonigal et al. 2014, Bate et al. 2015). We examine the populations of Sag DIG in this regard by splitting the galaxy into inner and outer sections. "Inner" is defined to be within $2r_s$ (excluding the inner 0.5' which is highly impacted by crowding) and "outer" is defined to be within 2 and $4r_s$. The CMDs are shown in the left and right upper panels of Figure 4.11, respectively.

Inspection of the CMDs in Figure 7 shows that there is a much higher concentration of young stars (blue loop and main sequence) in the central regions of Sag DIG than the outer regions (the outer CMD spans an area 4 times larger than the inner CMD, yet still has fewer stars with $(g-i)_0 \lesssim 1$). Moreover, the outer region lacks very bright young blue stars in comparisons to the inner region, for example young

stars brighter than $i \simeq 22$ mags. Overlaying the younger isochrones shown previously in Figure 4.11, we can see that the brightest blue stars in the central regions correspond to a population approximately 50 Myrs old, whereas the brightest blue stars in the outer region are better fitted with an isochrone that is at least $\gtrsim 100$ Myrs old.

The RGB is well populated in both the inner and outer CMDs, however the color spread is larger in the inner region. In particular, there may be a deficit of blue RGB stars in the outer region (i.e. stars bluer than the reference isochrone 6 Gyrs, [Fe/H]=-2.2 dex). To quantify this difference and determine if it is significant, the color difference of each star from the reference isochrone is computed. Only stars between the TRGB and i_o=23.5 are included (to minimize uncertainties due to photometric errors), and only RGB stars are selected. These tramlines are chosen to be far enough from the RGB to generously include all possible RGB stars, so a small amount of foreground contamination will be present.

The lower panel of Figure 4.11 shows that the color distribution of the RGB stars in the inner and outer regions are qualitatively different, with more stars at negative color difference (i.e., the blue side of the isochrone) in the inner region compared to the outer region. To quantify the potential difference between the populations, a Kolmogorov-Smirnov test is applied. The resulting p value is reasonably large, hence we must conclude that any difference, if present, is not statistically significant. If the excess of bluer RGB stars in the center is real, then it implies either a younger RGB population or a more metal poor RGB population. A dwarf galaxy with a more metal poor interior would be quite unusual, since all radial gradients in metallicity so-far discovered act in the opposite direction (e.g., Ross et al. 2015 or Leaman et al. 2013). We prefer the interpretation that the difference in color is due to much younger ages in the center, obviously consistent with the centrally concentrated star formation of this galaxy.

4.6 Summary

The *Solo* survey provides resolved stars in all but the very centre of Sag DIG allowing us to use a CMD as a powerful tool. Sag DIG is a gas rich dwarf, with on-going star formation. While the old stars are clearly the dominant population, young bluer stars are also present. While we know from previous work, AGB population is present, we are unable to identify any bright AGB stars. Using the CMD, we can isolate the RGB branch, from which we can estimate the distance to be $1.16^{+0.08}_{-0.07}$ Mpc using the

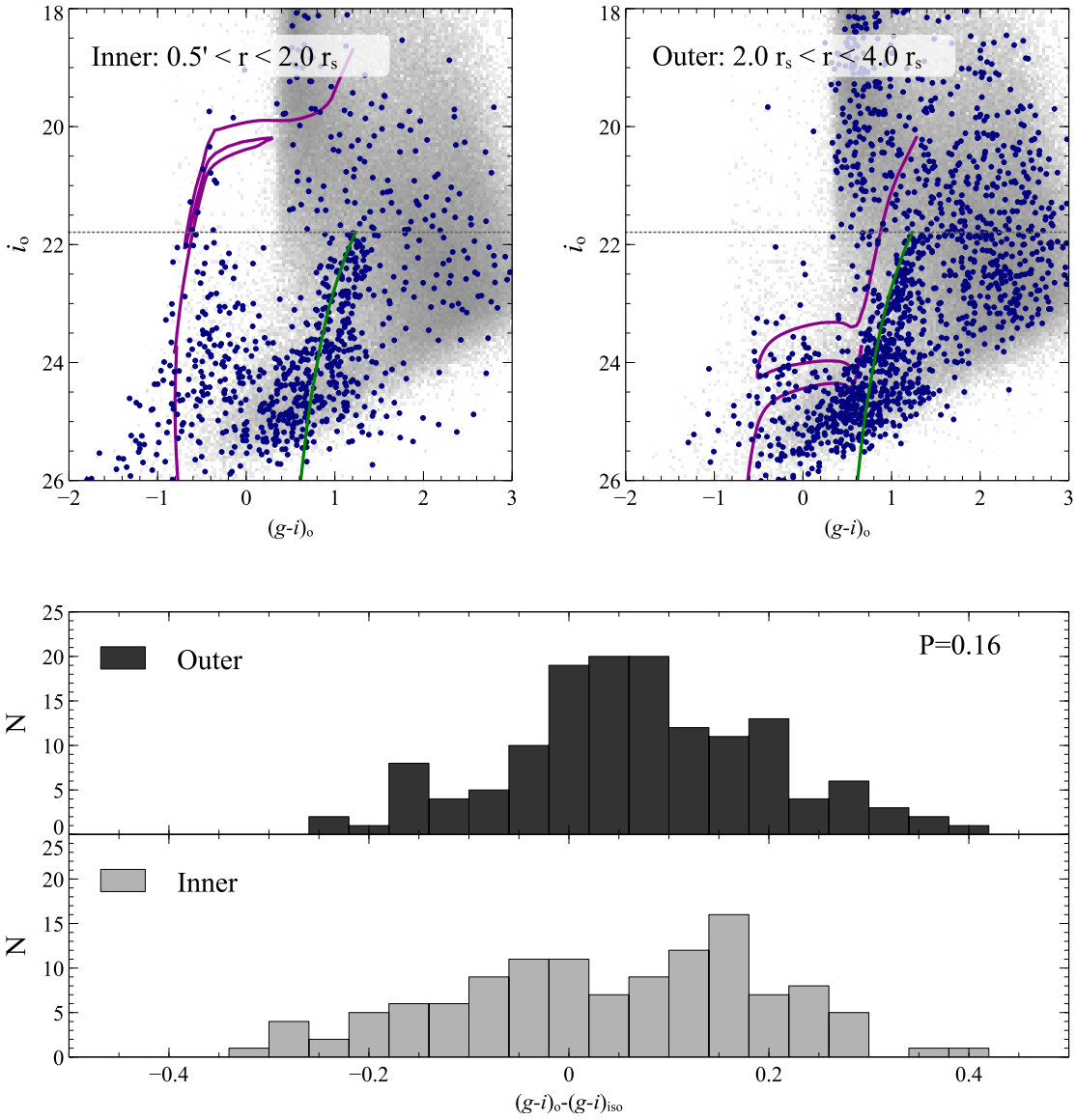

Figure 4.11 The upper panels show the CMD for the inner part of the galaxy (defined to be within $2r_s$) on the left and the outer part of galaxy (defined to be between 2 to $4r_s$) on the right shown relative to the 6 Gyr isochrone in green with a metallicity of [Fe/H]=-2.2 dex (Dotter et al. 2008). Younger isochrones are shown in purple with ages of 50 Myrs and 500 Myrs in the left and right panels respectively. The color difference of RGB stars relative to the 6 Gyr isochrone is shown in the lower panels, along with the Kolmogorov-Smirnov test result between the two color distributions.

TRGB. We also confirm that RGB population is metal poor, and shows a possible radial gradient. In the next chapter, we use the RGB stars in combination with an integrated light analysis to study the radial profile and extended structure of Sag DIG.

Chapter 5

Low Surface Brightness Structure

While *Solo* targets those galaxies for which studying their resolved stellar content is possible, most of the galaxies have central regions that cannot be resolved from the ground under natural seeing conditions. The observations are wide field to analyze the extended structure, with the trade off being a lack spatial resolution in the central regions. Some nearby dwarfs, like Sag DIG, have been observed with HST, which greatly improves the resolution and decreases the effects of crowding, but the small field of view limits the spatial extent. For a more complete view of the galaxy, we use our wide field observations and start by analyzing the integrated light. With careful consideration of contamination from foreground stars, we are able to determine the integrated light profile and color profile. To extend this profile to extremely faint limts and large radii, we can combine the integrated light profile with RGB stellar density, using both CFHT and HST data. By fitting this profile, we parameterize the surface brightness profile of Sag DIG.

5.1 Integrated Light Profiles

Due to crowding in the centre, we cannot resolve stars. However, we can use the total integrated light to understand the radial profile. This profile quickly becomes too faint away from the center and not distinguishable from the noise in the image. Hence we are restricted to only the center of the dwarf.

Integrated light radial profiles are generated by finding the total flux within a set of elliptical annuli placed on the reduced CCD image of Sag DIG. For simplicity and ease of comparison, the ellipticity (e) and position angle (PA) of the annuli is fixed

with radius. We adopt $e = 0.53$ and $PA = -0.52^{\circ}$ as determined later in Section 5.2.

The foreground Milky Way stars contaminate the underlying light from Sag DIG and must be carefully subtracted as these foreground stars are significantly brighter than the diffuse signal from the dwarf galaxy. In the previous CMD analysis, the RGB branch of Sag DIG is obvious relative to the Milky Way foreground. Spatially however, stars belonging to Sag DIG do not dominate the foreground stars. To remove these stars before determining the integrated light profile, a pixel mask is generated by removing all pixels brighter than a cutoff level, or adjacent to one of these bright pixels. The appropriate cutoff level for each band is determined by analyzing the distribution of pixel values across the full image and by studying the resulting mask, for which all obvious foreground stars and artefacts should be blacked out. The resulting masks shown in Figures 5.2 and 5.1.

The total flux within each elliptical annuli for unmasked pixels is found, while ignoring the masked pixels. The uncertainties associated with the flux are Poisson photon noise. While the mask described above removes contamination from foreground stars, dust within the Milky Way may distort the radial profile, particularity if there are large gradients across the galaxy. Additionally, the central surface brightness will be reduced by dust, and Sag DIG may appear reddened. We corrected the flux in each pixel for the appropriate value of extinction as derived from the Schlafly & Finkbeiner (2011) dust maps at the position of that pixel. The $E(B-V)$ extinction values across Sag DIG are shown in Figure 5.3. The spatial resolution of the dust maps is a few arc minutes, due to the resolution of COBE/DIRBE and IRAS/ISSA, upon which the dust maps are constructed.

Using the calibrations for the MegaCam data found in the image header, the resulting flux, in photon counts per pixel, is converted to the conventional units magnitude per square arcsecond. Specifically, we convert ADU per pixel to magnitudes per square arcsecond using

$$\mu_i = -2.5 log_{10}\left(\frac{ADU}{a_{pix}^2 exptime}\right) + phot_c + phot_k(airmass - 1.0) \qquad (5.1)$$

where a_{pix} is the area of the pixels (in arcseconds), and $exptime$, $phot_c$, $phot_k$ and $airmass$ are all observing parameters and zeropoints given in the image header.

The resulting integrated light profile is shown in the upper panel of Figure 5.4 for both bands. We can also determine a $(g-i)_o$ color profile by subtracting the two radial profiles, and is shown in the lower panel of Figure 5.4.

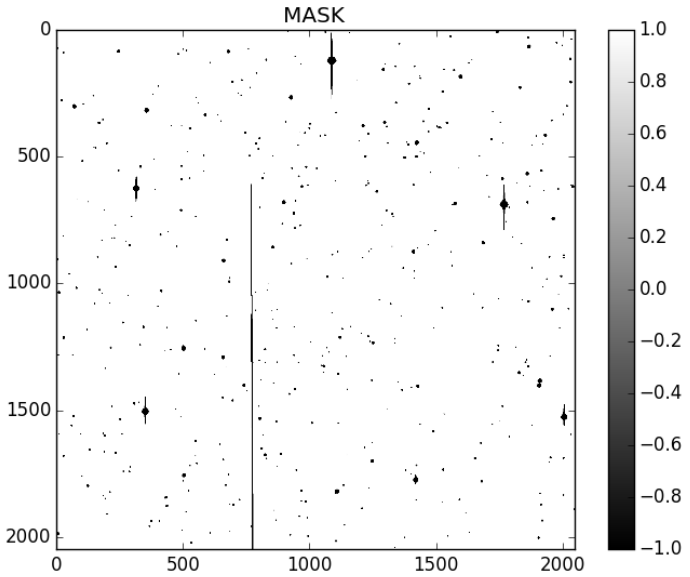

Figure 5.1 Masked pixels in the g band, removing all pixels with a value above 6500 ADU.

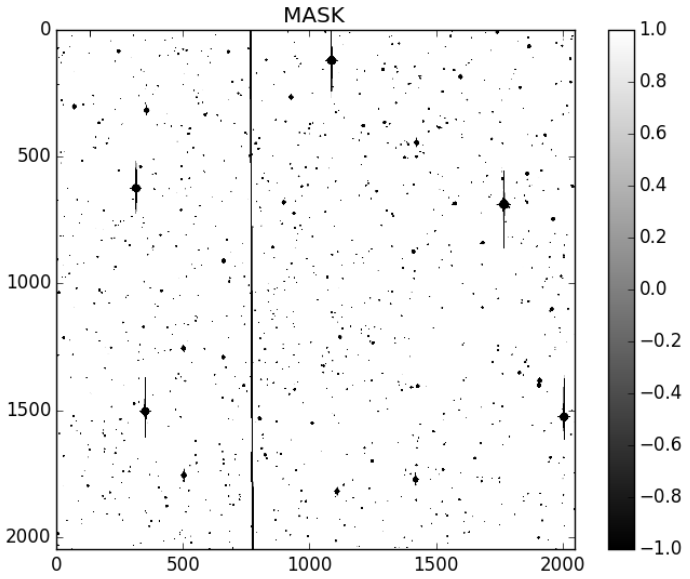

Figure 5.2 Masked pixels in the i band, removing all pixels with a value above 6500 ADU.

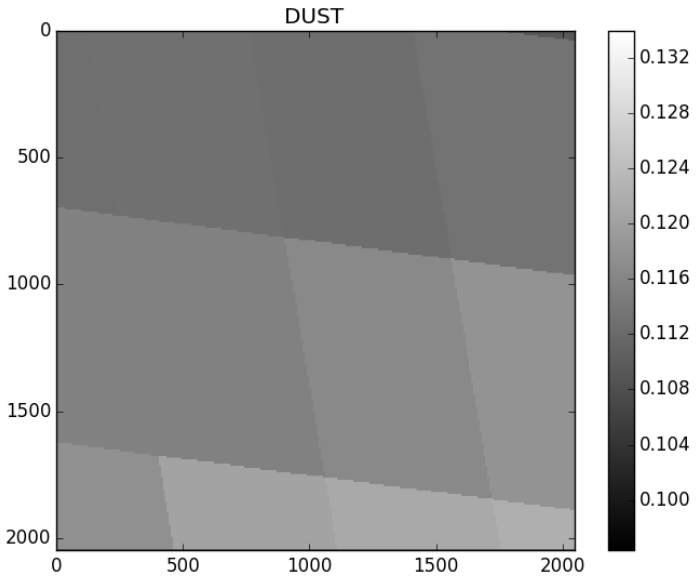

Figure 5.3 The $E(B-V)$ extinction values across Sag DIG from the Schlafly & Finkbeiner (2011) dust maps. The axes are in pixels, where each pixel is 0.187 arcseconds. The resolution of the dust maps is about 2 arcminutes, hence the visible squares.

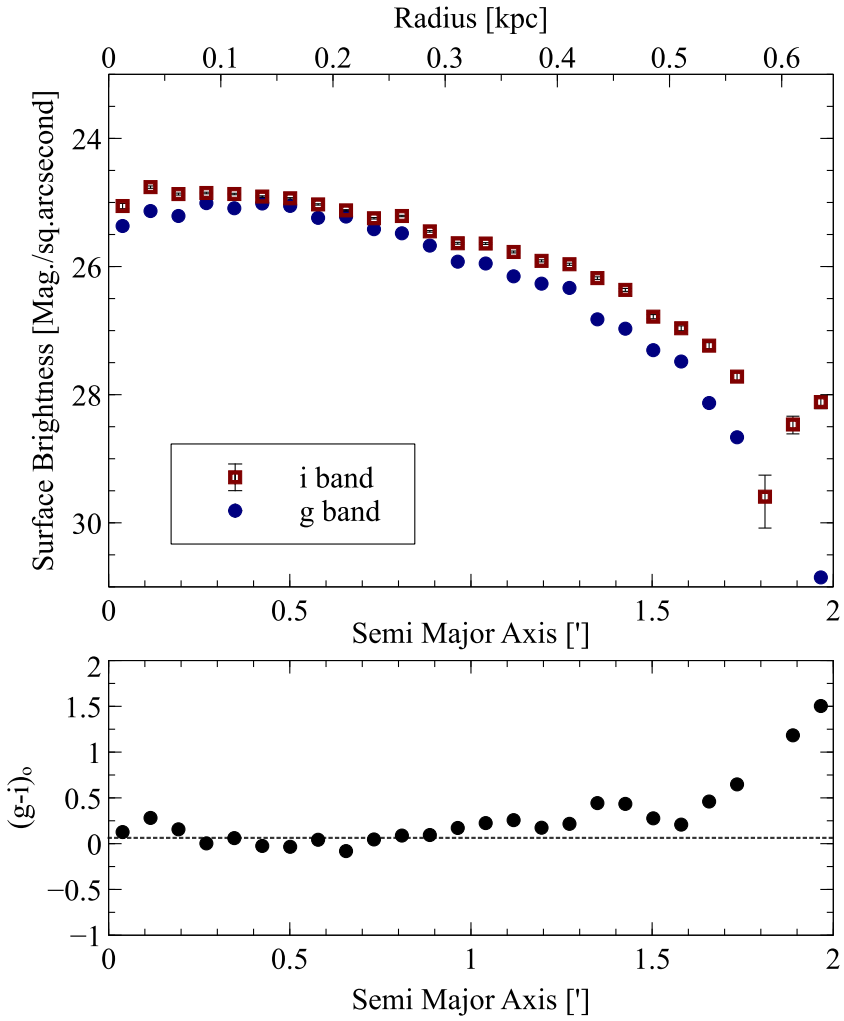

Figure 5.4 The upper panel shows integrated light profiles in both the i and g bands, calculated using elliptical annuli with bright sources masked as described in the text. The lower panel shows the color profile as a function radius.

In generally, the profiles in both g and i are broadly exponential, with no notable features. There is a possible "kink" in both profiles near 1 arcmin which is most likely due to the irregular distribution of young stars, visible in Figure 3.1. From the color profile, we can see a gradual reddening towards larger radii, particularly beyond $\sim$ 1 arcmin, consistent with the fact that we see bluer stellar populations are more centrally concentrated. The dashed line in the lower panel is the average color of the galaxy interior to 1 arcmin with a value of $(g-i)_o = 0.06$.

5.2 The Outer Low Surface Brightness Structure

Whereas the integrated light allows us to probe the central regions of Sag DIG to a moderately low surface brightness level of $\sim$ 28 mags/sq.arcsec, we can use resolved star counts as a proxy to characterize the low surface brightness shape and extent of Sag DIG. Specifically, we use RGB stars selected from the CMD to trace Sag DIG to very faint surface brightness, where in the previous analysis based on unresolved light, the foreground stars and intrinsic detector background overwhelm the extremely diffuse signal. By selecting only RGB stars, the distribution is now dominated by stars belonging to Sag DIG. We can use the edges of the wide field image to characterize a background level of Milky Way stars which occupy the same region in color magnitude space. This uniform background is characterized and is subtracted from radial profiles to probe the extended structure to much larger radii than the integrated light.

However, a caveat on this approach is necessary due to the dominant populations in each method. The extended stellar structure is dominated by RGB stars, hence we trace the presence of intermediate and old stellar populations. In contrast, the integrated light used in the previous section is a luminosity-weighted mapping of the structure of the galaxy and is generally biased to the younger, brighter populations present in Sag DIG. We must bear this inconsistency in mind when interpreting these profiles, particularly in combination with each other.

Prior to analyzing the stellar distribution, a correction must be applied for the large gaps between the CCDs in the CFHT/MegaCam focal plane, since star counts are artificially low (zero) in these regions. These gaps are clearly visible in the full CCD shown in Figure 3.1. While the chip gaps are located about 15' from the center of Sag DIG, they still pose a potential problem in generating a reliable radial profile and create an artificial feature in the spatial distribution. To minimize the impact of these gaps on a radial profile, we artificially generate RGB stars within gaps. The

spatial distribution of RGB stars are binned into pixels with a size 0.6' × 0.6' and those pixels with anomalously low star counts are identified. A low star count is determined to be more than $\sim 3\sigma$ lower than the mean values within the column across the detector. Artificial stars are added at random positions with these pixels until the total number of stars in this pixel is equal to the interpolated value based on its neighbours, allowing for Poissonian scatter. An example of star counts across a column in the detector is shown in Figure 5.5. The number of RGB stars is generally quite flat across the image, and the chip gaps are very distinct. Figure 5.6 shows the resulting spatial distribution of RGB stars with the gaps filled and Sag DIG is clearly visible. We can see that a few RGB stars are also added where there are saturated Milky Way stars. Just as with the chip gaps, these regions are artificially low due to the bright star, hence the added RGB stars help to generate a reliable radial profile and a smooth background. We use these artificial stars in what follows only when constructing 1 and 2-D density distributions of the RGB maps. The artificially added stars do not require color information, since we only consider RGB star density in the distribution.

RGB stars are selected from the CMD using the same selection criteria as used when deriving the luminosity function. An image of the density distribution of these stars is created using pixels with dimensions $0.1' \times 0.1'$. A Gaussian filter is applied, with $\sigma = 0.3$ arcmins. The mean background value and its standard deviation is estimated from the outskirts of the image (around a border with width 10 arcmins), and that is used to set appropriate contour levels. The resulting RGB density map is shown in the left panel of Figure 5.7 for the entire CFHT/MegaCam field, with contour levels at $1.5, 3$ and $10\,\sigma$ above the background. The right panel shows an enlargement of a 20 × 20 arcmins region centered on Sag DIG. Blue points are the positions of young blue stars, $-1 < (g-i)_o < 0$ and i_o <25 mags., for comparison.

5.3 Quantifying Shape

Figure 5.7 shows that the outer regions of Sag DIG is well described as a highly elliptical system. The faint extension are at a level of approximately $1.5 - 3\sigma$ above the background level.

To quantify the value for the ellipticity and position angle as a function of radius, we use the moments of the stellar distribution. We follow the procedure in McConnachie & Irwin (2006) and use an iterative process to define the parameters,

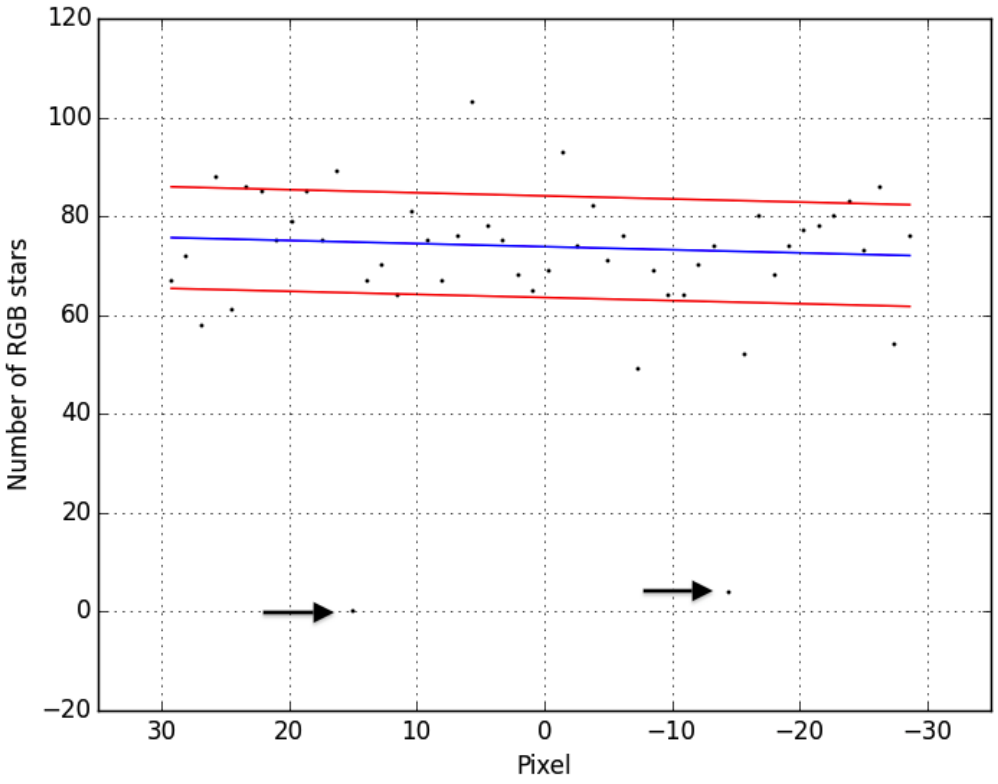

Figure 5.5 An example of the star counts binned in 0.6' × 0.6' pixels along one full column of the detector. The 2 wide chip gaps are clearly visible at approximately 15' and -15', symmetric about the center of the image. These points are highlighted with the black arrows. The blue line shows a linear fit to the data with the red lines being plus and minus 1.5σ.

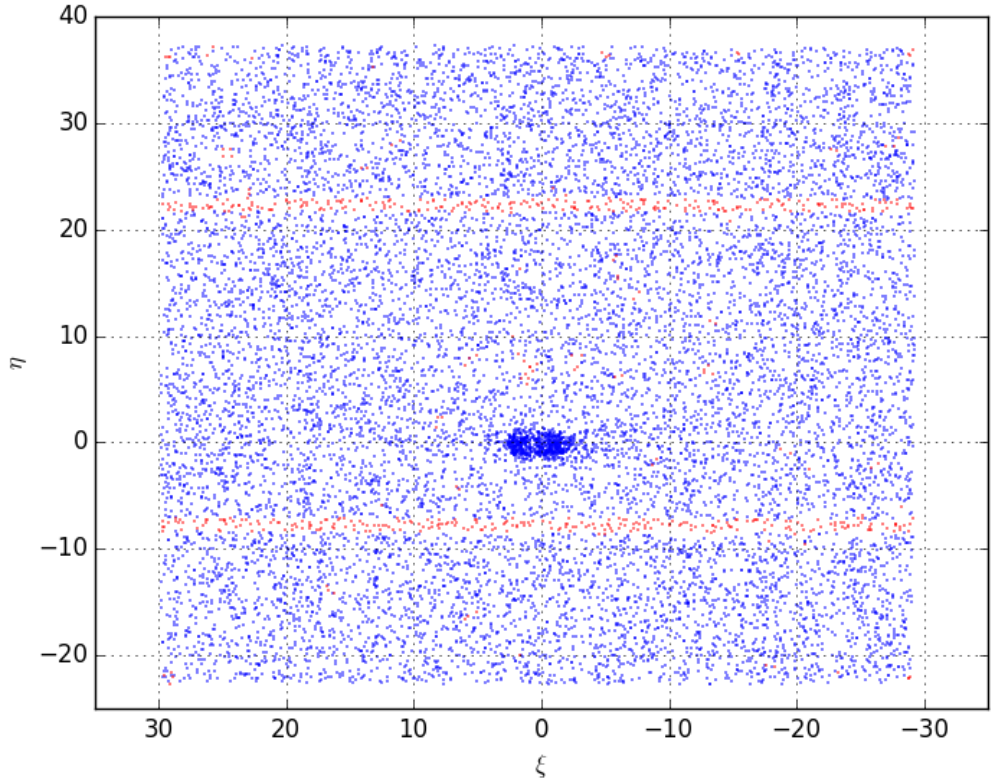

Figure 5.6 The artificially added stars are shown in red with the real stars shown in blue. We can clearly see that gaps have been filled, creating a smooth background. Some stars have also been added where a particularly bright foreground star exists.

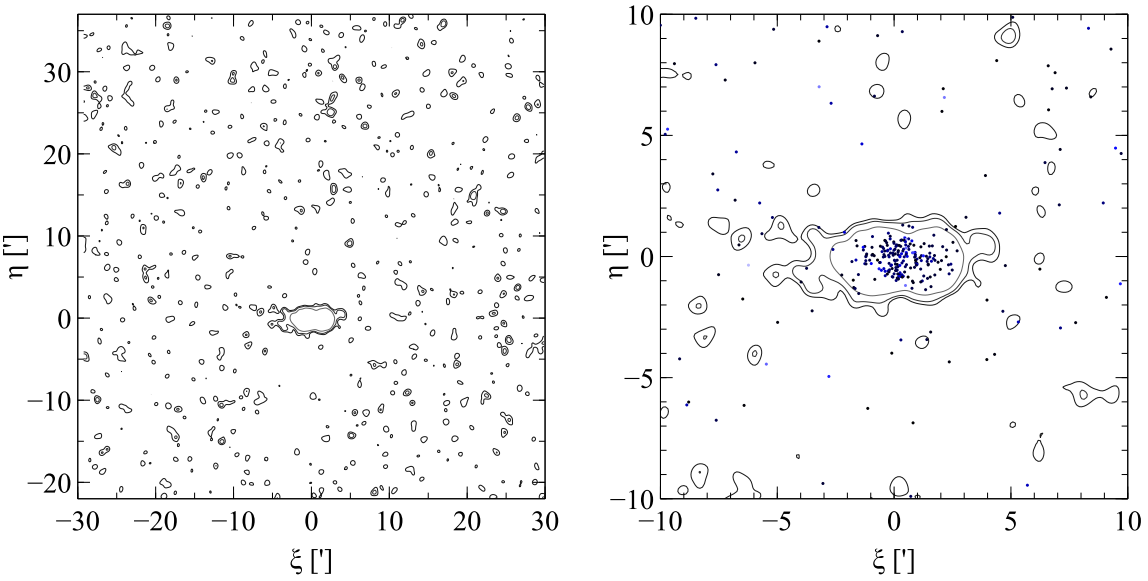

Figure 5.7 The left panel shows the RGB star distribution (RGB stars per unit area, relative to the median background) in the full 1° by 1° image. The right panel shows the inner region of the RGB stellar distribution with blue stars (selected with $-1 < (g-i)_o < 0$ and i_o <25 mags.) plotted as points. Contours: 1.5, 3 and 10 σ above the mean background. Bins are 0.1' and are smoothed using a gaussian filter with $\sigma = 0.3$ arcmins.

relative to the center of Sag DIG. Due to crowding, the center of Sag DIG is hard to define from these observations hence, we fix the center of Sag DIG at the literature value of $\alpha = 19^h29^m59.0^s$ and $\delta = -17^d40^m41^s$ (McConnachie, 2012). At a fixed distance from Sag DIG, we use all pixels that are within that distance from Sag DIG to calculate the moments of the distribution and hence the position angle and ellipticity. The moments are basically an intensity weighted mean. Specifically, from McConnachie & Irwin (2006), the position angle (P.A) and ellipticity (e) are given by:

$$P.A. = \frac{1}{2} arctan\left(\frac{2\sigma_{xy}}{\sigma_{yy} - \sigma_{xx}}\right) \tag{5.2}$$

$$e = \frac{\sqrt{(\sigma_{xx} - \sigma_{yy})^2 + \sigma_{xy}^2}}{\sigma_{yy} + \sigma_{xx}} \tag{5.3}$$

where σ_{xx}, σ_{xy}, and σ_{yy} are the intensity weighted second moments. Specifically, these moments are given by:

$$\sigma_{xx} = \frac{\sum_i (x_i - X)^2 I_i}{I_{tot}} \tag{5.4}$$

$$\sigma_{yy} = \frac{\sum_i (y_i - Y)^2 I_i}{I_{tot}} \tag{5.5}$$

$$\sigma_{xy} = \frac{\sum_i (x_i - X)(y_i - Y) I_i}{I_{tot}} \tag{5.6}$$

$$\tag{5.7}$$

where (X, Y) is the center of the galaxy, and (x_i, y_i) is the location of the i^{th} pixel with intensity I_i.

We then repeat the analysis, but this time using only those pixels contained within an ellipse with the newly derived ellipticity and position angle. This process is repeated until convergence. The resulting position angle and ellipticity are shown as a function of major axis radius in Figure 5.8. The hatched regions of these plots correspond to the approximate regions where crowding is problematic and so the estimates are unreliable. Solid lines indicate the adopted mean position angle and ellipticity of the outer points, between a semi-major axis of 2.5' and 7.5'. We find that $e = 0.53 \pm 0.04$ and $PA \simeq -0.52^\circ \pm 0.14^\circ$ with very little radial variation away from the center of the dwarf.

We also repeat this analysis using the HI gas from Hunter et al. (2012), which is

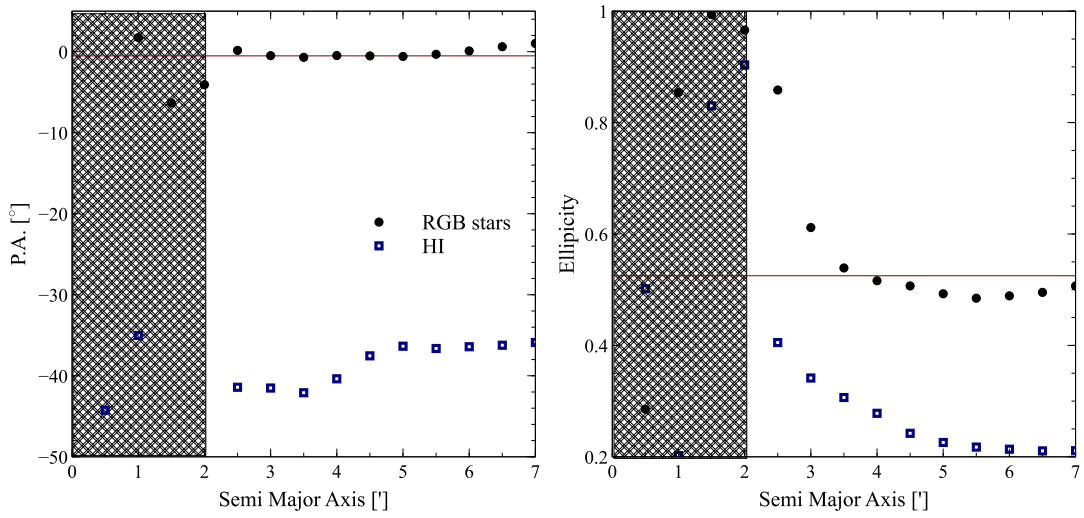

Figure 5.8 *Left:* The position angle as a function of the semi major axis, as described in the text. *Right:* The ellipticity as a function of the semi major axis, as described in the text. The shaded regions in all four plots indicate the region where the estimates are heavily influenced by crowding. The lines indicate the mean values for the shape parameters of Sag DIG adopted for this study.

discussed in more detail in Section 6.1. The position angle and ellipticity are shown in Figure 5.8 and are clearly distinct from the stellar values at all radii. This difference is explored further in Chapter 6.

5.4 Radial Profiles

The integrated light radial profile, introduced in Section 5.1, is limited by the lack of stars relative to the background at larger radii. We can extend this radial profile using RGB stars selected from the CMD, which will isolate Sag DIG's stars from the background contamination. Using the mean position angle and ellipticity, a series of elliptical annuli are used to determine a radial profile for the RGB density map shown in Figure 5.7, with the background value that was previously estimated subtracted from the final profile. Crowding in the CFHT imaging is a significant concern at radii smaller than approximately 2 arcmins. Within this radius, the radial structure is well mapped by the integrated light analysis conducted earlier. The RGB density profile (in units of stars/square arcminute) can be scaled to match the integrated light profile

(in units of magnitude/square arcsecond) by requiring that the average values of the points in the overlapping region between the integrated light and CFHT/MegaCam profile align. The blue points in Figure 5.9 show the i_0 band integrated light profile derived in Section 5.1.

Since the overlap region in the radial profile includes some points for which crowding issues are a concern, we choose to augment the star count data with similar star count data from the HST/ACS analysis by Momany et al. (2005). A DAOphot stellar catalogue was retrieved from the Hubble Legacy Archive, as described by Momany et al. (2005). In the same manner as described above, a CMD was constructed using the bluest (F475W) and reddest (F814W) filters and a set of tramlines used to isolate the RGB, shown previously in Figure 4.4. As the HST field of view is much smaller than that of CFHT MegaCam, there are no "background" reference fields, and the image is dominated by Sag DIG stars. The spatial distribution of RGB stars identified from the CMD are then used to construct a radial profile. The HST star counts data is shown in Figure 5.9 as green squares. The radial extent of this profile is limited by the field of view of the observations.

By combining the i_o band integrated light profile, the ground-based CFHT/MegaCam star counts data and the HST/ACS star counts data, Figure 5.9 shows the complete radial profile for Sag DIG over fully 8 magnitudes in surface brightness (a factor of 1500 in luminosity), extending down to as faint as nearly 33 mags/sq.arcsec. The shape of the annuli is fixed and is consistent across the full radial range of the combined profile. We remind the reader that the RGB and integrated light profiles are, in fact, potentially tracing different populations. The integrated light traces the luminosity-weighted stellar populations, and so is biased towards bright stars (i.e. the young stellar population that dominates the central regions) whereas the RGB profile traces intermediate and old stellar populations. We have used the i_0 integrated light profile, since it is likely a closer match to the population traced by the RGB than the bluer g_0 filter. From the absence of any significant "kinks" in the profile at the points at which we transition from one tracer to another, however, it appears that the net effect of using the different tracers is small.

We fit multiple profiles to all the points defining the overall radial profile in Figure 5.9, shown with the black lines. An exponential and a Plummer profile (with two free parameters) are shown in the left hand panel and Sersic and King fits (with three free parameters) are shown in the right hand panel. The exponential form used is the similar to the one preferred by Faber & Lin (1983):

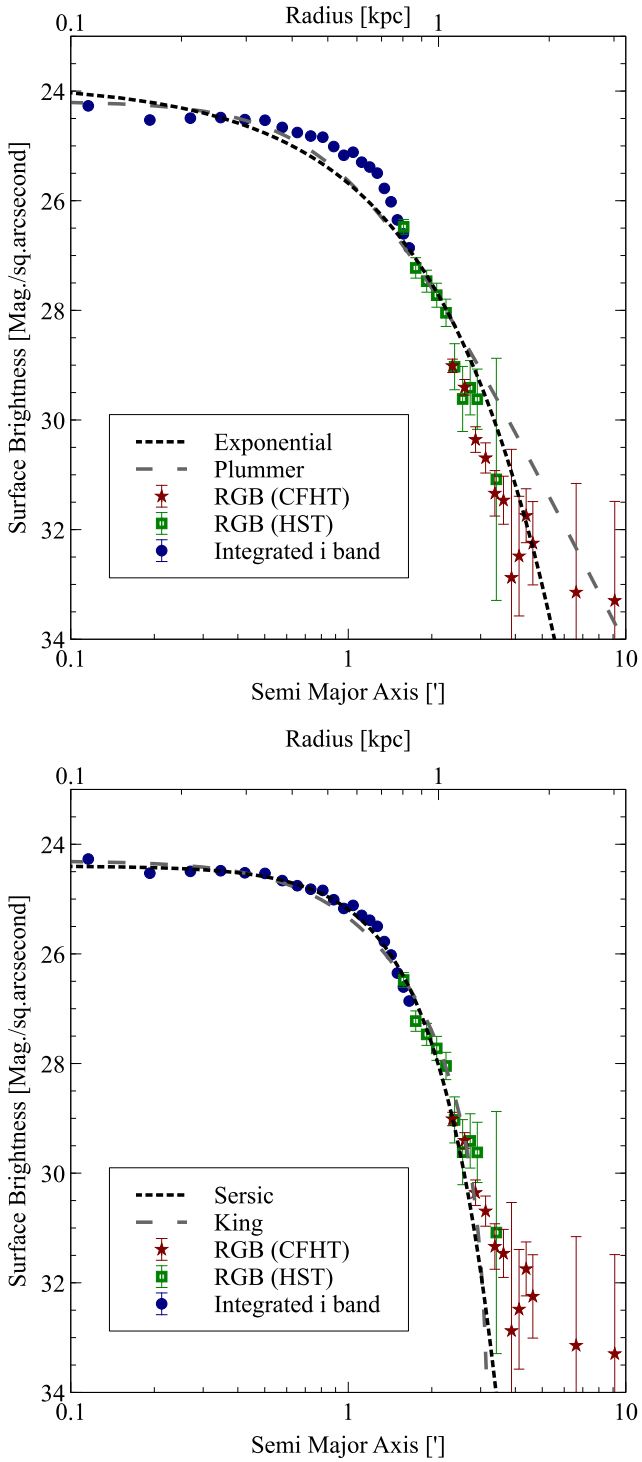

Figure 5.9 Radial profile for Sag DIG, using a combination of integrated light (blue points) and star counts from HST (green squares) and CFHT (red stars). The star count profiles are scaled vertically to match the integrated light profile in overlapping regions. The best-fit Sersic model is shown with the dashed line. See text for details.

$$I(r) = I_{o,e} exp\left(-\frac{r}{r_e}\right) \ . \tag{5.8}$$

The Plummer fit (for example, used by Law et al. 2005) is given by:

$$I(r) = I_{o,p} r_e^2 (r_e^2 + r^2)^{-2} \ . \tag{5.9}$$

The functional form for the Sersic fit (e.g. Graham & Driver (2005)) used is:

$$I(r) = I_{o,s} exp\left(-b_n \left(\frac{r}{r_e}\right)^{\frac{1}{n}}\right) \text{ where } b_n = 1.9992n - 0.3271 \ . \tag{5.10}$$

Finally, the King profile (King, 1962) is given by:

$$I(r) = I_{o,k} \left(\left(1 + \left(\frac{r}{r_c}\right)^2\right)^{-\frac{1}{2}} - \left(1 + \left(\frac{r_t}{r_c}\right)^2\right)^{-\frac{1}{2}}\right)^2 \ . \tag{5.11}$$

In fitting to the full profile, the uncertainty on the integrated light portion is artificially increased relative to the star-count portions. This increase partially reflects the systematic errors in this profile due to contamination from flux from the halos of foreground stars, and it gives more equal weight to the inner and outer portions of the profile in determining the best overall fit. The best-fit parameters (and derived quantities) for all fits are given in Table 5.1.

Adequate fits are obtained for both the Sersic and King profiles, whereas the exponential and Plummer profiles are unable to describe simultaneously the inner and outer portions of the radial profile. Specifically, the profile is considerably more cored than an exponential, as revealed by the Sersic $n = 0.49$. This is typical of many dwarf galaxies (e.g., Ferrarese et al. 2006). It is also clear that the best fit profiles systematically underestimate the surface brightness of Sag DIG in its extreme outskirts (i.e., beyond $\sim$ 4 arcmins, or $\sim$ 1.3 kpc). In this region, the profile is still monotonically decreasing, implying the presence of an extremely faint, extended population of RGB stars, the origins of which will be discussed in the next chapter.

From the King profile, we can also determine a concentration parameter c, given by:

$$c = log_{10}\left(\frac{r_t}{r_c}\right). \tag{5.12}$$

For Sag DIG, this value is $c \approx 0.47$, which is somewhat smaller than the value of

Table 5.1 Summary of parameters for sersic, exponential, king and plummer fits to the surface brightness profile. For explanation of the parameters, see Equations 5.8, 5.9, 5.10 and 5.11. The integrated magnitude and central surface brightness are derived for the i band.

Parameter	Value	
P.A.	$-0.5^\circ \pm 0.1^\circ$	
Ellipticity	0.53 ± 0.04	
r_e (Exponential)	0.59 ± 0.03'	0.199 ± 0.010 kpc
r_e (Plummer)	1.02 ± 0.05'	0.344 ± 0.017 kpc
r_c (King)	1.11 ± 0.06'	0.37 ± 0.02 kpc
r_t (King)	3.25 ± 0.07'	1.10 ± 0.02 kpc
r_s (Sersic)	0.949 ± 0.012'	0.320 ± 0.012 kpc
n (Sersic)	0.49 ± 0.02	
i_{total} (Sersic)	14.8 ± 0.2	mags.
i_{abs}(Sersic)	-10.6 ± 0.2	mags.
μ_o (Sersic[a])	24.40 ± 0.03	mags./sq.arcsecond

[a] Computed in the i band.

$c \approx 0.62$ found by Lee & Kim (2000).

5.5 Summary

By combining the integrated light profile in the crowded center of Sag DIG with the resolved RGB stellar density in the outskirts of Sag DIG, we are able to parameterize the shape and radial profile of this dwarf. We are able to trace the profile to large radii ($>r_s$) and to extremely faint surface brightness limits ($\approx 33 - 34$ mag./sq. arcsecond). We find that the radial profile is well fit by a single component but does show a surplus of stars at very large radii, suggestive of a possible stellar halo. These extended structures and their possible origins are discussed in the following chapter.

Chapter 6

Sag DIG's Components and Comparison with Other Dwarfs

We now study the gaseous HI component of Sag DIG in comparison the stellar structure traced by the RGB stars. Looking at the distribution and kinematics of the HI and the stellar distribution, we explore the possibility of these components being disk – like, and how they would relate.

Sag DIG is not alone in its morphology and structures. We compare it to Aquarius (also know as DDO 210) which has similar HI and stellar structures. In contrast, we look at the larger, but also well isolated, dwarf Wolf – Lundmark – Mellote (WLM), which has a very different structure.

6.1 On the Content and Structure of Sag DIG

Our CFHT/MegaCam CMD of Sag DIG shown in Figure 4.1 demonstrates the broad mix of stellar ages and recent star formation in this galaxy previously shown by multiple authors (e.g., Karachentsev et al. 1999, Momany et al. 2005, Weisz et al. 2014), and consistent with the findings for other isolated dwarf irregulars (see Weisz et al. 2014). Sag DIG contains a young population of massive blue stars (blue-loop and main sequence), the brightest of which imply star formation as recent as 50 Myrs years ago. A well populated RGB reveals a considerably older population. Using the TRGB, the distance modulus is estimated to be $(m\text{-}M)_o = 25.32^{+0.14}_{-0.13}$ (corresponding to a distance of $1.16^{+0.08}_{-0.07}$ Mpc). The color of the RGB is remarkably blue, and if this effect is due to metallicity then it implies a mean metallicity of order [Fe/H]$\simeq$

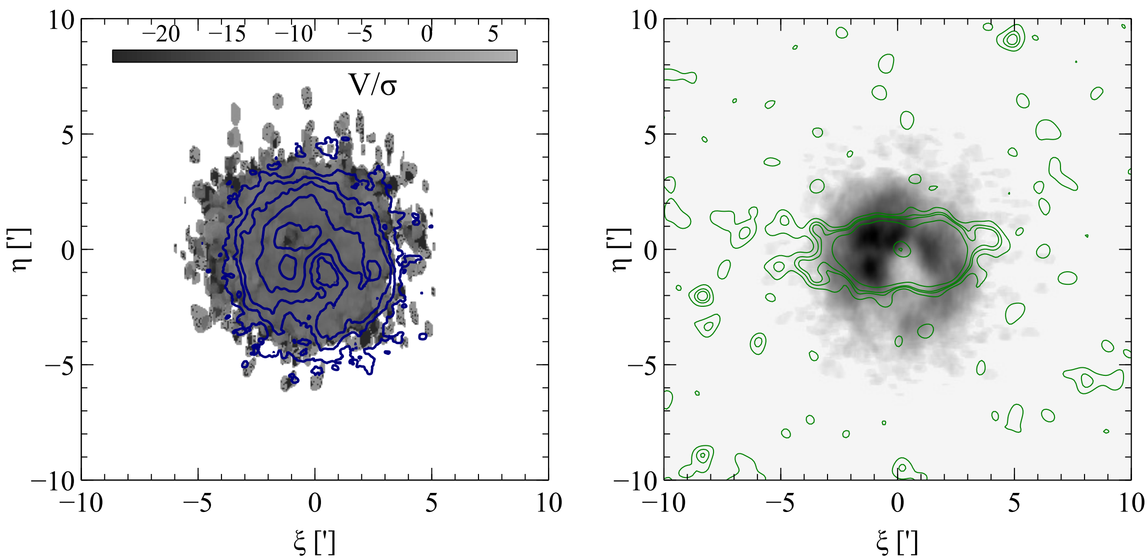

Figure 6.1 *Left:* HI is shown with contours at 10, 50, 100, 250, 500 (Jy/beam)(m/s) as seen previously in Figure 3.1. The underlying grey scale is shows the velocity divided by dispersion from the analysis by Hunter et al. (2012). *Right:* The RGB star distribution is shown in the contours (1.5, 3,10 σ above the mean background) overlaying the HI distribution in greyscale.

-2.2 dex. While the "red" loop of He burning stars may contribute to the RGB width, the lack of a clear vertical sequence suggest that this effect is minor. Comparison of the inner and outer regions of Sag DIG shows that there is a spatial gradient in the stellar populations. The majority of the young stars are centrally concentrated, and those bright main sequence stars in the central regions appear to extend to younger ages than the bright main sequence stars at larger radius. The RGB stars in the central regions also appear to extend to bluer colors – implying a larger contribution of RGB stars from intermediate age stellar populations compared to the older stars in the outer regions – although this difference is not statistically significant.

We can trace the low surface brightness structure of Sag DIG using the RGB star count maps. The main body of the dwarf is highly elliptical in shape ($e = 0.53$) with no obvious isophote twisting as a function of radius. Instead, it looks similar to an inclined stellar disk (although we note that, in the absence of stellar velocities, it is also possible that Sag DIG is a highly ellipsoidal system). Under the assumption of an inclined disk, we can use the shape of the observed distribution of RGB stars to constrain the possible inclination angle of Sag DIG. As a low mass system, several observational studies have shown that we do not expect the stars to be in a thin disk akin to large galaxies (see Roychowdhury et al. 2010; Sánchez-Janssen et al. 2010). From a theoretical perspective, we expect pressure support to be more important in low mass dark matter halos, leading to puffier disks (Kaufmann et al. 2007). We therefore assume that the galaxy is in a circular disk with a radius (A) equal to the semi-major axis, a, and a uniform thickness C. The observed semi-minor axis, b, is therefore a function of both C and the inclination, i, such that

$$b = Acos(i) + Csin(i) \ . \tag{6.1}$$

The resulting inclination is shown in Figure 6.2. For the measured ellipticity of $e = 0.53$ and an infinitely thin disk, then the minimum inclination of Sag DIG is $i \approx 62°$. At the other limit – i.e. assuming we are seeing Sag DIG edge-on – then the maximum thickness of Sag DIG is $C/A \approx 0.48$. Thus, even if the main body of Sag DIG is a thickened disk, we are observing it relatively close to edge on.

The HI structure of Sag DIG has been analyzed in detail previously by Lo et al. (1993), Young & Lo (1997) and Beccari et al. (2014) and it is interesting to compare this structure with our extended stellar maps. Figure 6.1 shows the integrated HI map of Sag DIG from the LITTLE THINGS Survey (Hunter et al., 2012) in comparison

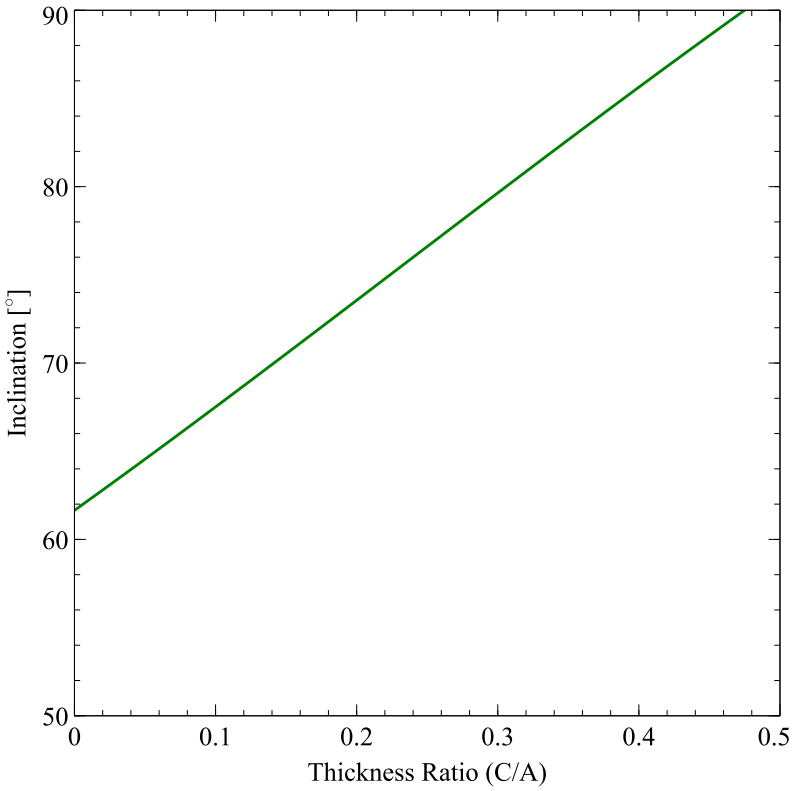

Figure 6.2 The inclination given observed shape as a function of thickness considering the galaxy as a thick circular disk (cylindrical in shape) with the mean ellipticity found for the RGB stars.

to the RGB stellar distribution discussed previously. Two aspects are particularly notable. Firstly, the distribution of stars and gas are strikingly different within this galaxy, with the stars showing an elongated distribution and the gas showing a much more circular shape. We note that there is a prominent feature (a hole) in the HI distribution, and Momany et al. (2002) have previously suggested that the hole is due to stellar feedback, although they were unable to find any significant correlation between the location of the hole and the location of the most recent star formation for Sag DIG. Secondly there is no clear signature of rotation of the gas in Sag DIG in the left panel of Figure 6.1, showing $\frac{V_r}{\sigma}$. Indeed, the gas is either nearly entirely pressure supported or we are observing the disk face on. For the stars, we have established that if the stars are distributed in a disk, we must be observing this disk closer to edge on, not face on. It would be quite unusual to have disk of gas presented nearly perpendicular to the stellar disk, although not unprecedented, even in the Local Group. NGC6822 has been shown by Battinelli et al. (2006) to have the gas oriented at a large angle relative to the stars, making it the closest example of a polar ring galaxy and necessitating a merger at some point in its relatively recent past. As well as demonstrating Sag DIG to be a highly elliptical system, Figure 5.7 shows that the outermost few contours of the galaxy (at 1.5σ and 3σ above the background) have a mild distortion that looks like a stretching of the contours along the major axis direction. It is difficult to interpret what, if anything, this feature indicates without ancillary data such as stellar radial velocities. If Sag DIG was closer to a large galaxy it could be interpreted tentatively as evidence for a tidal interaction. Additional insight into the extended structure of Sag DIG comes from analysis of the radial surface brightness profile. We augment the $i-$band integrated surface brightness profile of Sag DIG with RGB star counts from the CFHT/MegaCam data at large radius, and RGB star counts from HST at intermediate radii. The resulting surface brightness profile extends over 8 magnitudes and is remarkably smooth. It is generally well fit by a Sersic or King profile over most of its radius (exponential and Pummer profiles with one less parameter do not do a satisfactory job of fitting the inner and outer regions of the profile simultaneously), but it still shows a very low level excess of stars at large radius (> 3 arcmins) in comparison to both of these model fits. These four profiles are fit to both characterize the profile and for easy comparison to other studies in the literature. Of the four, only the King profile has a physical interpretation. This profile makes the assumption that each star is equally massive, are on radial orbits and that the whole system resides in a larger potential

well. This external potential truncates the potential at a tidal radius. In contrast, the Plummer profile does not have a cutoff and is a more extended function. The King profile generally well describes Milky Way globular clusters, which are clearly influence by our galaxy. In contrast, Sag DIG does not reside in a more massive dominant potential, hence we do not expect it to be truncated at the tidal radius. As expected, we do see stars at large radii, not well fit by the King profile. If indeed Sag DIG were to be truncated, this would have interesting implications for the idea that this is an isolated dwarfs.

What could be the origin of this excess of stars at large radius in Sag DIG compared to the single component fits? Irwin & Hatzidimitriou (1995) originally called this signature "extra-tidal stars". These authors coined this phrase since they were fitting King profiles to Milky Way dwarf spheroidal satellites, and this excess was seen beyond the nominal King tidal radius. One physically plausible origin for them is that they are stars that were heated from the dwarf in its orbit around the Milky Way due to tidal effects. For Sag DIG, however, its extremely large distance from any large galaxy makes this unlikely, since tidal distortions are transitory in nature. Thus, even if Sag DIG had at one point been tidally harassed by a large galaxy, any signature would long since have disappeared (e.g. Peñarrubia et al. 2009). If the very low level distortion on the outermost contours of the two dimensional surface brightness profile are related to this feature in the radial surface brightness profiles, then a more likely tidal scenario for Sag DIG is that it has experienced a merger of a much smaller object – perhaps a globular cluster – and that we are observing the remnants of this interaction.

Another possible interpretation of the radial surface brightness profile, that we deem more likely than the tidal interaction scenario, is that Sag DIG is not well described by a single component model because Sag DIG does not consist of only a single component. Rather, there is a secondary, much more extended, lower surface brightness and lower luminosity component to the galaxy that surrounds the highly elliptical main body i.e., a stellar halo. Indeed, such a scenario is not particularly unusual; bright galaxies are known to possess multiple stellar components and more recent work on nearby dwarf galaxies have suggested that multiple components are ubiquitous even at low stellar mass (e.g., Martínez-Delgado et al. 1999; Lee et al. 1999; Lee & Byun 1999; Lee & Kim 2000; Kleyna et al. 2003; Tolstoy et al. 2004; Kleyna et al. 2004; Vansevičius et al. 2004; Battaglia et al. 2006, 2008, 2011; McConnachie et al. 2007a; Hidalgo et al. 2008; Bellazzini et al. 2014).

Table 6.1 Summary of parameters for Sag DIG, Aquarius (DDO 210) and Wolf Lundmark Mellote (WLM).

	Sag DIG	Ref.	Aquarius	Ref.	WLM	Ref.
Distance [Mpc]	$1.16^{+0.08}_{-0.07}$	(1)	0.977 ± 0.045	(2)	0.985 ± 0.033	(11)
E(B-V) [mag.]	0.12^{a}	(3)	0.045	(3)	0.035	(12)
Stellar Mass [$M_\odot$]	1.14×10^{6b}	(1)	$1 - 2 \times 10^6$	(2,4,5)	1.1×10^7	(13)
HI Mass [$M_\odot$]	1.0×10^7	(6)	8.8×10^6	(7)	$(6.3 \pm 0.3) \times 10^7$	(14)
Stellar [Fe/H] [dex]	~ -2.2	(1)	-1.44 ± 0.03^{c}	(8)	-1.28 ± 0.02^{e}	(11)
Mean Age [Gyrs.]	6	(9)	13	(9)	3	(9)
Stellar Ellipticity	0.53	(1)	0.6 [d]	(10)	~ 0.5	(11)

References: (1) this work (2) Cole et al. (2014) (3) Schlafly & Finkbeiner (2011) (4) Young & Lo (1997) (5) McConnachie (2012) (6) Young & Lo (1997) (7) Young et al. (2003) (8) Kirby et al. (2013) (9) Weisz et al. (2014) (10) McConnachie et al. (2006) (11) Leaman et al. (2012) (12) McConnachie et al. (2005) (13) Jackson et al. (2007) (14) Kepley et al. (2007)

[a] In agreement with Table 1, computed here as the mean value for each star, where as Table 1 is the central value.

[b] Computed using M/L$\sim$ 1 and $i_\odot$ =4.58 mags Blanton et al. (2003)

[c] Derived from spectra of individual RGB stars, with uncertainty reflecting the spread in metallicity between stars.

[d] In the central part, varies to 0.4 at larger radii.

[e] Determined spectroscopically from RGB stars. Photometric estimate from RGB stars is -1.45 ± 0.2 dex from Minniti & Zijlstra (1997).

We note that the recent analysis of Sag DIG by Beccari et al. (2014) trace the profile to approximately 4 arcminutes and did not observe this an excess. Comparison of the surface brightness profiles shows that our CFHT/MegaCam data and large field of view have allowed us to push to larger radii and lower effective surface brightness required to identify this feature.

6.2 Sag DIG in Comparison to Other Local Group Dwarfs

As an extremely isolated, very low mass dwarf galaxy, Sag DIG is an important target for understanding galaxy evolution at the lowest mass end. However, it is not unique. The closest known galaxy to Sag DIG is the Aquarius dwarf (DDO 210) at a separation of $\sim$ 400 kpc. These two galaxies bear some similarities that makes comparison of

their properties particularly interesting. Both are located at large distances (>1 Mpc; McConnachie 2012) from the Milky Way and M31, making recent tidal interactions with these large systems unlikely. Both are comparable in luminosity ($M_V = -11.5$ and -10.6 for Sag DIG and Aquarius, respectively), implying their stellar masses are the same to within a factor of a few. Both systems are relatively gas rich, with HI masses of $M_* = 4.1 \times 10^6 M_\odot$ and $M_* = 8.8 \times 10^6 M_\odot$ for Aquarius and Sag DIG respectively. The general properties of these two systems are summarized in Table 6.1, along with a third dwarf, WLM, introduced later.

Recently, the detailed star formation history of Aquarius has been determined through deep CMD analysis by Cole et al. (2014) that reaches one magnitude below the oldest main sequence turn-off. Aquarius is found to possess a very small old (>10 Gyrs) population, with a peak in its star formation approximately 6 - 8 Gyrs ago, after which the star formation rate has been declining until the present day. Without similarly deep CMDs for Sag DIG, it is not possible to derive a SFH of similar quality for this galaxy. However, as previously discussed, the SFH derived by Weisz et al. (2014) suggests that Sag DIG is not dominated by an old population like many Local Group galaxies. On a qualitative note, the stellar content of Sag DIG and Aquarius are broadly similar; ground based CMDs for both galaxies (see McConnachie et al. 2006 for a ground-based CMD of Aquarius) have well defined RGB populations, weak AGB populations and significant numbers of bright main sequence/blue loop stars. However, in contrast to Sag DIG, Aquarius is not observed to be forming stars at the present, although it was forming stars as recently as a few tens of Myrs ago. For this reason, it is formally classed as a transition-type galaxy. At the low mass end, there may not be a fundamental distinction between a dwarf irregular and a transition-type galaxy, since low level star formation in a dwarf irregular may naturally lead to periods of little or no star formation (so-called "gasping" e.g., Tosi et al. 1991 and also Weisz et al. 2011).

Both Aquarius and Sag DIG also share similarities in their HI structure relative to their stars. The main stellar bodies of both galaxies are relatively elliptical in extent yet both have integrated HI maps that imply a more spherical gas distribution (or a disk that is inclined at a significantly different angle to the stellar disk; see Young et al. (2003) for an HI map of Aquarius). Figure 6.3 from McConnachie et al. (2006) shows the HI structure relative to the stars. Sag DIG shows no evidence of rotation in the HI, and Aquarius shows a low level systematic rotation with a peak velocity near $\sim$16 km s^{-1} (Begum & Chengalur, 2004).

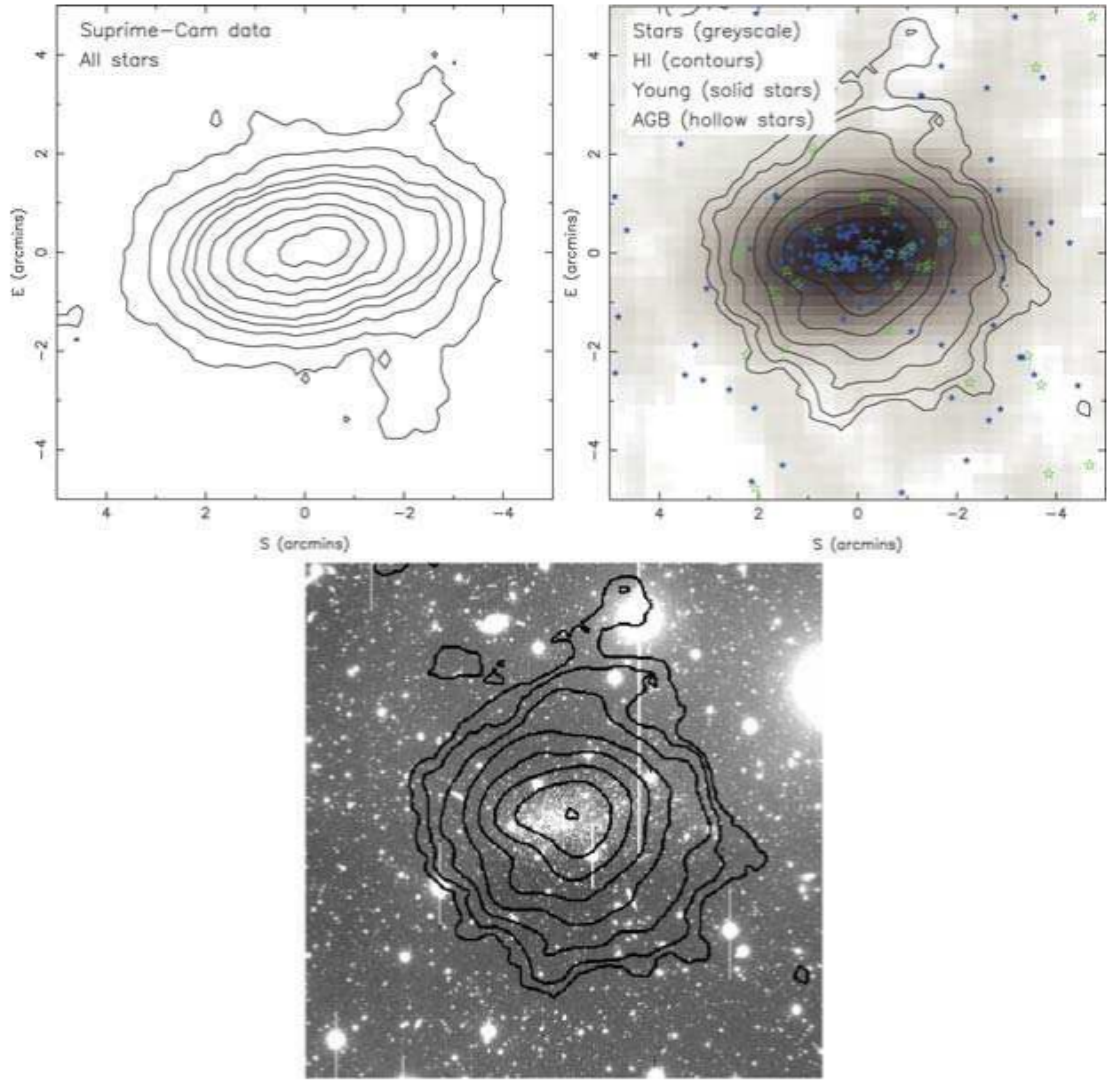

Figure 6.3 From McConnachie et al. (2006), the stellar and HI distribution in Aquarius. The *Upper Left* panel shows the RBG star distribution, which is shown as a grey scale in the *Upper Right* panel, along with the HI gas in contours. The HI contours are shown in the *Lower* panel again with the stellar image.

We can contrast the similar structures of Aquarius and Sag DIG with another, well studied dwarf, Wolf – Lundmark – Mellote (WLM). Leaman et al. (2012) studies this isolated dwarf irregular galaxy in detail. Its general characteristics are included in Table 6.1. Overall, it is similarly isolated, but is younger, more metal rich and more massive by about a factor of 10. Looking at its stellar and HI structure, shown in Figure 6.4 from Leaman et al. (2012), we can see that the young and older stellar components, and HI all follow very similar structures. For WLM, the RGB stellar distribution is slightly more spherical than the HI component. The HI gas is also marginally more extended, but overall, the stellar and gaseous components seem to trace each other well, in contrast to Aquarius and WLM.

The stellar kinematics of both WLM and Aquarius are studied by Leaman et al. (2012) and Kirby et al. (2014) respectively. As mentioned above, the HI gas of Aquarius does show some systematic rotation, unlike Sag DIG. The stellar component is also found to be rotating by Oh et al. (2015) who find the rotation curve of Aquarius to be well fit by both an NFW profile and a pseudo isothermal model. The stellar and HI kinematics in WLM were characterized in detail by Leaman et al. (2012) using spectroscopy of RGB stars. Neither the rotational nor dispersion component dominates. The stellar populations of all ages show rotation, but it agrees with the rotation shown by the HI. The stellar dispersion is larger than that of the HI. Leaman et al. (2012) suggests that the kinematics are likely due feedback mechanisms within isolated evolution.

The extended star formation of both Aquarius and Sag DIG is a feature common to all dwarf irregular/transition-type galaxies (e.g., Weisz et al. 2011). However, delayed star formation, such as that in Aquarius, appears to be relatively common for highly isolated low mass systems (see Cole et al. 2014 for a discussion relating to Aquarius and Leo A) and so it will be important to determine if Sag DIG also follows this behaviour. Certainly, it is possible that the lack of any nearby large antagonists means that interactions at early times do not trigger star formation in these systems as might occur for closer satellites. Further, at the low mass end, the relationship between the accretion of dark matter and the accretion of baryons may be much more stochastic, such that these galaxies might not have accreted large amounts of gas at early times to fuel significant star formation. WLM's SFH shows a much larger fraction has formed at more recent times as compared to Sag DIG and Aquarius (Weisz et al. 2014). Reionisation is also often argued to have a significant impact on the early star formation of low mass dwarfs, but there is little evidence

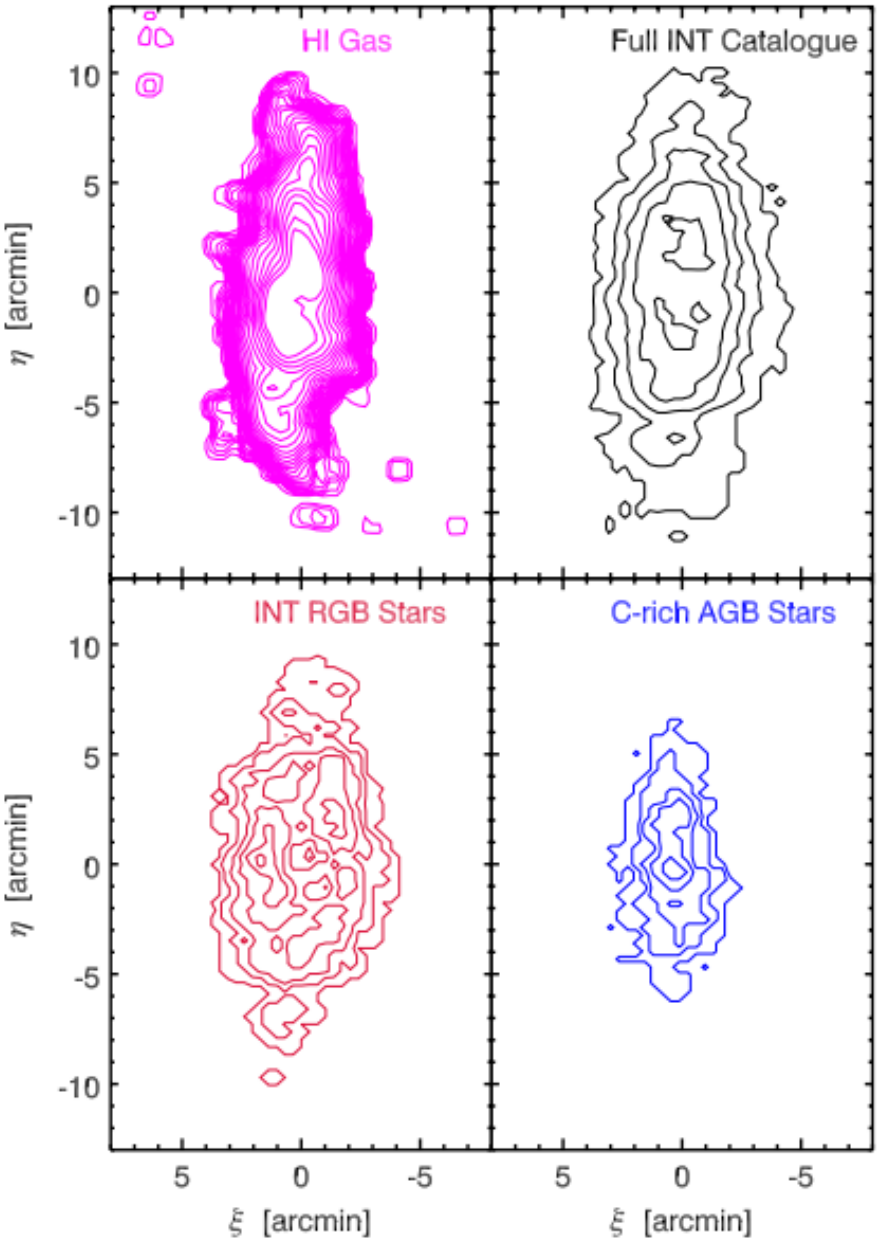

Figure 6.4 From Leaman et al. (2012), the stellar and HI content of WLM. The *Upper Left* panel shows the HI gas, *Upper Right* shows all resolved stars. *Lower Right* shows the RGB stars and *Lower Left* shows just the carbon right AGB stars.

for this amongst those galaxies that have accurate star formations at early times (see Weisz et al. 2014). It is nevertheless conceivable that the gas that is accreted at early times in these low mass galaxies is heated by reionization and does not cool sufficiently until later times at which point it start forming stars again.

Indeed, a process whereby the gas is heated in these small systems could be necessary to explain the difference between the stellar distribution (as traced by older RGB stars) and HI structures seen in Sag DIG and Aquarius. In particular, it is plausible that the gas has been re-shaped by internal processes like star formation or supernova feedback that heats up the gas. Once heated, the gas stays in the vicinity of the dwarf until it cools again. Once it has cooled again, the structure of the HI and the stellar structure of the galaxy can appear decoupled from each other, as is seen in these two galaxies. This idea is tentatively supported by the fact that the youngest stars in Aquarius are offset by several arcminutes from the center of the galaxy as traced by the oldest populations, and align with a slight "dent" in the HI, perhaps suggesting that the gas is not virialised and the HI is relatively recently accreted. This scenario is also interesting as it applies specifically to low mass and isolated systems: for more massive dwarf galaxies, like WLM, it is harder to heat the gas significantly, and so the gas and the stellar component are more likely to remain closer coupled; for satellite systems, once gas is heated and no longer at the center of the gravitational potential of the galaxy, it is more easily tidally stripped such that it does not have the chance to cool again. Clearly, however, Aquarius and Sag DIG are good examples of the inadequacy of assuming that the HI resides in a thin, rotationally supported disk, and that this disk bears any similarity to the structure of the bulk of the stellar populations. While this assumption appears true from WLM, it is clearly incorrect at lower stellar masses.

6.3 Summary

The HI and stellar components of Sag DIG are intriguing in the stark difference in their shape and structure. Without stellar kinematics, it is challenging to determine how these components relate to each other, and whether they are disk – like. These structures are similar to DDO 210 and in distinct contrast to the structure of WLM. It is possible that the differing masses of these dwarfs or their own SFH histories generate these differences.

Chapter 7

Conclusions and Extensions

The general properties of Sag DIG derived here are summarized. The remaining dwarfs in the *Solo* data set will be analyzed in an analogous manner. Additionally, extensions to this initial analysis, such as using stellar kinematics, are explored.

7.1 Future Work

Work on the dwarfs in *Solo* Survey will continue with all dwarfs analyzed using the same methods as applied to Sag DIG. The resulting data set will be consistent, so the general characteristics of dwarfs can be determined, both for all isolated nearby dwarfs, and subsets within the survey. The amount of previous analysis for these isolated dwarfs varies substantially. For instance, those in Kirby et al. (2014) have stellar kinematics, and the majority are in the LITTLE THINGS sample from Hunter et al. (2012) with detailed HI analysis. Additionally some, like Sag DIG, do have HST imaging available. Following the example set by this work, the remaining *Solo* dwarfs will be studied, taking into account the archival data available, and limitations, like very low stellar mass.

This survey is ideal for characterizing the irregular types. As stated in the introduction, most dwarf irregulars are isolated, where as dwarf spheroidals are generally close to a host. One comparison of interest using the full *Solo* sample will be the size verse magnitude of the isolated dwarfs in comparison to the satellites of M31 and the Milky Way. As described initially by McConnachie & Irwin (2006), the characteristic sizes of dwarfs of a given luminosity are different for these two subsets. However, with additional dwarfs discovered, Brasseur et al. (2011) found no statistical differ-

ence between the two populations, corroborated by McConnachie (2012) . It will be interesting to determine how the isolated dwarfs fit into this picture.

Of course, each individual dwarf in the survey is also interesting in its own right. The extended structure for many of the dwarfs has not be studied and could reveal unusual or interesting features. Indeed, the extended elliptical stellar structure of Sag DIG was not anticipated in this current analysis. These faint structures should be visible in the entirety of the *Solo* dataset. Indeed, using resolved stellar analysis is the only way in which such structures may be observed. At greater distances, crowding in the central regions will become increasingly problematic, but the outskirts remain resolved. The depth of the CMD will decrease and for the most distant dwarfs, only the brightest magnitude of the RGB branch will be observable. However, using the same methods, we can trace structures much fainter than would be possible using unresolved light. For dwarfs at low galactic latitude, like Sag DIG, the high level of foreground contamination makes finding faint structures is more challenging. Fortunately, most of the dwarfs at large distances (>2 Mpc) are, in fact, away from the Galactic disk (with an obvious exception of KKH 86).

We can also look for globular clusters for these dwarfs. For example, using similar CFHT observations Huxor et al. (2014) find a number of globular clusters in M31's halo within the PAndAS data, which is a similar distance as several *Solo* dwarfs. Using comparable techniques, identifying globular clusters in the *Solo* dwarfs is possible.

For Sag DIG in particular, stellar kinematics would be very interesting to add to this analysis. While we know that the HI appears spherical and shows no rotation, we are limited to only the stellar distribution without kinematics. It would be enlightening to know if the stellar component also exhibits no rotation like the gas, or if it looks more like a rotating disk as the stellar distribution might suggest. Kirby et al. (2014) did look at the stellar dynamics of seven isolated local group dwarfs, however excluded Sag DIG due to its low galactic latitude and resulting high Galactic contamination in the field. A similar analysis, using a multi-object spectrograph, could be used for Sag DIG, with very careful identification of sources to be sure that they do, in fact, belong to the dwarf.

In addition, the ideally suited, wide field imaging from the *Solo* Survey can be used to look for very faint satellites of nearby isolated dwarfs. Dark matter simulations rely on the fact that dark matter is scale free. That is, the hierarchy of structures does not depend on size. This scale-free nature is clearly seen in Figure 7.1 from Moore et al. (1999) where, without a scale given, it is impossible to tell a galaxy

cluster from a galaxy halo. We therefore expect, just as large galaxies have satellites, these small dwarfs also could have satellites. These satellites would be very faint and extremely low surface brightness, hence have not yet been observed. However, we do predict their presence (Wheeler et al. 2015). By looking in the vicinity of the isolated dwarfs, we maximize our chance of discovering these satellites of dwarfs. Any discoveries would join the growing list of nearby dwarfs. These new dwarfs would also help alleviate the tension between the number of dwarfs predicted by dark matter simulations and the deficit observed today, dubbed "the missing satellite problem". These possible satellites of dwarfs can constrain the size of the smallest dark matter halos which have a the ability to form stars, a necessary and unknown parameter such simulations (Peñarrubia et al. (2008)).

7.2 Summary

In this paper, we have introduced *Solo*, the *So*litary *Lo*cal Dwarfs survey. *Solo* is a wide field photometric survey targeting every isolated dwarf galaxy within 3 Mpc of the Milky Way, based on $(u)gi$ multi-band imaging from CFHT/MegaCam in the north, and Magellan/Megacam in the south. All galaxies fainter than $M_V \simeq -18$ situated beyond the nominal virial radius of the Milky Way and M31 are included in this volume-limited sample, for a total of 42 targets. We also present first results for Sag DIG, one of the most isolated, low mass galaxies at the edge of the Local Group.

The resolved stellar populations analyzed here are consistent with previous ground based studies of this galaxy. We provide updated estimates of its central surface brightness and integrated luminosity, and trace its surface brightness profile to a level fainter than 30 mags./sq.arcsec using a combination of integrated light and resolved stars. Sag DIG is well described by a highly elliptical (disk-like) system following a single component Sersic model, with a low-level distortion present at the outer edges of the galaxy. Were Sag DIG not so isolated, these distortions would likely be attributed to some kind of previous tidal interaction. We also show that Sag DIG has an excess of stars at large radius, over and above that expected for a single component Sersic fit to the inner regions. We suggest that this is evidence of an extended stellar halo around this galaxy, although much deeper imaging data will be required to confirm this hypothesis to obtain sufficient star counts at large radius.

The stellar and HI structures of SagDIG are compared with those in Aquarius, a similarly isolated low mass galaxy also at the edge of the Local Group. Both

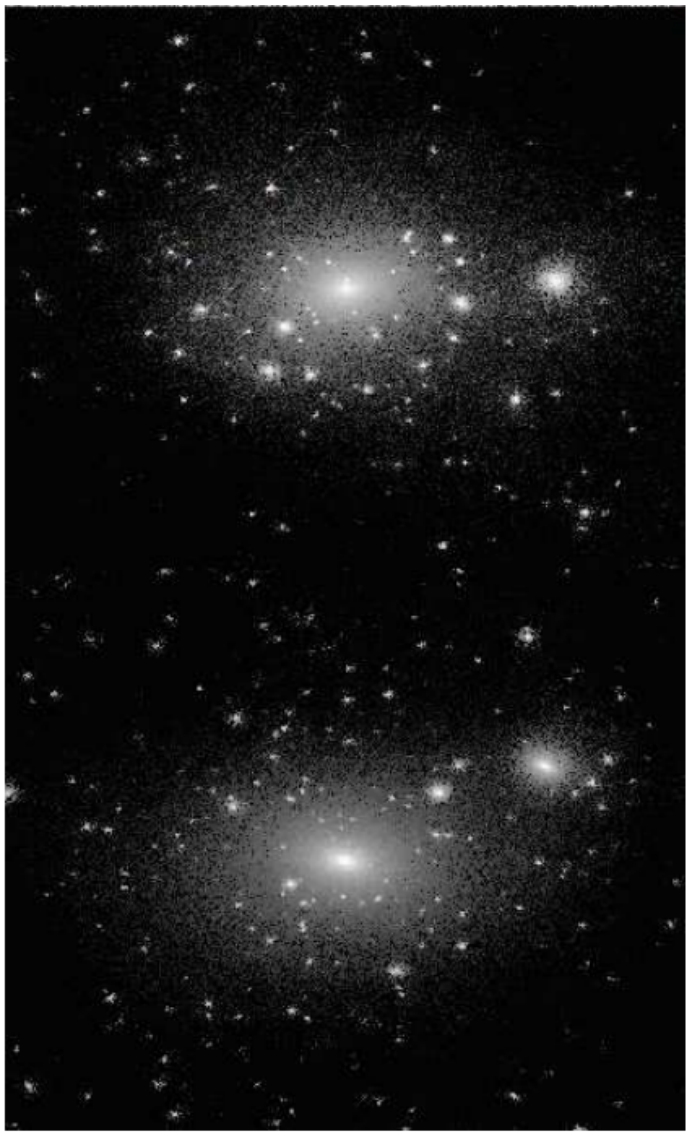

Figure 7.1 From Moore et al. (1999), showing the dark matter density from two snapshots within their simulation. The *upper panel* shows a galaxy cluster with a mass of $5 \times 10^{14} M_{\odot}$ and the *lower panel* shows a galaxy halo with a mass of $2 \times 10^{12} M_{\odot}$.

systems have a clear mismatch between their integrated stellar and HI structures. This difference in structures may be related to both their low mass and isolated locations, which permits the re-accretion of HI into their central regions after this gas was puffed up via some heating mechanism (likely earlier generations of star formation in the galaxy). In contrast, WLM is a similarly isolated, but slightly more massive dwarf. This dwarf shows a clear correlation in the spatial and kinematic distribution of its stellar and gaseous components.

The derivation of a comprehensive set of parameters to describe the global properties of Sag DIG is the first step to the derivation of a comprehensive set of parameters for all galaxies in the *Solo* sample, using a homogeneous dataset and consistent analysis procedures. Our comparison of Sag DIG with Aquarius and WLM also highlights the early usefulness of *Solo* in building up a more systematic understanding of the structures of dwarf galaxies in the very local Universe, that can inform interpretation of other systems for which resolved stellar analyses are not possible. The *Solo* dwarfs offer the opportunity to build a comprehensive understanding of the properties of low mass systems that have evolved in isolation for comparison to the satellite systems of the Local Group and other galaxy groups.

Bibliography

Abadi, M. G., Navarro, J. F., Steinmetz, M., & Eke, V. R. 2003, Astrophysical Journal, 591, 499

Barber, C., Starkenburg, E., Navarro, J. F., McConnachie, A. W., & Fattahi, A. 2014, Monthly Notices of the RAS, 437, 959

Bate, N. F., McMonigal, B., Lewis, G. F., et al. 2015, Monthly Notices of the RAS, 453, 690

Battaglia, G., Fraternali, F., Oosterloo, T., & Sancisi, R. 2006, Astronomy and Astrophysics, 447, 49

Battaglia, G., Helmi, A., Tolstoy, E., et al. 2008, Astrophysical Journal, Letters to the Editor, 681, L13

Battaglia, G., Tolstoy, E., Helmi, A., et al. 2011, Monthly Notices of the RAS, 411, 1013

Battinelli, P., Demers, S., & Kunkel, W. E. 2006, Astronomy and Astrophysics, 451, 99

Beccari, G., Bellazzini, M., Fraternali, F., et al. 2014, Astronomy and Astrophysics, 570, A78

Bechtol, K., Drlica-Wagner, A., Balbinot, E., et al. 2015, Astrophysical Journal, 807, 50

Begum, A., & Chengalur, J. N. 2004, Astronomy and Astrophysics, 413, 525

Bellazzini, M., Cacciari, C., Federici, L., Fusi Pecci, F., & Rich, M. 2003, Astronomy and Astrophysics, 405, 867

Bellazzini, M., Ferraro, F. R., & Pancino, E. 2001, Astrophysical Journal, 556, 635

Bellazzini, M., Beccari, G., Fraternali, F., et al. 2014, Astronomy and Astrophysics, 566, A44

Bernard, E. J., Gallart, C., Monelli, M., et al. 2008, Astrophysical Journal, Letters to the Editor, 678, L21

Blanton, M. R., Hogg, D. W., Bahcall, N. A., et al. 2003, Astrophysical Journal, 592, 819

Boselli, A., & Gavazzi, G. 2014, Astronomy and Astrophysics Reviews, 22, 74

Bouchard, A., Da Costa, G. S., & Jerjen, H. 2009, Astronomical Journal, 137, 3038

Boylan-Kolchin, M., Bullock, J. S., & Kaplinghat, M. 2011, Monthly Notices of the RAS, 415, L40

Bradford, J. D., Geha, M. C., & Blanton, M. R. 2015, Astrophysical Journal, 809, 146

Brasseur, C. M., Martin, N. F., Macciò, A. V., Rix, H.-W., & Kang, X. 2011, Astrophysical Journal, 743, 179

Bressan, A., Marigo, P., Girardi, L., et al. 2012, Monthly Notices of the RAS, 427, 127

Cesarsky, D. A., Lequeux, J., Laustsen, S., Schuster, H.-E., & West, R. M. 1977, Astronomy and Astrophysics, 61, L31

Cole, A. A., Weisz, D. R., Dolphin, A. E., et al. 2014, Astrophysical Journal, 795, 54

Cook, K. 1987, University of Arizona

Cutri, R. M., Skrutskie, M. F., van Dyk, S., et al. 2003, 2MASS All Sky Catalog of point sources.

Czekaj, M. A., Robin, A. C., Figueras, F., Luri, X., & Haywood, M. 2014, Astronomy and Astrophysics, 564, A102

Dalcanton, J. J., Williams, B. F., Seth, A. C., et al. 2009, Astrophysical Journal, Supplement Series, 183, 67

de Vaucouleurs, G., de Vaucouleurs, A., Corwin, Jr., H. G., et al. 1991, Third Reference Catalogue of Bright Galaxies (Volume 1-3, XII, 2069 pp. 7 figs.. Springer-Verlag Berlin Heidelberg New York)

Dekel, A., & Silk, J. 1986, Astrophysical Journal, 303, 39

Dekel, A., & Woo, J. 2003, Monthly Notices of the RAS, 344, 1131

Di Cintio, A., Brook, C. B., Macciò, A. V., et al. 2014, Monthly Notices of the RAS, 437, 415

Dotter, A., Chaboyer, B., Jevremović, D., et al. 2008, Astrophysical Journal, Supplement Series, 178, 89

Eggen, O. J., Lynden-Bell, D., & Sandage, A. R. 1962, Astrophysical Journal, 136, 748

Einasto, J., Saar, E., Kaasik, A., & Chernin, A. D. 1974, Nature, 252, 111

Faber, S. M., & Lin, D. N. C. 1983, Astrophysical Journal, Letters to the Editor, 266, L17

Ferrarese, L., Côté, P., Jordán, A., et al. 2006, Astrophysical Journal, Supplement Series, 164, 334

Ferrarese, L., Côté, P., Cuillandre, J.-C., et al. 2012, Astrophysical Journal, Supplement Series, 200, 4

Garrison-Kimmel, S., Boylan-Kolchin, M., Bullock, J. S., & Lee, K. 2014, Monthly Notices of the RAS, 438, 2578

Geha, M., Blanton, M. R., Yan, R., & Tinker, J. L. 2012, Astrophysical Journal, 757, 85

Gill, S. P. D., Knebe, A., & Gibson, B. K. 2005, Monthly Notices of the RAS, 356, 1327

Governato, F., Zolotov, A., Pontzen, A., et al. 2012, Monthly Notices of the RAS, 422, 1231

Graham, A. W., & Driver, S. P. 2005, PASA, 22, 118

Grebel, E. K., Gallagher, J. S., & Harbeck, D. 2003, Astronomical Journal, 125, 1926

Greisen, E. W., & Calabretta, M. R. 2002, Astronomy and Astrophysics, 395, 1061

Harbeck, D., Grebel, E. K., Holtzman, J., et al. 2001, Astronomical Journal, 122, 3092

Hidalgo, S. L., Aparicio, A., & Gallart, C. 2008, Astronomical Journal, 136, 2332

Hodge, P., Lee, M. G., & Kennicutt, Jr., R. C. 1988, Publications of the ASP, 100, 917

Hunter, D. A., Ficut-Vicas, D., Ashley, T., et al. 2012, Astronomical Journal, 144, 134

Huxor, A. P., Mackey, A. D., Ferguson, A. M. N., et al. 2014, Monthly Notices of the RAS, 442, 2165

Ibata, R., Irwin, M., Lewis, G. F., & Stolte, A. 2001, Astrophysical Journal, Letters to the Editor, 547, L133

Ibata, R. A., Gilmore, G., & Irwin, M. J. 1994, Nature, 370, 194

Irwin, M., & Hatzidimitriou, D. 1995, Monthly Notices of the RAS, 277, 1354

Irwin, M., & Lewis, J. 2001, NAR, 45, 105

Irwin, M. J. 1985, Monthly Notices of the RAS, 214, 575

—. 1997, Detectors and data analysis techniques for wide field optical imaging., 35–74

Irwin, M. J., Lewis, J., Hodgkin, S., et al. 2004, in Society of Photo-Optical Instrumentation Engineers (SPIE) Conference Series, Vol. 5493, Optimizing Scientific Return for Astronomy through Information Technologies, ed. P. J. Quinn & A. Bridger, 411–422

Ishibashi, W., & Fabian, A. C. 2012, Monthly Notices of the RAS, 427, 2998

Jackson, D. C., Skillman, E. D., Gehrz, R. D., Polomski, E., & Woodward, C. E. 2007, Astrophysical Journal, 656, 818

Karachentsev, I., Aparicio, A., & Makarova, L. 1999, Astronomy and Astrophysics, 352, 363

Karachentsev, I. D. 2005, Astronomical Journal, 129, 178

Karachentsev, I. D., Makarova, L. N., Makarov, D. I., Tully, R. B., & Rizzi, L. 2015, Monthly Notices of the RAS, 447, L85

Karachentsev, I. D., Makarova, L. N., Tully, R. B., Wu, P.-F., & Kniazev, A. Y. 2014, Monthly Notices of the RAS, 443, 1281

Kaufmann, T., Wheeler, C., & Bullock, J. S. 2007, Monthly Notices of the RAS, 382, 1187

Kawata, D., & Mulchaey, J. S. 2008, Astrophysical Journal, Letters to the Editor, 672, L103

Kepley, A. A., Wilcots, E. M., Hunter, D. A., & Nordgren, T. 2007, Astronomical Journal, 133, 2242

King, I. 1962, Astronomical Journal, 67, 471

Kirby, E. N., Bullock, J. S., Boylan-Kolchin, M., Kaplinghat, M., & Cohen, J. G. 2014, Monthly Notices of the RAS, 439, 1015

Kirby, E. N., Cohen, J. G., Guhathakurta, P., et al. 2013, Astrophysical Journal, 779, 102

Kirby, E. N., Simon, J. D., & Cohen, J. G. 2015, ArXiv e-prints, arXiv:1506.01021

Kleyna, J. T., Wilkinson, M. I., Evans, N. W., & Gilmore, G. 2004, Monthly Notices of the RAS, 354, L66

Kleyna, J. T., Wilkinson, M. I., Gilmore, G., & Evans, N. W. 2003, Astrophysical Journal, Letters to the Editor, 588, L21

Klypin, A., Kravtsov, A. V., Valenzuela, O., & Prada, F. 1999, Astrophysical Journal, 522, 82

Klypin, A., Zhao, H., & Somerville, R. S. 2002, Astrophysical Journal, 573, 597

Koposov, S. E., Belokurov, V., Torrealba, G., & Evans, N. W. 2015, Astrophysical Journal, 805, 130

Kormendy, J. 1985, Astrophysical Journal, 295, 73

Kormendy, J., Fisher, D. B., Cornell, M. E., & Bender, R. 2009, Astrophysical Journal, Supplement Series, 182, 216

Law, D. R., Johnston, K. V., & Majewski, S. R. 2005, Astrophysical Journal, 619, 807

Law, D. R., & Majewski, S. R. 2010, Astrophysical Journal, 714, 229

Leaman, R., Venn, K. A., Brooks, A. M., et al. 2012, Astrophysical Journal, 750, 33

—. 2013, Astrophysical Journal, 767, 131

Lee, M. G., Aparicio, A., Tikonov, N., Byun, Y.-I., & Kim, E. 1999, Astronomical Journal, 118, 853

Lee, M. G., & Byun, Y.-I. 1999, Astronomical Journal, 118, 817

Lee, M. G., Freedman, W. L., & Madore, B. F. 1993, Astrophysical Journal, 417, 553

Lee, M. G., & Kim, S. C. 2000, Astronomical Journal, 119, 777

Lianou, S., Grebel, E. K., Da Costa, G. S., et al. 2013, Astronomy and Astrophysics, 550, A7

Lo, K. Y., Sargent, W. L. W., & Young, K. 1993, Astronomical Journal, 106, 507

Longmore, A. J., Hawarden, T. G., Webster, B. L., Goss, W. M., & Mebold, U. 1978, Monthly Notices of the RAS, 183, 97P

Madore, B. F., Mager, V., & Freedman, W. L. 2009, Astrophysical Journal, 690, 389

Majewski, S. R., Skrutskie, M. F., Weinberg, M. D., & Ostheimer, J. C. 2003, Astrophysical Journal, 599, 1082

Martínez-Delgado, D., Aparicio, A., & Gallart, C. 1999, Astronomical Journal, 118, 2229

Massey, P., Olsen, K. A. G., Hodge, P. W., et al. 2006, Astronomical Journal, 131, 2478

Mayer, L., Mastropietro, C., Wadsley, J., Stadel, J., & Moore, B. 2006, Monthly Notices of the RAS, 369, 1021

McConnachie, A. W. 2012, Astronomical Journal, 144, 4

McConnachie, A. W., Arimoto, N., Irwin, M., & Tolstoy, E. 2006, Monthly Notices of the RAS, 373, 715

McConnachie, A. W., & Côté, P. 2010, Astrophysical Journal, Letters to the Editor, 722, L209

McConnachie, A. W., Ferguson, A. M. N., Irwin, M. J., et al. 2010, Astrophysical Journal, 723, 1038

McConnachie, A. W., & Irwin, M. J. 2006, Monthly Notices of the RAS, 365, 1263

McConnachie, A. W., Irwin, M. J., Ferguson, A. M. N., et al. 2005, Monthly Notices of the RAS, 356, 979

McConnachie, A. W., Peñarrubia, J., & Navarro, J. F. 2007a, Monthly Notices of the RAS, 380, L75

McConnachie, A. W., Venn, K. A., Irwin, M. J., Young, L. M., & Geehan, J. J. 2007b, Astrophysical Journal, Letters to the Editor, 671, L33

McConnachie, A. W., Irwin, M. J., Ibata, R. A., et al. 2009, Nature, 461, 66

McMonigal, B., Bate, N. F., Lewis, G. F., et al. 2014, Monthly Notices of the RAS, 444, 3139

Minniti, D., & Zijlstra, A. A. 1997, Astronomical Journal, 114, 147

Momany, Y., Held, E. V., Saviane, I., & Rizzi, L. 2002, Astronomy and Astrophysics, 384, 393

Momany, Y., Held, E. V., Saviane, I., et al. 2005, Astronomy and Astrophysics, 439, 111

Monelli, M., Bernard, E. J., Gallart, C., et al. 2012, Monthly Notices of the RAS, 422, 89

Moore, B., Ghigna, S., Governato, F., et al. 1999, Astrophysical Journal, Letters to the Editor, 524, L19

Oh, S.-H., Hunter, D. A., Brinks, E., et al. 2015, Astronomical Journal, 149, 180

Ordoñez, A. J., & Sarajedini, A. 2015, Astronomical Journal, 149, 201

Peñarrubia, J., Navarro, J. F., & McConnachie, A. W. 2008, Astronomische Nachrichten, 329, 934

Peñarrubia, J., Navarro, J. F., McConnachie, A. W., & Martin, N. F. 2009, Astrophysical Journal, 698, 222

Richardson, J. C., Irwin, M. J., McConnachie, A. W., et al. 2011, Astrophysical Journal, 732, 76

Rizzi, L., Held, E. V., Bertelli, G., & Saviane, I. 2004, Mem. Soc. Astron. Italiana, 75, 110

Robin, A. C., Reylé, C., Derrière, S., & Picaud, S. 2003, Astronomy and Astrophysics, 409, 523

Ross, T. L., Holtzman, J., Saha, A., & Anthony-Twarog, B. J. 2015, Astronomical Journal, 149, 198

Roychowdhury, S., Chengalur, J. N., Begum, A., & Karachentsev, I. D. 2010, Monthly Notices of the RAS, 404, L60

Sakai, S., Madore, B. F., & Freedman, W. L. 1996, Astrophysical Journal, 461, 713

Salaris, M., & Cassisi, S. 1997, Monthly Notices of the RAS, 289, 406

Sánchez-Janssen, R., Méndez-Abreu, J., & Aguerri, J. A. L. 2010, Monthly Notices of the RAS, 406, L65

Sand, D. J., Spekkens, K., Crnojević, D., et al. 2015, Astrophysical Journal, Letters to the Editor, 812, L13

Sandage, A., & Tammann, G. A. 1976, Astrophysical Journal, 210, 7

Sarajedini, A., & Jablonka, P. 2005, Astronomical Journal, 130, 1627

Saviane, I., Rizzi, L., Held, E. V., Bresolin, F., & Momany, Y. 2002, Astronomy and Astrophysics, 390, 59

Schlafly, E. F., & Finkbeiner, D. P. 2011, Astrophysical Journal, 737, 103

Schlegel, D. J., Finkbeiner, D. P., & Davis, M. 1998, Astrophysical Journal, 500, 525

Scudder, J. M., Ellison, S. L., Torrey, P., Patton, D. R., & Mendel, J. T. 2012, Monthly Notices of the RAS, 426, 549

Searle, L., & Zinn, R. 1978, The Astrophysical Journal, 225, 357

Simon, J. D., & Geha, M. 2007, Astrophysical Journal, 670, 313

Skillman, E. D., Terlevich, R., & Melnick, J. 1989, Monthly Notices of the RAS, 240, 563

Spekkens, K., Urbancic, N., Mason, B. S., Willman, B., & Aguirre, J. E. 2014, Astrophysical Journal, Letters to the Editor, 795, L5

Strobel, N. V., Hodge, P., & Kennicutt, Jr., R. C. 1991, Astrophysical Journal, 383, 148

Teyssier, R., Pontzen, A., Dubois, Y., & Read, J. I. 2013, Monthly Notices of the RAS, 429, 3068

Tolstoy, E., Hill, V., & Tosi, M. 2009, Annual Review of Astronomy and Astrophysics, 47, 371

Tolstoy, E., Irwin, M. J., Helmi, A., et al. 2004, Astrophysical Journal, Letters to the Editor, 617, L119

Tosi, M., Greggio, L., Marconi, G., & Focardi, P. 1991, Astronomical Journal, 102, 951

van de Rydt, F., Demers, S., & Kunkel, W. E. 1991, Astronomical Journal, 102, 130

van Dokkum, P. G., Abraham, R., & Merritt, A. 2014, Astrophysical Journal, Letters to the Editor, 782, L24

van Dokkum, P. G., Abraham, R., Merritt, A., et al. 2015, Astrophysical Journal, Letters to the Editor, 798, L45

Vansevičius, V., Arimoto, N., Hasegawa, T., et al. 2004, Astrophysical Journal, Letters to the Editor, 611, L93

Verbeke, R., Vandenbroucke, B., & De Rijcke, S. 2015, ArXiv e-prints, arXiv:1511.01484

Vollmer, B., Marcelin, M., Amram, P., et al. 2000, Astronomy and Astrophysics, 364, 532

Weisz, D. R., Dolphin, A. E., Skillman, E. D., et al. 2014, Astrophysical Journal, 789, 147

Weisz, D. R., Dalcanton, J. J., Williams, B. F., et al. 2011, Astrophysical Journal, 739, 5

Wheeler, C., Oñorbe, J., Bullock, J. S., et al. 2015, Monthly Notices of the RAS, 453, 1305

Willman, B., & Strader, J. 2012, Astronomical Journal, 144, 76

Young, L. M., & Lo, K. Y. 1997, Astrophysical Journal, 490, 710

Young, L. M., van Zee, L., Lo, K. Y., Dohm-Palmer, R. C., & Beierle, M. E. 2003, Astrophysical Journal, 592, 111